European Journal of Medicinal Chemistry 271 (2024) 116357

Contents lists available at ScienceDirect

European Journal of Medicinal Chemistry

journal homepage: www.elsevier.com/locate/ejmech

Research paper

# Discovery and optimization of narrow spectrum inhibitors of Tousled like kinase 2 (TLK2) using quantitative structure activity relationships

Christopher R.M. Asquith [a,b,c,*], Michael P. East [a], Tuomo Laitinen [b], Carla Alamillo-Ferrer [c], Erkka Hartikainen [b], Carrow I. Wells [c], Alison D. Axtman [c], David H. Drewry [c,d], Graham J. Tizzard [e], Antti Poso [b], Timothy M. Willson [c], Gary L. Johnson [a,d,**]

[a] Department of Pharmacology, School of Medicine, University of North Carolina at Chapel Hill, NC, 27599, USA
[b] School of Pharmacy, Faculty of Health Sciences, University of Eastern Finland, 70211, Kuopio, Finland
[c] Structural Genomics Consortium and Division of Chemical Biology and Medicinal Chemistry, UNC Eshelman School of Pharmacy, University of North Carolina at Chapel Hill, Chapel Hill, NC, 27599, USA
[d] Lineberger Comprehensive Cancer Center, University of North Carolina at Chapel Hill, Chapel Hill, NC, 27599, USA
[e] UK National Crystallography Service, School of Chemistry, University of Southampton, Highfield Campus, Southampton, SO17 1BJ, UK

ARTICLE INFO

*Keywords:*
Kinase inhibitors
Oxindole
Kinase chemical tool
Tousled like kinase 2 (TLK2)
Quantitative structure-activity relationship (QSAR)

ABSTRACT

The oxindole scaffold has been the center of several kinase drug discovery programs, some of which have led to approved medicines. A series of two oxindole matched pairs from the literature were identified where TLK2 was potently inhibited as an off-target kinase. The oxindole has long been considered a promiscuous kinase inhibitor template, but across these four specific literature oxindoles TLK2 activity was consistent, while the kinome profile was radically different ranging from narrow to broad spectrum kinome coverage. We synthesized a large series of analogues, utilizing quantitative structure-activity relationship (QSAR) analysis, water mapping of the kinase ATP binding sites, kinome profiling, and small-molecule x-ray structural analysis to optimize TLK2 inhibition and kinome selectivity. This resulted in the identification of several narrow spectrum, sub-family selective, chemical tool compounds including **128** (UNC-CA2-103) that could enable elucidation of TLK2 biology.

## 1. Introduction

Tousled-like kinase 2 (TLK2) is a ubiquitously expressed nuclear serine/threonine kinase. The kinase activity of TLK2 and its closest human paralog TLK1 is activated by autophosphorylation, hetero- and homo-dimerization, and oligomerization through conserved coiled-coiled domains [1]. TLK kinase activity is highest during S-phase where TLKs phosphorylate ASF1 histone chaperones [2]. DNA rapidly associates with histones during replication and the ASF1 chaperones regulate the soluble pool of histones H3 and H4 during this process [3]. Phosphorylation of ASF1 chaperones by TLKs stabilizes ASF1 protein [4], and promotes interactions between ASF1 and histones as well as histones with downstream chaperones CAF1 and HIRA1. TLK2, but not TLK1, was also shown to regulate G2/M checkpoint recovery after DNA damage through an ASF1A dependent mechanism [5]. TLKs have ASF1 independent functions during DNA replication through the regulation of replication forks [6]. Depletion of TLKs results in replication fork stalling, the accumulation of single-stranded DNA, and ultimately, DNA damage and cell cycle arrest in G1. These phenotypes were rescued by ectopic expression of WT TLKs but not kinase dead TLKs. Analysis of chromatin accessibility using the Assay for Transposase-Accessible Chromatin using sequencing (ATAC-seq) following knockdown of TLK1 or TLK2 increased accessibility and transcription of heterochromatin. As a result, loss of TLKs induced alternate lengthening of telomeres thereby activating the cGAS-STING-TBK1 mediated immune response. Consistent with this function, high levels of TLK2 in patients were associated with poor innate and adaptive immune responses in tumors and, potentially, immune evasion [7]. TLK2 was recently shown to interact directly with the transcription factor ATF4 to regulate amino acid metabolism through transcriptional activation of the asparagine synthesis enzyme ASNS [8]. Thus, TLKs, and more specifically their kinase activity, are essential for proper chromatin assembly, DNA replication, transcriptional activation, and maintenance of heterochromatin.

The cellular functions of TLK1 and TLK2 are predominantly

* Corresponding author. School of Pharmacy, Faculty of Health Sciences, University of Eastern Finland, 70211, Kuopio, Finland.
** Corresponding author. Department of Pharmacology, School of Medicine, University of North Carolina at Chapel Hill, NC, 27599, USA.
*E-mail addresses:* christopher.asquith@uef.fi (C.R.M. Asquith), gary_johnson@med.unc.edu (G.L. Johnson).

https://doi.org/10.1016/j.ejmech.2024.116357
Received 24 December 2023; Received in revised form 24 March 2024; Accepted 24 March 2024
Available online 2 April 2024
0223-5234/© 2024 The Authors. Published by Elsevier Masson SAS. This is an open access article under the CC BY-NC license (http://creativecommons.org/licenses/by-nc/4.0/).

overlapping but their clinical implications are more diverse which may suggest other distinct functions. In the present study, we focus on TLK2. TLK2 has been implicated in neurodevelopmental disease and intellectual deficiency [9–11]. Neurodevelopmental defects manifested with TLK2 haploinsufficiency and were more severe in a single, homozygous case. TLK2 mutations observed in these studies resulted in loss of TLK2 kinase activity [12]. In cellular models of latent gammaherpesvirus infections, knockdown of TLK1 or TLK2 was sufficient to reactivate latent Epstein-Barr virus infection whereas only knockdown of TLK2 resulted in reactivation of latent Kaposi sarcoma-associated herpesvirus [13]. Latency allows viral infections to evade the immune system and antiviral therapies resulting in lifelong, incurable infection. Reactivation of virus in combination with antiviral therapy is a promising approach known as "shock and kill" that could potentially cure these latent viral infections [14]. TLK2 has also been implicated in breast cancer, glioblastoma, and gastric cancer where TLK2 is amplified or over-expressed in a high percentage of patients and where higher expression levels are associated with poor patient outcomes [8,15–17]. In cell lines from all three cancer types, ectopic expression of TLK2 lead to enhanced aggressiveness whereas knockdown or pharmacological inhibition slowed growth and inhibited invasion. In breast cancer and glioblastoma, TLK2 was shown to activate SRC signaling [15–17]. In gastric cancer, TLK2 regulated amino acid metabolism through the mTOR pathway [8]. In large-scale CRISPR knockout screens across 1100 cancer cell lines (DepMap.org), TLK1 was essential for growth of only 12 cell lines strongly selective for colorectal lineages whereas TLK2 was essential for 996 cell lines spanning all cancer types suggesting TLK2 may be an important target in a much broader spectrum of human cancers. Knockout of TLK2 in mice resulted in late embryonic lethality due to defective trophoblast differentiation and placental failure [18]. Conditional knockout of TLK2 to bypass the placental defect led to healthy mice suggesting that TLK2 was otherwise dispensable for development and viability. These findings suggest that inhibition of TLK2 may be tolerable in normal, healthy cells in patients. Thus, TLK2 is a very promising target for drug development in multiple cancer types and as a latency reversing agent in shock and kill approaches for latent viral infections [14–16].

While some recent advances have been made around TLK2 chemical tools, with one recent advancement based on indirubin based derivatives, these analogues still inhibit both TLK1 and TLK2 with limited selectivity information [19]. There are currently no potent and selective TLK2 inhibitors as chemical probes to investigate TLK2 biology [20]. This, despite several concerted efforts to map and identify leads within existing ATP-competitive kinase inhibitors and to define inhibitor chemical space [20–30].

## 2. Results

Currently the only small molecule inhibitors available to modulate TLK2 are compounds with very broad kinome coverage including staurosporine, SYK inhibitor R406, and RTK inhibitor sunitinib, all of which inhibit TLK2 as an undesired off-target with low relative potency (Fig. 1). However, the sunitinib oxindole based scaffold has demonstrated tractability on TLK2 where small modifications to afford SU14813 still maintain potency on TLK2 even when coverage has been reduced from 187 to 149 kinases. This is further supported by additional results of an enzyme assay-based panel identifying two further oxindoles, GW506033X and SU9516, that had 84% and 57% inhibition of TLK2 at 0.5 μM, respectively [23]. The narrower kinome profile of SU9516 provided an attractive starting point for progress towards the development of a selective chemical probe for TLK2. Herein we report the synthesis, modelling, and characterization of oxindole based inhibitors as potent narrow-spectrum TLK2 inhibitors.

Having identified the oxindole scaffold as a promising inhibitor chemotype, we first screened 21 commercially available oxindole based kinase inhibitors (Fig. 2) [31–37] in a TLK2 enzyme assay (Table S1-S2) [24]. This enabled us to quickly map the TLK2 vs the close kinome landscape and to prioritize our efforts around the smaller SU9516 and GW506033X oxindoles.

Several interchangeable matched pairs including sunitinib (SU11248), toceranib (SU11654), SU12662 and SU14813 all demonstrated consistent low single digit micromolar activity against TLK2. While all these compounds have promiscuous kinome profiles [21–23], this data increased our confidence that the oxindole may provide a good starting point for TLK2 probe development. The two indirubin derivatives had the same activity against TLK2 ($IC_{50} = 0.44$ μM) indicating that oxindoles were bound in the traditional binding mode, with space to

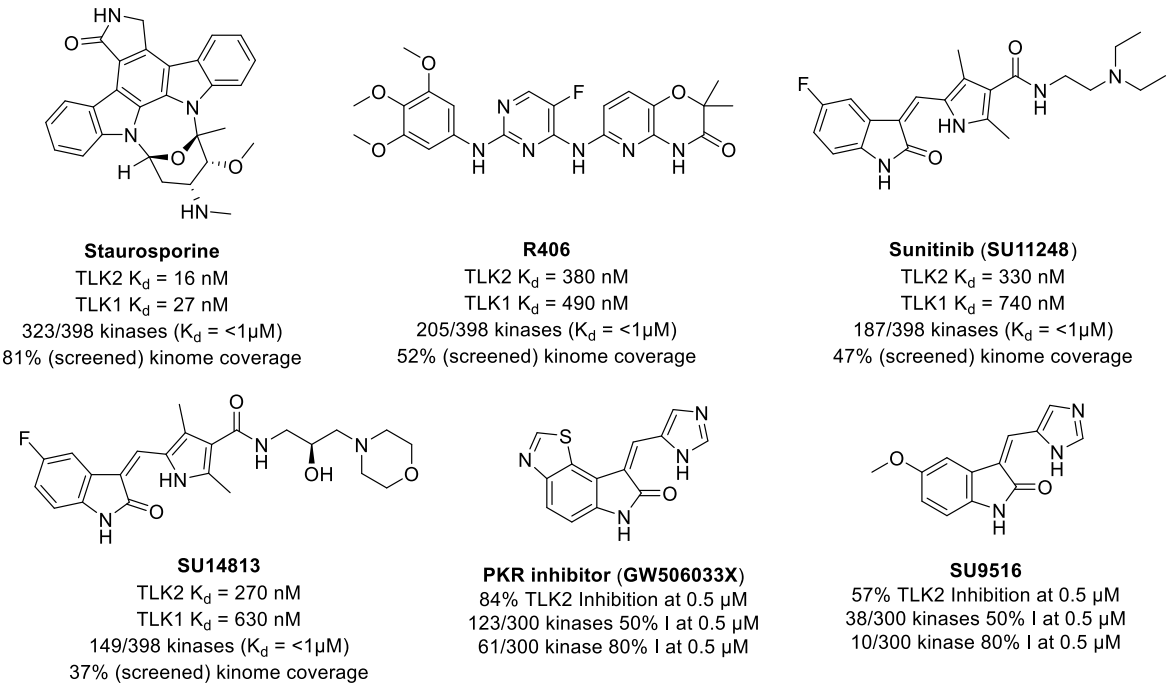


**Fig. 1.** Previously reported kinase inhibitors with off-target of TLK2 inhibition, including two matched pair oxindoles.

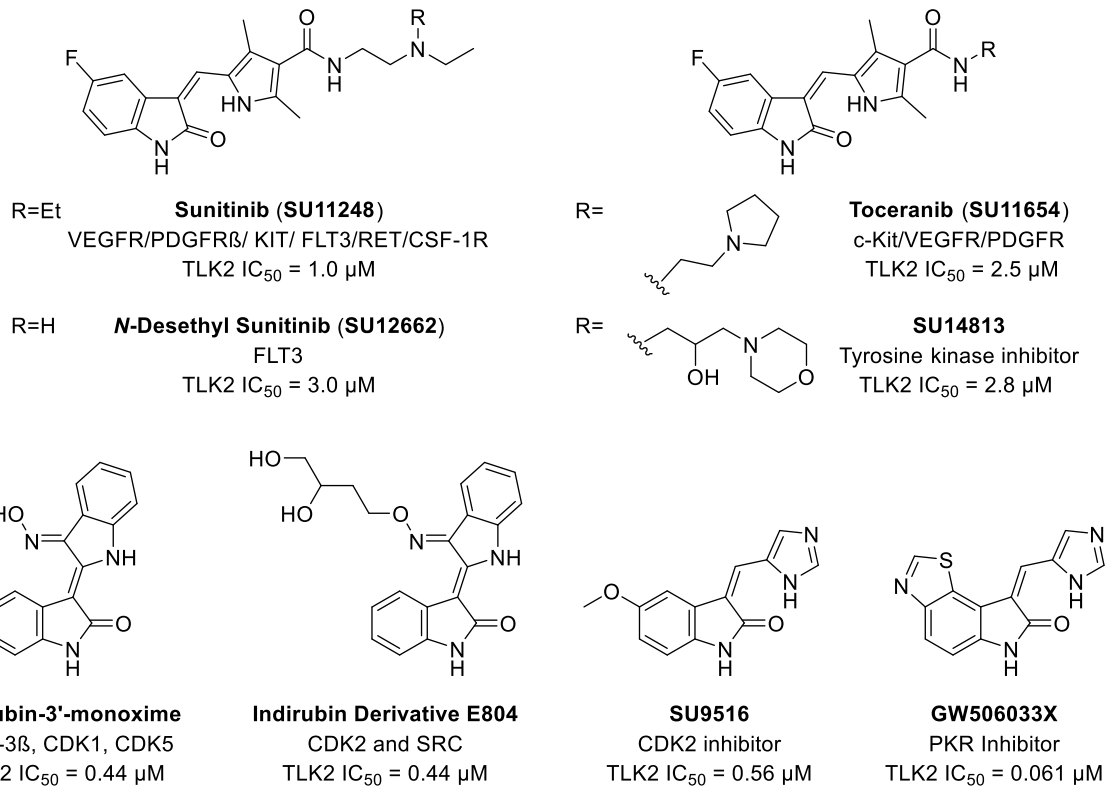


**Fig. 2.** Screening of literature inhibitors with the oxindole scaffold with activities below 10 μM (see Fig. S1 for additional screening and structures). Format: Name, primary target, TLK2 $IC_{50}$.

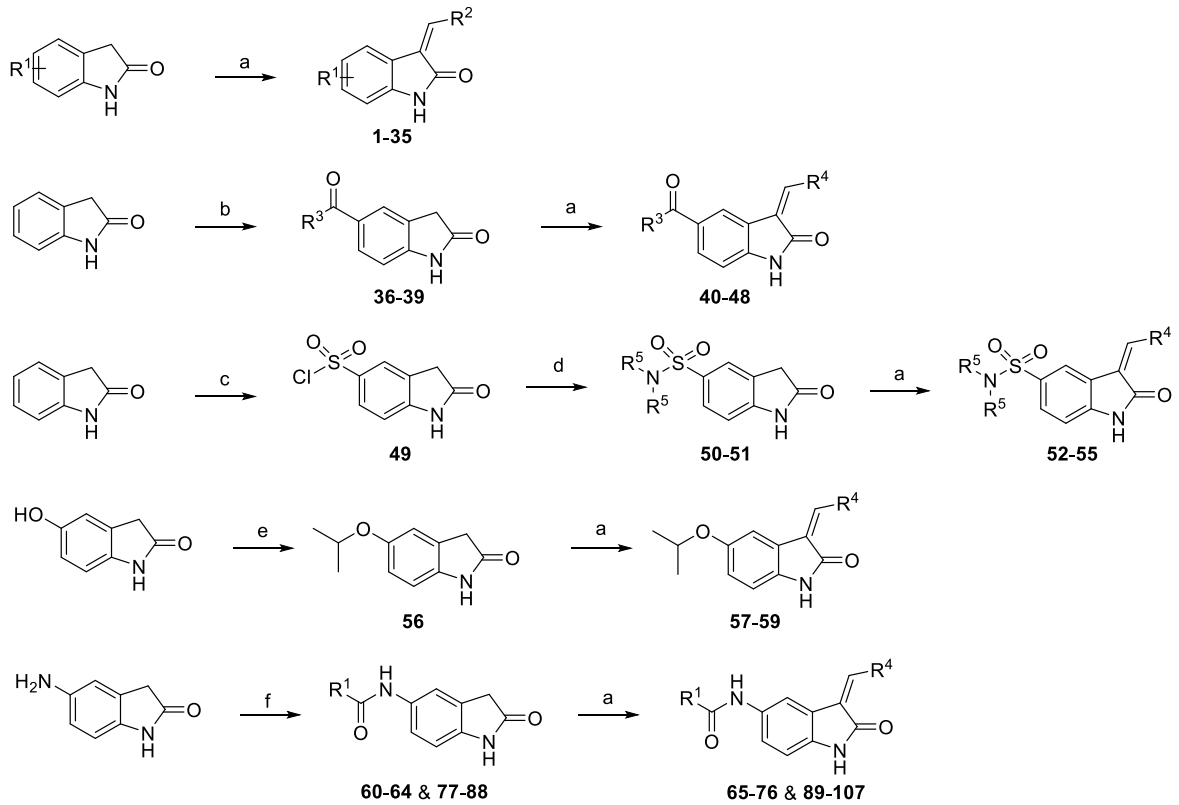


**Scheme 1.** Synthetic route to prepare the oxindole analogues - *reagents and conditions* a) $R_2CHO$, piperidine, EtOH, reflux, 4–24 h; b) $R^1COCl$, $AlCl_3$, $CH_2Cl_2$, rt, 48 h; c) $ClSO_3H$, −5 °C, 2 h; d) $(R^1)_2NH$, $EtN(CH(CH_3)_2)_2$ THF, rt, 12 h; e) $R^1OH$, diethyl azadicarboxylate (DEAD), $PPh_3$, rt, −5 °C to rt; f) $R^1COCl$, HATU, $EtN(CH(CH_3)_2)_2$, THF, rt, 12 h.

grow the solvent exposed region of the molecule (Fig. S1) [31–37]. The only other two oxindoles that showed activity below 1 μM were SU9516 and GW506033X, both containing an imidazole head group (Fig. S1 and Fig. 2). The narrow kinome spectrum of SU9516 (10 kinases inhibited to 80% at 1 μM) combined with the potency of GW506033X ($IC_{50} = 0.061$ μM) afforded a promising indication that a potent narrow spectrum compound was possible [24]. We also noted that the same major kinase off-targets namely, fms-like tyrosine kinase 3 (FLT3) and tropomyosin receptor kinase C (TRKC) were recurring themes and likely a prognostic marker for further promiscuity across the kinome. In addition to screening for TLK2 potency, we screened these two off-targets as a micro-panel to check for selectivity between molecules before kinome-wide screening [38–40].

Having decided to focus our attention on SU9516 (**1**) and related GW506033X, we first sought to explore the structural features required for TLK2 inhibition (Scheme 1). Initially we synthesized a series of direct SU9516 analogues (**1**–**35**) using commercially available 5- and/or 6-substituted oxindoles and the Knoevenagel condensation [41–43]. The oxindoles along with a corresponding aldehyde were suspended in ethanol and treated with piperidine under reflux to afford condensation products **1**–**35**

in varying yields (15–85%). The products were isolated by direct crystallization from the crude reaction mixture or following chromatographic purification. A second set of analogues was synthesized in a two-step procedure, first using a Friedel–Crafts acylation by treatment of unsubstituted oxindole with aluminum (III) chloride and the corresponding acid chloride in dichloromethane to afford the 5-position ketone substituted products **36**–**39** in acceptable to good yields (30–74%) [44–46]. Second, the ketone products (**36**–**39**) were then treated with the corresponding aldehyde, piperidine under reflux to afford condensation products **40**–**48** in acceptable to good yields (30–74%). To afford a series of sulphonamide analogues, we first treated the unsubstituted oxindole with neat chlorosulphonic acid at −10 °C, affording **49** in good yield (68%) [47]. The sulfonyl chloride **49** was treated with the corresponding amine to afford the sulphonamide building blocks **50**–**51** in excellent yields, 78% and 85% respectively. The sulphonamides **50**–**51** were then treated with the previous Knoevenagel conditions with the respective aldehyde to afford the condensation products **52**–**55** in good yield (41–75%).

To access a novel 5-position *iso*propyl ether oxindole, a standard Mitsunobu reaction was performed on the 5-hydroxy oxindole with diethyl azadicarboxylate (DEAD), triphenylphosphine, *iso*propyl alcohol in THF at 0 °C to afford 5-*iso*propoxyindolin-2-one (**56**) in 30% yield [48–50]. The ether **56** was then subject to the Knoevenagel conditions with the corresponding aldehyde to afford the desired condensation products **57**–**59** in good yields (53–62%). Finally, we prepared a series of substituted oxindole amides, furnished with a standard HATU coupling [51], in the presence of DIPEA and THF. The first set **60**–**64** was afforded in good yields (63–78%), followed by a series of condensations under standard conditions to render a series of 5-postion substituted amide final products **65**–**76** in a range of yields (15–71%). The second set of amide substitutions **77**–**88** were also afforded in good to excellent yields (48–91%) followed by standard Knoevenagel conditions with the appropriate aldehyde to produce the condensation products **89**–**107** in a range of yields (11–71%).

Having prepared a series of oxindole analogues, these were screened in a TLK2 enzyme assay [24] in a 10-point dose dependent format for TLK2 to determine an $IC_{50}$ value. The maximum concentration used was 20 μM with an ATP concentration of 10 μM. The corresponding collateral target evaluation was performed on FLT3 and TRKC which were screened at a 0.5 μM with an ATP concentration of 10 μM, consistent with previous reports [24]. The most advanced compounds were then subjected to an in-house Kinase-Glo assay. The lead compounds were then screened in a DiscoverX kinome panel assay (>400 kinases) to assess their selectivity across the kinome [21–23].

In the first series of analogues, we followed up on the initial hit compound (*Z*)-3-((1*H*-imidazole-5-yl)methylene)-5-methoxyindolin-2-one (**1**) which when resynthesized produced a compound with consistent potency on TLK2 ($IC_{50} = 240$ nM) (Table 1). The substitution of the imidazole with the pyrrole **2** resulted in a 6-fold drop in potency on TLK2. Introduction of the sterically hindered dimethyl group **3** afforded no inhibition of TLK2 at the maximum concentration tested but still showed activity against FLT3 and TRKC. The introduction of a pyrazole group **4** lead to a 36-fold reduction of TLK2 activity with respect to **1**. The 2-substituted imidazole **5** afforded a compound that was near equipotent with **1** against TLK2. However, none of the simple 5 membered analogues **2**–**5** improved activity on TLK2. A switch to a 6-member 2-pyridyl **6** or 3-pyridyl **7** head group ring system, demonstrated limited activity against TLK2 at the maximum concentration tested, but also no activity against TRKC and FLT3. Removal of the 5-methoxy group to afford the unsubstituted oxindole **8** led to a 2-fold drop in potency against TLK2. Interestingly the pyrrole substitution **9** shows the same potency as **8** unlike the corresponding drop observed between **1** and **2**. The corresponding 3,5-dimethyl pyrrole substitution **10** was inactive against TLK2, while the pyrazole **11** showed a 13-fold drop compared with **8**. The 2-substituted imidazole analogue **12** was equipotent with **8**, while the two pyridyl analogues **13** and **14** demonstrated no activity against TLK2 or TRKC/FLT3. Switching to the 6-methoxy oxindole substitution **15**–**20** lead to a net reduction of around 10-fold in activity on nearly all analogues with only the pyrrole maintaining TLK2 inhibition at the same level as **2**.

Given the decrease in inhibition of TLK2 activity at the 6-position, we decided to explore the 5,6-dimethxoyoxindole core **21**–**25** to assess potential synergistic effects of a double substitution pattern. The results of the five analogues were consistent with the mono-substituted 6-methoxy except for the pyrrole **22** that showed a 3-fold jump in potency against TLK2. However, **22** also showed a boost in TRKC and FLT3 inhibition, meaning it was also likely an overall increase in kinome inhibition rather than something solely related to TLK2. We decided to focus our attention on the 5-postion as this seemed to be preferable for TLK2 inhibition. Switching the core to the 5-acetyloxindole **26**–**32** afforded our first compound **26** with 3-fold drop in potency against TLK2 compared with **1**. However, the pyrrole **27** showed improvement on **1** with more potency against TLK2 with an $IC_{50} = 150$ nM. The 3,5-dimethylpyrrole analogue **28** also demonstrated inhibition of TLK2 for the first time with an $IC_{50} = 870$ nM. The pyrazole **29** was significantly weaker nearly 10-fold less potent than the imidazole parent **26**. The 2-substituted imidazole **30** was as active as the parent while the pyridyl analogues **31** and **32** showed no activity against TLK2 at the maximum concentration, but there was an increase in TRKC and FLT3 inhibition compared to the other pyridyl analogues synthesized.

There are clear trends observed between pyrrole, imidazole, 2-substituted imidazole, in addition to the unsubstituted-, 5-position methoxy- and acetyl-oxindoles. The docking of **1**, **3**, **27** and **28** in the TLK2 protein crystal structure [12], provided an insight into these trends (Fig. 3). The differences between **1** and **3** can be simply explained by the steric clash between the 3,5-dimethylpyrrole on **3**. However, the reduced solvation by removal of the additional nitrogen was also contributing to the reduced potency of **3** on TLK2 (Fig. 3A-**B**). However, the acetyl substitution of **27** and **28** allowed for a shift in overall binding position that was able to compensate for this steric clash (Fig. 3C-**D**) and enabled a closing of the gap of potency from >40-fold between **1** and **3** to equipotent between **26** and **28**. We used this knowledge in the design of our next series of ketone-based substituted oxindole analogues.

The (*Z*)-3-((1*H*-pyrrol-2-yl)methylene)-5-acetylindolin-2-one (**27**) was the most potent analogue from the initial matrix array (Table 1). The 5-position acetyl showed a good trend towards TLK2 inhibition even enabling the 3,5-dimethyl pyrrole substitution **28** to have activity against TLK2 below 1 μM. These two results together with a TLK2 inhibition preference for the pyrrole and imidazoles prompted us to focus on the acetyl derivatives (Table 2).

First, we looked at the simple carboxylic acid derivatives **33**–**35**. The

**Table 1**
Matrix array of SU9516 derivatives with 5,6-oxindole substitutions and different heterocyclic head groups.

| | | | | | | | | |
|---|---|---|---|---|---|---|---|---|
| | **Name** | **1** | **2** | **3** | **4** | **5** | **6** | **7**[c] |
| | **TLK2 ($IC_{50}$)**[a] | 0.24 μM | 1.5 μM | >20 μM | 8.7 μM | 0.38 μM | >20 μM | >20 μM |
| | **FLT3 (% Inh.)**[b] | 93 | 81 | 98 | 43 | 90 | 6.7 | 8.6 |
| | **TRKC (% Inh.)**[b] | 96 | 80 | 97 | 61 | 93 | 15 | 20 |
| | **Name** | **8**[c] | **9** | **10** | **11** | **12**[c] | **13** | **14** |
| | **TLK2 ($IC_{50}$)**[a] | 0.44 μM | 0.47 μM | >20 μM | 5.9 μM | 0.60 μM | >20 μM | >20 μM |
| | **FLT3 (% Inh.)**[b] | 81 | 94 | 97 | 31 | 71 | 0 | 0 |
| | **TRKC (% Inh.)**[b] | 92 | 97 | 94 | 55 | 89 | 7.7 | 1.1 |
| | **Name** | – | **15** | **16** | **17** | **18** | **19** | **20**[c] |
| | **TLK2 ($IC_{50}$)**[a] | | 1.7 μM | >20 μM | >20 μM | 2.2 μM | >20 μM | >20 μM |
| | **FLT3 (% Inh.)**[b] | | 87 | 76 | 11 | 67 | 0 | 13 |
| | **TRKC (% Inh.)**[b] | | 81 | 64 | 25 | 63 | 5.2 | 23 |
| | **Name** | **21** | **22** | **23** | **24** | **25**[c] | – | – |
| | **TLK2 ($IC_{50}$)**[a] | 1.8 μM | 0.63 μM | >20 μM | >20 μM | 2.1 μM | | |
| | **FLT3 (% Inh.)**[b] | 87 | 95 | 82 | 35 | 80 | | |
| | **TRKC (% Inh.)**[b] | 64 | 89 | 65 | 19 | 55 | | |
| | **Name** | **26** | **27** | **28** | **29** | **30**[c] | **31** | **32**[c] |
| | **TLK2 ($IC_{50}$)**[a] | 0.77 μM | 0.15 μM | 0.87 μM | 7.6 μM | 0.62 μM | >20 μM | >20 μM |
| | **FLT3 (% Inh.)**[b] | 94 | 97 | 98 | 75 | 89 | 23 | 15 |
| | **TRKC (% Inh.)**[b] | 91 | 97 | 99 | 62 | 82 | 33 | 21 |

[a] 8-point dose response (n = 1).
[b] Percentage inhibition at 0.5 μM (n = 2).
[c] *E:Z* ratio: **7** (50:50); **8** (33:67); **12** (40:60); **20** (28:72); **25** (44:56); **26** (32:68); **30** (47:53); **32** (48:52) [41].

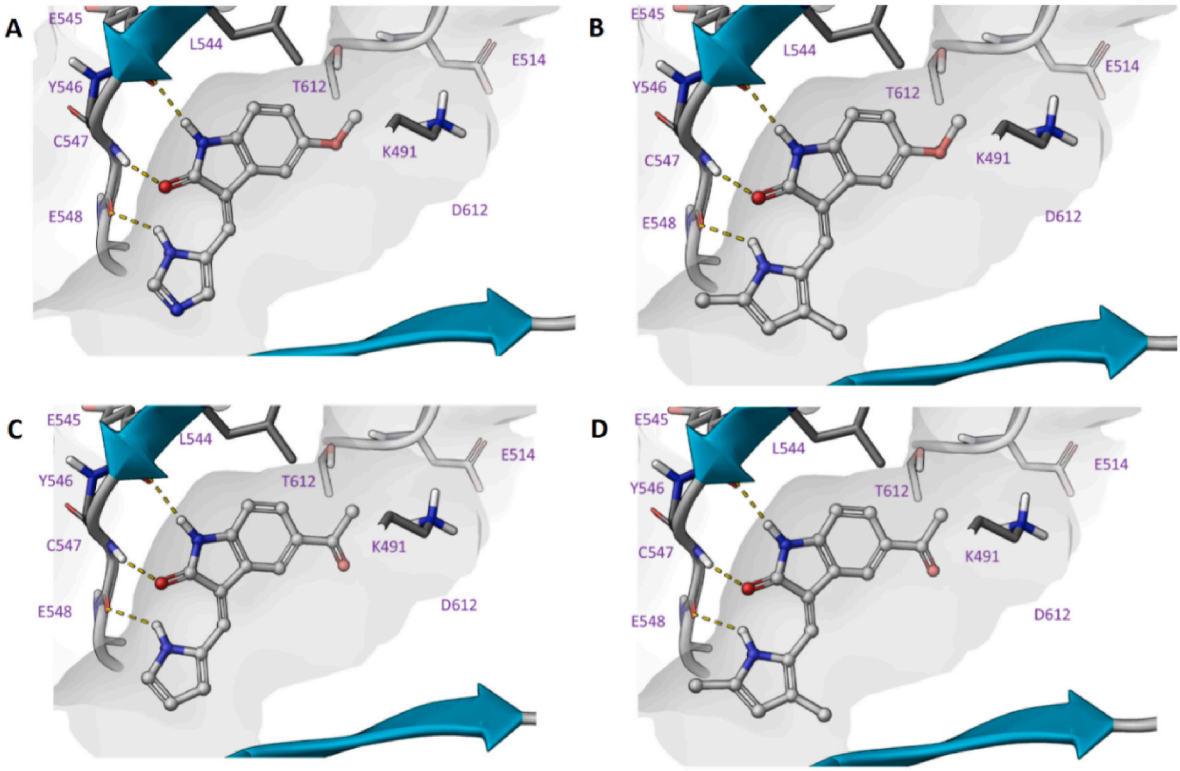


**Fig. 3.** Inhibitor docking of A) **1**, B) **3**, C) **27**, D) **28** in TLK2 (PDB: 5O0Y), demonstrating key hinge binding interactions and space in the hydrophobic pocket.

direct replacement of the acetyl to form the carboxylic acid **33** demonstrated a 2-fold improvement in TLK2 inhibition, while the imidazole **34** was equipotent. However, the 2-substituted imidazole **35** showed a 6-fold boost in potency against TLK2 ($IC_{50}$ = 26 nM). Interestingly, both imidazole substituted compounds also had good selectivity over the two off-targets FLT3 and TRKC. To pursue the aim of a TLK2 probe quality compound with single digit nanomolar activity against TLK2, we hence investigated larger substituents. The *n*-butyl substituent analogues **40**–**42** showed a slight decrease in inhibition compared to **27** with flat structure-activity relationship (SAR) across the three analogues. The larger phenyl analogues **43**–**44** showed no improvement with an overall 5-6-fold decrease compared with **27**. Introduction of a 4-fluoro substitution **45**–**46** mitigated some of the decrease in TLK2 inhibition to 2-3-fold compared with **27** with the same off-target FLT3/TRKC profile. Switching from a phenyl to a furan afforded compounds **47**–**48** that were near equipotent with **27**. Despite decreased ligand efficiency compared with **27**, these furan analogues **47**–**48** presented a potential expansion point for further optimization.

**Table 2**
Investigation of derivatives of **27** with pyrrole and imidazole heterocyclic head groups.

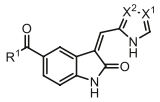

| Name | $R^1$ | $X^1$ | $X^2$ | TLK2 $IC_{50}$ (nM)[a] | FLT3 (%)[b] | TRKC (%)[b] |
|---|---|---|---|---|---|---|
| **33** | | C–H | C–H | 62 | 94 | 91 |
| **34**[c] | | N | C–H | 140 | 67 | 54 |
| **35** | | C–H | N | 26 | 70 | 63 |
| **40** | | C–H | C–H | 220 | 96 | 98 |
| **41** | | N | C–H | 230 | 91 | 96 |
| **42** | | C–H | N | 250 | 86 | 91 |
| **43** | | C–H | C–H | 870 | 94 | 98 |
| **44** | | N | C–H | 700 | 83 | 97 |
| **45** | | C–H | C–H | 340 | 97 | 99 |
| **46** | | N | C–H | 340 | 85 | 98 |
| **47** | | C–H | C–H | 100 | 99 | 99 |
| **48** | | C–H | N | 340 | 90 | 95 |

[a]8-point dose response (n = 1).
[b]Percentage inhibition at 0.5 μM (n = 2).
[c]*E*:*Z* ratio: **33** (30:70) [41].

The docking of **44**, **46**, and **47** supported our initial observations with **27** (Fig. 4). The aromatic groups that are able to interact with the catalytic lysine in **44**, **46**, and **47** appeared to be preferable to a simple alkyl when attempting to drive potency on TLK2 below $IC_{50}$ = 100 nM (Fig. 4). Comparing the unsubstituted **44** to the 4-fluoro substituted **46**, we observed a potential halogen bond between the fluorine and a backbone carbonyl which may explain the 3-fold boost in potency against TLK2 (Fig. 4A-**B**) [52–54]. However, further analysis of the binding and water network of **35** highlighted untapped potential within a network of interactions in the hydrophobic pocket (Fig. 5). The carboxylic acid motif of **35** was able to align with the Thr612 which in-turn coordinated a main chain amide, which was used in the next phase of development. The water network is not disrupted by this series of interactions, but this simulation highlights that the oxindole occupies an optimal hinge binding position.

The relatively flat SAR of the ketone substitution towards TLK2 inhibition led us to expand our search to other 5-position substitution patterns including two different sulphonamides **52**–**55** and an *iso*propyl ether **57**–**59** (Table 3). Surprisingly, despite the relatively high potency of the acetyl **27**, the sulphonamides **60**–**65** were inactive on TLK2 at the top concentration. The 5-*iso*propyl ether oxindole showed some potential. The pyrrole analog **57** was 3-fold more potent for TLK2 than the 5-methyl ether version **2**. The imidazole **58** was 7-fold less potent on TLK2 than the corresponding 5-methyl ether **1**. While the 2-subsitituted imidazole **59** was the only analog to show an improvement over the methyl counterpart with a 2-fold increase in potency against TLK2.

However, these limited improvements meant we switched to the 5-amide substituted oxindoles **65**–**76** in hope of driving down potency on TLK2 (Table 4). We first screened a direct *n*-propyl analog **65** that showed similar potency to **27** with a slight reduction in off-target potency on FLT3 and TRKC. The addition of a pendent ethyl group to form a pentan-3-yl substitution **66**–**68** dropped potency by around 10-fold against TLK2 compared to the corresponding *n*-propyl analogue **65**. The cyclohexane substitution **69**–**71** was broadly similar in potency with **27** on TLK2, but with a significant improvement on the off-target profile with a reduction in potency on FLT3 and TRKC compared to **27**. The unsubstituted phenyl **72**–**74** has an asymmetric SAR for TLK2 with the pyrrole **72** 5-fold weaker than **27**. While the imidazole **73** was 4-fold more potent and both improved off-target selectivity against FLT3 and TRKC. The 2-subsitituted imidazole **74**, was 3-fold less potent than **73** and equipotent to **27**. The furan substitution analogues **75** and **76** were equipotent with **27** on TLK2 but both demonstrated improved off-target selectivity against FLT3 and TRKC.

The unsubstituted phenyl **72**, is about an order of magnitude less active than close derivatives **73** and **74**. This was likely due to the water network coordination as the 5-membered imidazoles and pyrrole ring systems are all pointing towards the solvent exposed region of the TLK2 ATP binding site. The interactions in the hydrophobic pocket region were identical for all three compounds, with the designed interaction of Thr612 and the cation-pi interaction between Lys491 and the phenyl ring observed in each of the docked examples (Fig. 6A–C). However, we observed through WaterMap that analog **72** was not able to make a stable hydrogen bond network with first solvation shell waters (Fig. 7), likely leading to weaker binding [55–59]. The lack of solvent coordination coupled with the ability of **74** to hydrophobically stack with Leu468 (Fig. 7), which was not possible with **72** and **73**, provided a rational explanation for the results we observed.

To build on the encouraging results of **73** and **74**, we decided to explore the amide derivatives with a series of modifications to the phenyl ring system **88**–**106** and focused on the imidazole and 2-subsitituted imidazole head groups (Table 5). First, we probed the 4-position of the phenyl ring by introducing a nitrile group with the imidazole head group to afford the most potent compound **88** against TLK2 observed so far ($IC_{50}$ = 12 nM); 13-fold more potent than **27**, with good selectivity over FLT3/TRKC. The 3-position nitrile with the imidazole head group **89** afforded 8-fold less potency for TLK2 than **88**, but with slightly improved selectivity over FLT3/TRKC, however the 2-subsitituted imidazole **90** only had a 4-fold drop in potency for TLK2. The 2-position nitrile was not well tolerated with 2-subsitituted imidazole **91** having an $IC_{50}$ = >1 μM on TLK2. The 4-methoxy substitution analogues **92**–**93** were 7-9-fold less potent on TLK2 than **89**. The 3-methoxy with the imidazole head group **94** was consistent with **92**–**93**, but the 2-subsitituted imidazole **95** was 28-fold less potent on TLK2 than **94**. In contrast to **91**, the 2-methoxy derivatives **96**–**97** were potent against

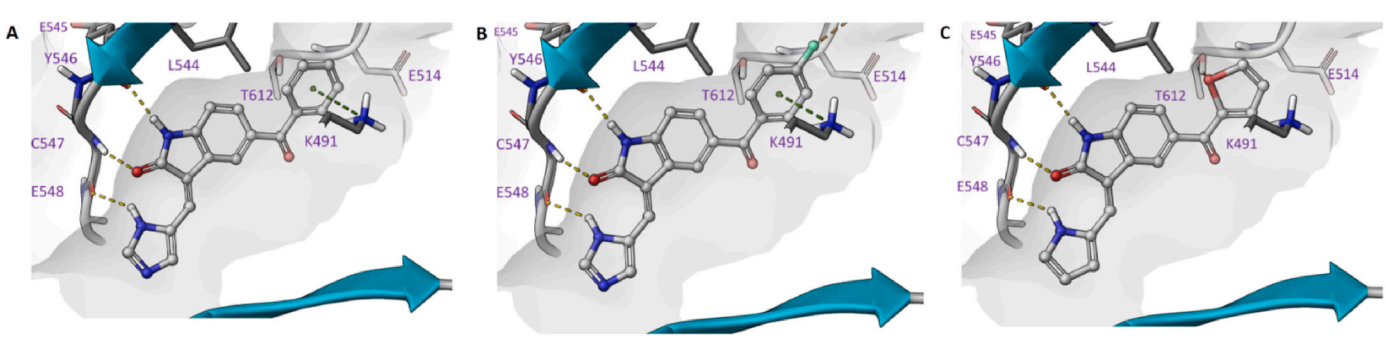


**Fig. 4.** Inhibitor docking comparing of A) **44**, B) **46** and C) **47** in TLK2 (PDB: 5O0Y) all demonstrating key hinge binding interactions and an expansion in the hydrophobic pocket.

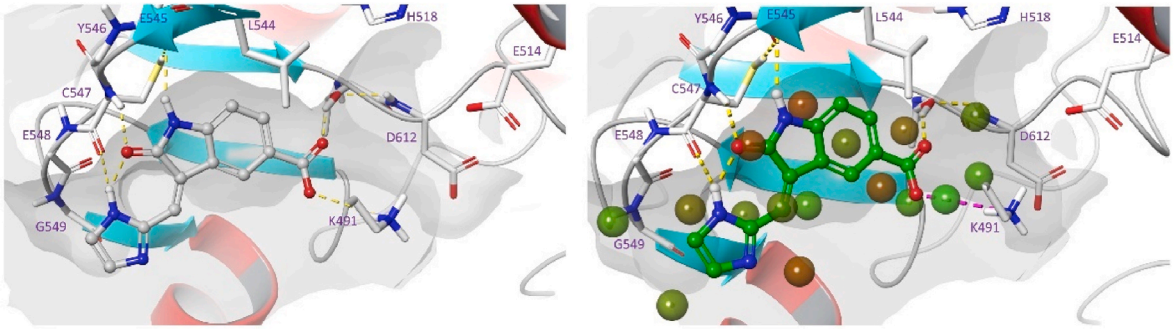


**Fig. 5.** Left: Favorable docking pose of compound **35**. Right: Visualization of hydration sites from a WaterMap simulation of docked compound **35**. WaterMap - green water is favorable and low energy, red water is unfavorable and higher energy. Hydrogen bonds denoted using yellow dotted line and salt bridges with magenta.

**Table 3**
Investigation of sulphonamide and ether derivatives.

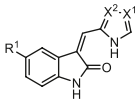

| Name | $R^1$ | $X^1$ | $X^2$ | TLK2 $IC_{50}$ (nM)[a] | FLT3 (%)[b] | TRKC (%)[b] |
|---|---|---|---|---|---|---|
| **52** | | C–H | C–H | >20000 | 69 | 98 |
| **53** | | N | C–H | >20000 | 45 | 88 |
| **54** | | C–H | C–H | >20000 | 73 | 97 |
| **55** | | N | C–H | >20000 | 38 | 73 |
| **57** | | C–H | C–H | 560 | 92 | 97 |
| **58** | | N | C–H | 1600 | 67 | 89 |
| **59** | | C–H | N | 160 | 75 | 94 |

[a]8-point dose response (n = 1).
[b]Percentage inhibition at 0.5 μM (n = 2).

**Table 4**
Initial investigation of amide derivatives.

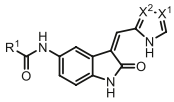

| Name | $R^1$ | $X^1$ | $X^2$ | TLK2 $IC_{50}$ (nM)[a] | FLT3 (%)[b] | TRKC (%)[b] |
|---|---|---|---|---|---|---|
| **65** | | C–H | C–H | 170 | 89 | 95 |
| **66** | | C–H | C–H | 2400 | 75 | 98 |
| **67** | | N | C–H | 2300 | 39 | 94 |
| **68** | | C–H | N | 2500 | 25 | 85 |
| **69** | | C–H | C–H | 150 | 72 | 89 |
| **70** | | N | C–H | 100 | 54 | 84 |
| **71** | | C–H | N | 130 | 42 | 68 |
| **72** | | C–H | C–H | 820 | 79 | 81 |
| **73**[c] | | N | C–H | 34 | 56 | 70 |
| **74** | | C–H | N | 110 | 52 | 67 |
| **75** | | C–H | C–H | 120 | 70 | 72 |
| **76** | | C–H | N | 130 | 58 | 67 |

[a]8-point dose response (n = 1).
[b]Percentage inhibition at 0.5 μM (n = 2).
[c]Not able to distinguish E/Z isomers for **73**: ratio 43:57 [41].

TLK2 with the imidazole head group **96** being single digit nanomolar ($IC_{50}$ = 9.1 nM), the most potent compound to date. The 2-subsitituted imidazole derivative **97** was 7-fold less potent on TLK2 but had good selectivity over FLT3/TRKC. The fluorine substitutions around the phenyl ring system **98**–**102** had relatively flat SAR for TLK2. The 2-position fluoro imidazole **102** was the most potent against TLK2 ($IC_{50}$ = 110 nM) and all analogues **98**–**102** had good selectivity against FLT3 and TRKC. The larger trifluoromethyl substitution in the 4-postion was partly tolerated with the imidazole head group **103** showing only a 3-fold drop on TLK2 with respect to **102**. However, the 2-subsitituted imidazole **104** showed limited to no activity against TLK2 at the highest concentration tested, potentially due to the inactive geometric *E*-isomer contribution. The 2-position analogues **105**–**106** were consistent with **98**–**102**, with equipotency on TLK2 and good selectivity over FLT3. Interestingly, **105**–**106** both display reduced selectivity over TRKC compared with **103**.

The docking of **73**, **88**, and **96** provided further evidence of the key interaction at the Thr612 residue with the amide bond carbonyl and the catalytic lysine (Lys491) and afforded high potency low double and single digit nanomolar compounds against TLK2 (Fig. 8). The high affinity was dependent on an aromatic ring system close to the active site but away from the hinge. We looked to exploit these traits to further optimize the analogues towards TLK2 inhibition and potentially increase kinome specificity in the process.

The recently released solved x-ray structures of TLK2 together with our molecular docking simulations were also helpful in the design of more effective TLK2 inhibitors [12]. A 3D-quantitative structure–activity relationship (3D-QSAR) model was constructed so that the main fields could be overlaid with co-crystallized ligands and verifiable favorable docking poses. We constructed a 3D-QSAR model for TLK2 using the field-based QSAR functionality of Schrödinger Maestro (Tables 6 and 7). The flexible ligand alignments were performed using a Bemis-Mucko method [60]. The 3D-QSAR model allowed recognition of the largest common scaffold and utilized a favorable docking pose of structurally representative derivatives as alignment templates. Torsion angles of larger substituents, including methoxy groups, were manually adjusted as required. The models were constructed with 80% of compounds defined randomly as training sets with the rest of the compounds as a test set (Fig. 9). The field values were calculated utilizing a grid spacing approach of 1.0 Å extended 3.0 Å beyond training

set limits. Variables with |T-value| < 2 were eliminated from final model build. The R-squared value of the TLK2 model with all four partial least squares regression (PLS) components were 0.75. The model had above average internal predictivities with a Q-square value of 0.75, which was determined by leave-one out (LOO) cross-validation. The stability of the model was 0.92 with four (PLS) components having demonstrated a robust predictivity of structure to activity output.

The shape of the oxindole series had a good alignment in the TLK2 ATP binding pocket with a strong interaction with hinge residues with semi-optimized back pocket QSAR fields (Fig. 10A–F). The pyrrole/imidazole head group assisted the hinge interacting with an additional anchor point. The oxindole scaffold was able to form two direct hydrogen bond interactions *via* the oxindole amide functionality to the

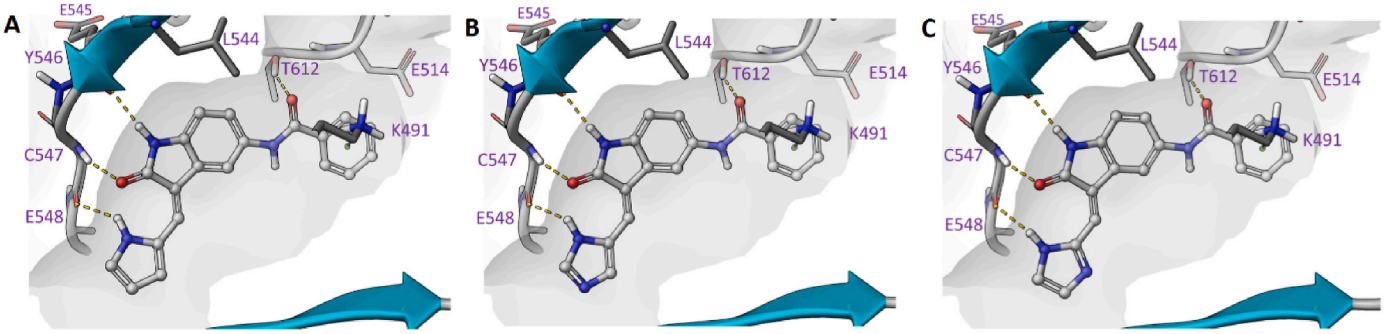


**Fig. 6.** Inhibitor docking comparing A) **72**, B) **73**, C) **74** in TLK2 (PDB: 5O0Y) demonstrating key hinge binding interactions and an expansion in the hydrophobic pocket.

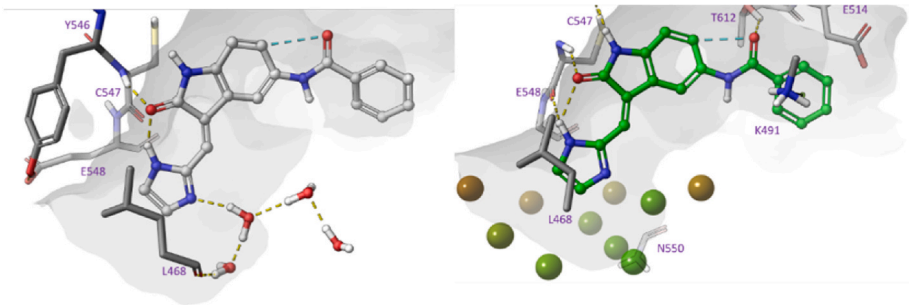


**Fig. 7.** Snapshot of trajectory waters from WaterMap simulation illustrating favorable solvent interactions of **73**. For clarity, waters and hydration sites are shown only at the mouth of the pocket. WaterMap - green water is favorable and low energy, red water is unfavorable and higher energy.

**Table 5**
Advanced investigation of amide derivatives.

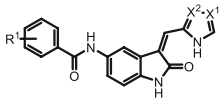

| Name | $R^1$ | $X^1$ | $X^2$ | TLK2 $IC_{50}$ (nM)[a] | FLT3 (%)[b] | TRKC (%)[b] |
|---|---|---|---|---|---|---|
| **88**[c] | 4-CN | N | C–H | 12 | 61 | 53 |
| **89**[c] | 3-CN | N | C–H | 95 | 44 | 48 |
| **90** | | C–H | N | 48 | 40 | 54 |
| **91** | 2-CN | C–H | N | 4000 | 25 | 67 |
| **92** | 4-OMe | N | C–H | 88 | 64 | 55 |
| **93** | | C–H | N | 110 | 56 | 50 |
| **94** | 3-OMe | N | C–H | 100 | 58 | 52 |
| **95**[c] | | C–H | N | 2800 | 16 | 20 |
| **96** | 2-OMe | N | C–H | 9.1 | 75 | 57 |
| **97** | | C–H | N | 67 | 60 | 66 |
| **98** | 4-F | N | C–H | 190 | 59 | 61 |
| **99** | | C–H | N | 140 | 54 | 47 |
| **100** | 3-F | N | C–H | 200 | 66 | 67 |
| **101**[c] | | C–H | N | 490 | 30 | 40 |
| **102** | 2-F | C–H | N | 110 | 74 | 76 |
| **103** | 4-$CF_3$ | N | C–H | 330 | 42 | 43 |
| **104**[c] | | C–H | N | 6100 | 12 | 17 |
| **105**[c] | 2-$CF_3$ | N | C–H | 400 | 40 | 83 |
| **106**[c] | | C–H | N | 190 | 38 | 80 |

[a]8-point dose response (n = 1).
[b]Percentage inhibition at 0.5 μM (n = 2).
[c]*E*:*Z* ratio: **88** (50:50); **89** (43:57); **95** (37:63); **101** (35:65); **104** (34:66); **105** (38:62); **106** (34:66) [41].

main chain amide of Tyr546 and Cys547. The N–H of the pyrrole/imidazole was then able to form an interaction with Glu548. The optimized amide derivatives were also able to interact *via* the carbonyl of the amide with Thr612 and had a cation-pi interaction with Lys491 forming with the pendent heterocycle. The internal conformational restriction of the oxindole scaffold between the carbonyl and amine of the pendant heterocycle was also assisting in the optimization of TLK2 binding, not only minimizing the entropic loss associated flexibility but also allowed the ligand to adopt a preferred conformation for binding [41].

We further explored the rigidity within the oxindole core with the solving of a series of small molecule crystal structures **1**, **2**, **15**, **19**, **72**, and **74** (Fig. 11, Table S3) and **4**, **9**, **11**, **13** and **16** (Fig. S1, Table S3). Structures **1**, **2**, **16** and **19** were planar due to intramolecular hydrogen bonding between the pyrrole **15** and imidazole **1** and **2** ring and the oxindole carbonyl oxygen atom (Fig. 11). The steric hindrance of the pyridine substituent of **19** and lack of hydrogen bond donor resulted in a deviation from planarity for this structure. Whilst the methylene pyrrole/imidazole rings were planar with the oxindole moiety, the benzamide substituents of **72** and **74** were not (Fig. 11). The methylene imidazole substituted structures **1** and **15** included a hydrogen bonded dimer between the amine of the imidazole and the oxindole carbonyl instead except **74** which formed flat 1D tapes along the crystallographic -*ac* plane *via* oxindole amine, imidazole imine hydrogen bonding. These tapes formed hydrogen bonds to those above and below *via* hydrogen bonds between the amide functionalities. The methylene pyrazole substituted structures showed no distinct packing motifs with **2** forming interleaved, corrugated tapes *via* oxindole amine, imidazole imine hydrogen bonding and **16** forming a hydrogen bonded, tetramer structure comprising two crystallographically independent molecules.

A series of oxindole derivatives were designed based on the 3D-QSAR model utilizing prior SAR knowledge and the small molecule crystal structure information. These were synthesized and tested using the same protocol as described above, with the addition of TLK1 screened at a 0.5 μM concentration with an ATP concentration of 10 μM, consistent with previous reports [24].

We synthesized the series of predicted analogues utilizing similar conditions as before (Scheme 1) with a few alterations in starting materials. The amide intermediates **107**–**129** were afforded by a routine

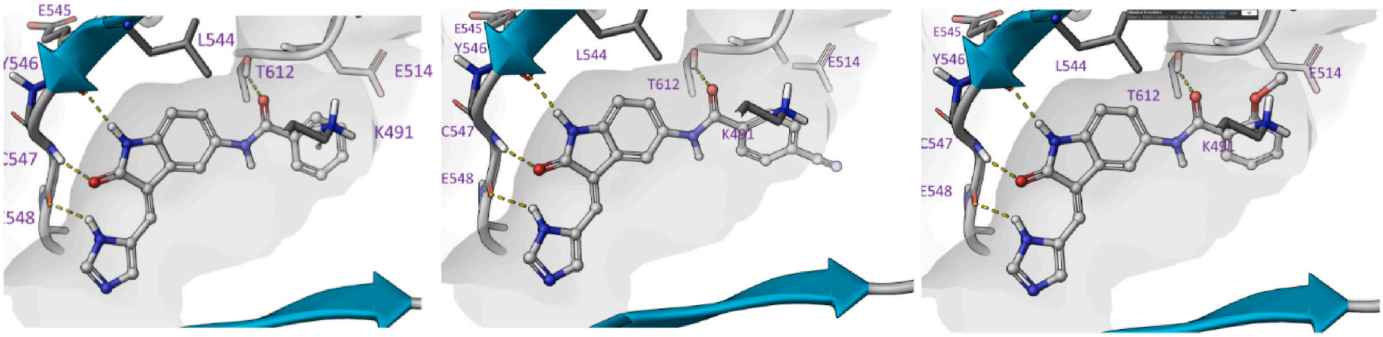


**Fig. 8.** Inhibitor docking in TLK2 (PDB: 5O0Y) comparing left: **73**, middle: **88** and right: **96**. All demonstrating key hinge binding interactions and a refined expansion in the hydrophobic pocket.

**Table 6**
Validation of 3D-QSAR models for TLK2.

| # Factors | SD | $R^2$ | R^2 CV | R^2 Scramble | Stability | F | P | RMSE | Q^2 | Pearsson-r |
|---|---|---|---|---|---|---|---|---|---|---|
| **1** | 0.74 | 0.43 | 0.38 | 0.055 | 0.997 | 56.1 | 1.01E-10 | 0.85 | 0.15 | 0.54 |
| **2** | 0.50 | 0.74 | 0.63 | 0.18 | 0.96 | 105.0 | 2.48E-27 | 0.57 | 0.61 | 0.83 |
| **3** | 0.22 | 0.80 | 0.68 | 0.27 | 0.94 | 98.5 | 1.43E-29 | 0.54 | 0.65 | 0.82 |
| **4** | 0.28 | 0.85 | 0.70 | 0.36 | 0.92 | 104.2 | 3.60E-30 | 0.52 | 0.68 | 0.83 |
| **5** | 0.33 | 0.89 | 0.71 | 0.43 | 0.92 | 116.9 | 7.54E-34 | 0.46 | 0.75 | 0.86 |
| **6** | 0.30 | 0.91 | 0.71 | 0.48 | 0.88 | 122.9 | 3.73E-38 | 0.47 | 0.74 | 0.86 |

**Table 7**
Regression Statistics for TLK2 QSAR model.

| #Factors | gauss_s | gauss_e | gauss_h | gauss_a | gauss_d |
|---|---|---|---|---|---|
| **1** | 0.53 | 0.062 | 0.13 | 0.19 | 0.09 |
| **2** | 0.27 | 0.070 | 0.32 | 0.26 | 0.09 |
| **3** | 0.28 | 0.069 | 0.31 | 0.24 | 0.10 |
| **4** | 0.29 | 0.067 | 0.28 | 0.25 | 0.12 |
| **5** | 0.30 | 0.068 | 0.25 | 0.25 | 0.14 |
| **6** | 0.31 | 0.068 | 0.23 | 0.27 | 0.13 |

HATU coupling to the respective 5-aminooxindole in good yields (57–84%) [51]. The amide was then treated with the previous Knoevenagel conditions with the respective aldehyde to afford the condensation products **117**–**129** in a range of yields (21–71%) (Scheme 2).

The QSAR modelling suggested that the phenyl ring could be reduced to a 5-member ring and coupled with earlier knowledge of the furan **75** and **76**, so we synthesized the thiophenes **117**–**121** (Table 8). The activities observed were broadly in line with the QSAR model. The unsubstituted thiophene with the imidazole head group **117** was potent on TLK2 ($IC_{50}$ = 23 nM) but lacked selectivity over FLT3/TRKC. The 2-subtitued imidazole **118** was equipotent but slightly more selective

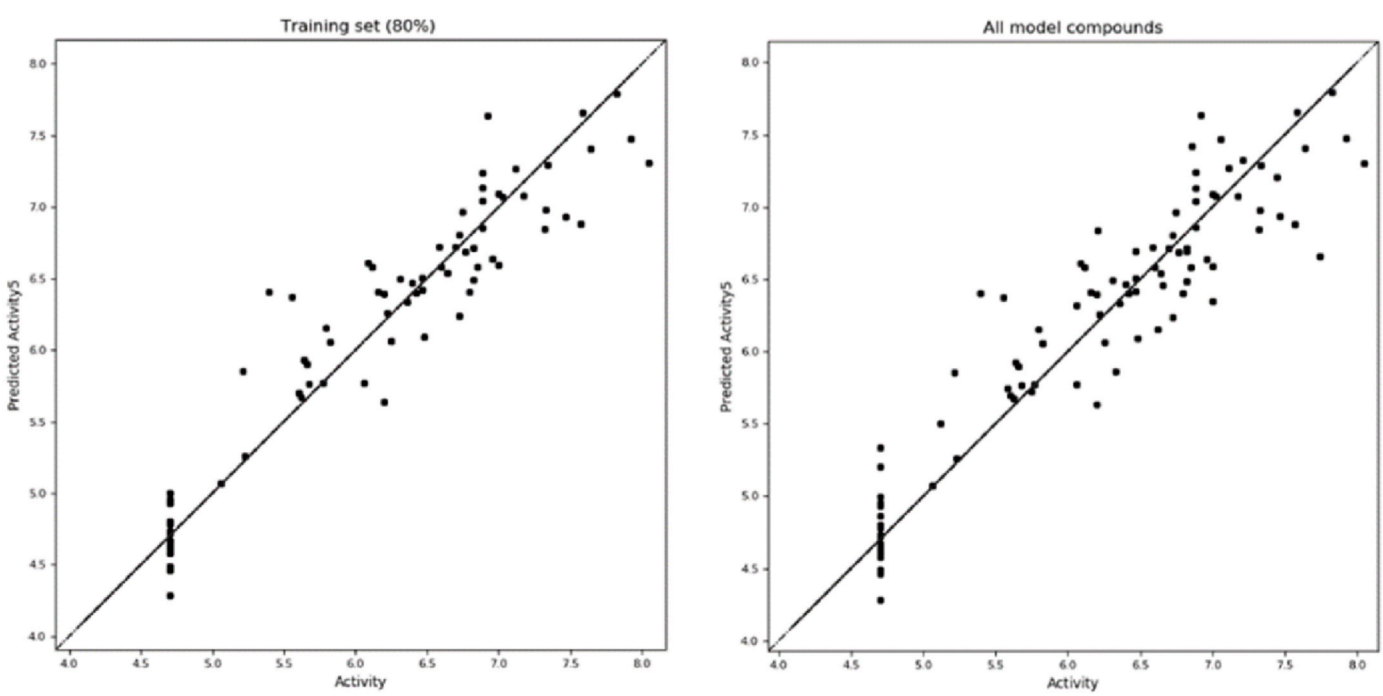


**Fig. 9.** Scatter plots of field-based 3D-QSAR models showing predicted versus measured binding affinities (nM) of active compounds printed at logarithmic scale with the TLK2 training set (left) and TLK2 all compounds (right).

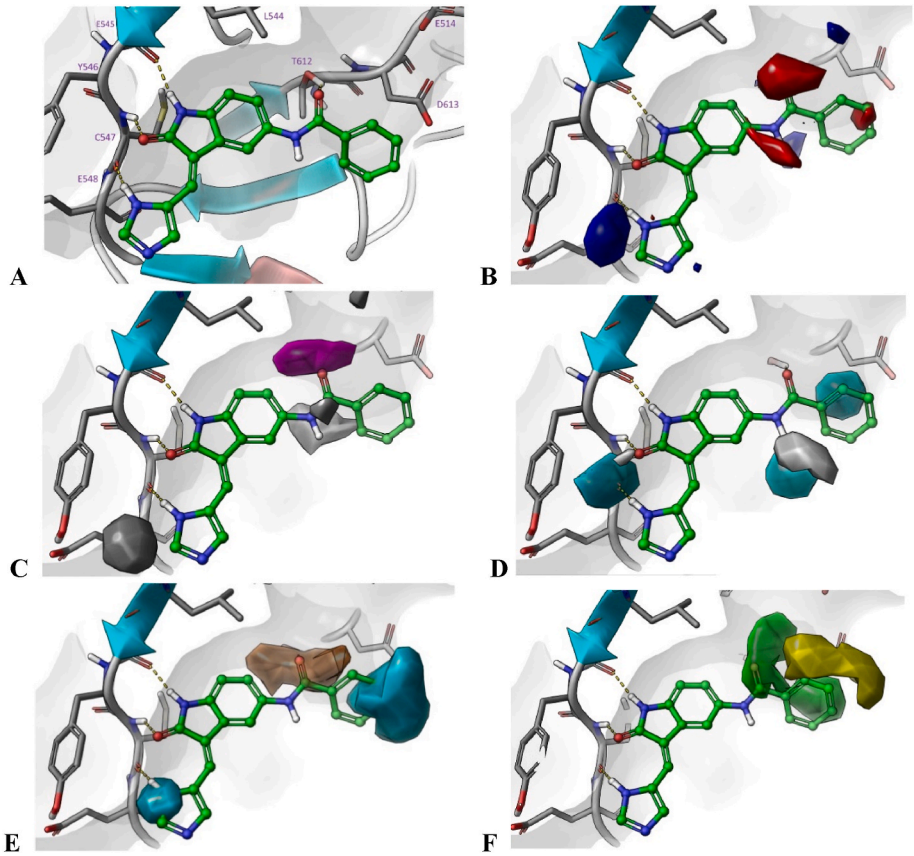


**Fig. 10.** QSAR modelling on **73** template: A) Standard docking of **73** in TLK2 (PDB:5O0Y); B) Electrostatics (blue = positive and red = negative); C) hydrogen bonding acceptor fields (magenta = positive and grey = negative); D) hydrogen bonding donor fields (cyan = positive and grey = negative); E) hydrophobic fields (orange = positive and cyan = negative); F) Steric fields (green = positive and yellow = negative).

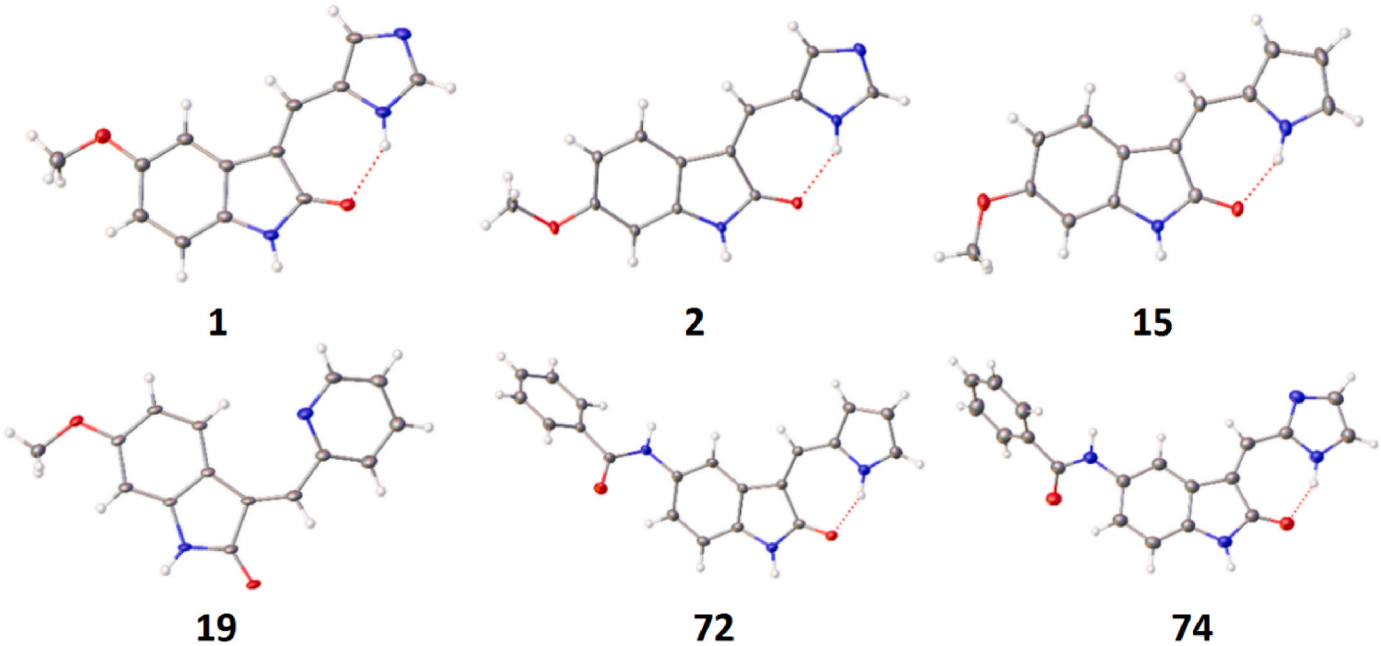


**Fig. 11.** Small molecule crystal structures of **1**, **2**, **15**, **19**, **72** and **74**.

against FLT3/TRKC. The introduction of a 4-methoxy group onto the thiophene **119** reduced potency for TLK2 by 3-fold compared to **117**. However, the 4-ethoxy group **120** was equipotent with **117** with equivalent selectivity over FLT3/TRKC. Interestingly **120** was the only compound to show any significant inhibition against TLK1 (46% inhibition at 1 μM). The final compound in this series, the 4-fluoro **121** was 8-fold less potent against TLK2 compared to **117**.

We then optimized these initial compounds to afford a series of more

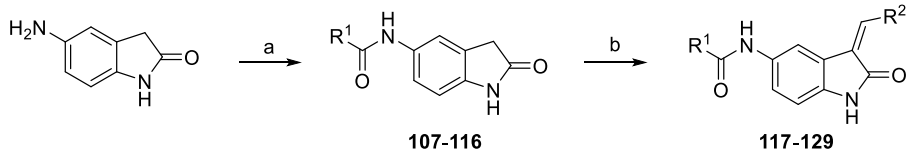


**Scheme 2.** Synthetic route to prepare predicted oxindole analogues - *reagents and conditions* a) $R^1COCl$, $EtN(CH(CH_3)_2)_2$, THF, rt, 12 h; b) $R^2CHO$, piperidine, EtOH, reflux, 4–24 h.

**Table 8**
Results of initial set of QSAR predicted compounds.

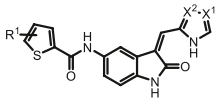

| Name | $R^1$ | $X^1$ | $X^2$ | TLK2 $IC_{50}$ (nM)[a] | FLT3 (%)[b] | TRKC (%)[b] | TLK1 (%)[b] |
|---|---|---|---|---|---|---|---|
| **117** | H | N | C–H | 23 | 88 | 84 | 11 |
| **118**[c] | H | C–H | N | 36 | 80 | 74 | 20 |
| **119** | 4-OMe | N | C–H | 77 | 80 | 78 | 13 |
| **120**[c] | 4-OEt | N | C–H | 27 | 91 | 92 | 46 |
| **121** | 4-F | N | C–H | 180 | 77 | 88 | 0 |

[a]8-point dose response (n = 1).
[b]Percentage inhibition at 0.5 μM (n = 2).
[c]*E*:*Z* ratio: **112** (34:66); **114** (28:72) [41].

advanced amide derivatives **122**–**127** (Table 9). The fused thiophene, **122** was 2-fold less potent compared with **117**, with no difference in selectivity. This larger 5,5-system was tolerated, so an expansion of the phenyl substitution patterns were synthesized to include 3-trifluoromethyl, 5-fluoro **123** and the fused 2,3-catacol **124.** Unfortunately, both these analogues lost significant activities against TLK2 compared with **117**. We also looked at smaller 5-member rings, thiazole **125**, oxazole **126**, and *iso*thiazole **127** all these analogues afforded good potency against TLK2, with the oxazole approaching towards single digit nanomolar against TLK2.

**Table 9**
Optimization of compounds based on QSAR.

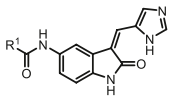

| Name | $R^1$ | TLK2 $IC_{50}$ (nM)[a] | FLT3 (%)[b] | TRKC (%)[b] | TLK1 (%)[b] |
|---|---|---|---|---|---|
| **122** | | 47 | 85 | 76 | 12 |
| **123** | | 630 | 45 | 70 | 0.5 |
| **124** | | 260 | 55 | 75 | 14 |
| **125** | | 120 | 82 | 89 | 2.8 |
| **126** | | 15 | 92 | 88 | 11 |
| **127**[c] | | 46 | 86 | 96 | 10 |

[c]E:Z ratio: 127 (30:70) [41].
[a] 8-point dose response (n = 1).
[b] Percentage inhibition at 0.5 μM (n = 2).

In a further effort to validate the model, two additional compounds **128** and **129** were synthesized (Table 10). These were based on the core structure of **73** and tested the predictive power of the model. The addition of the 2-methyl **128** to the imidazole head group afforded an 8-fold increase in potency against TLK2 over **73**, with no loss of selectivity against FLT3 and TRKC. The model was accurate for the pyrazole **129**, as the introduction of the extra nitrogen led to an over 15-fold drop in TLK2 inhibition compared with **73**, consistent with previous SAR in this series.

Aligning the results of the prediction with the experimental results, we found a good concordance (Table 11).

In addition to assessing the selectivity profile on the two near off-targets FLT3 and TRKC, we also investigated the wider kinome selectivity profile of nine of the most promising analogues using KinomeSCAN® at 1 μM across over 400 kinases (Table 12, Fig. 12) [21–23]. The original starting point **1** was moderately selective across the kinome hitting 15 kinases over 90%. The 5-acetyl analog **27**, was the most promiscuous analog with 62 kinases over 90%, possibly due to the small flexible ketone orientated favorably towards the common catalytic lysine motif (Fig. 3D). Interestingly, **1**, **27**, and **44** had similar hit kinases above 90%. Common kinases included MST2, CDKL2, ERK8, TRKA, JAK3(JH1domain-catalytic), and TNIK. The amide substitution in the 5-position, not only increased selectivity across the kinome but also changed the kinases inhibited. Compounds **72**–**74** consistently hit MYLK4, BIKE, GRK4, and SRPK3 above 90%, another four, PRP4, AAK1, PIP5K1A, and SRPK2 were revealed as consistent hits if the threshold was decreased to 80% inhibition, in addition to other kinases (see supporting information). The narrowest spectrum inhibitor across the kinome tested in the KinomeSCAN® assay was **97**, which hit only 7 kinases above 90% including BIKE, DRAK2, JAK1 (JH2domain-pseudokinase), MAST1, PIP5K1A, GRK4, and TYK2 (JH2domain-pseudokinase). The selectivity of the designed thiophene amide **111** was moderate with 15 kinases inhibited. The addition of a methyl **128** onto the 5-position of the imidazole head group of **73** changed the kinome profile subtly at 90% inhibition, reducing inhibition on TYK2(JH2domain-pseudokinase) and AAK1, but increasing inhibition on DRAK2, PIP5K1A, RIOK1, MAST1, and LKB1.

Finally, we screened the most promising compounds **97**, **117**, **128**,

**Table 10**
Optimization of compounds based on QSAR.

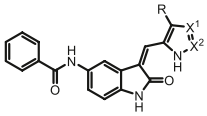

| Name | R | $X^1$ | $X^2$ | TLK2 $IC_{50}$ (nM) | FLT3 (%) | TRKC (%) | TLK1 (%) |
|---|---|---|---|---|---|---|---|
| **128** | Me | N | C–H | 18 | 76 | 65 | 16 |
| **129** | H | C–H | N | 2600 | 13 | 14 | 7.5 |

[a]8-point dose response (n = 1).
[b]Percentage inhibition at 0.5 μM (n = 2).

**Table 11**
Compound results ($IC_{50}$) based on QSAR prediction.

| Compound | TLK2 Inhibition Activity (nM) | | | |
|---|---|---|---|---|
| | Predicted | Found | Log Predicted | log Actual |
| **117** | 51 | 23 | 7.29 | 7.64 |
| **118** | 56 | 36 | 7.25 | 7.44 |
| **119** | 50 | 77 | 7.30 | 7.11 |
| **120** | 370 | 27 | 6.44 | 7.57 |
| **121** | 68 | 180 | 7.17 | 6.74 |
| **122** | 180 | 47 | 6.75 | 7.33 |
| **123** | 1800 | 630 | 5.76 | 6.20 |
| **124** | 40 | 260 | 7.40 | 6.59 |
| **125** | 8 | 120 | 8.08 | 6.92 |
| **126** | 8 | 15 | 8.12 | 7.82 |
| **127** | 37 | 46 | 7.44 | 7.34 |
| **128** | 180 | 18 | 6.74 | 7.74 |
| **129** | 960 | 2600 | 6.02 | 5.59 |

**Table 12**
Kinome selectivity profiling.

| Kinome profiling summary | | | | TLK2[b] |
|---|---|---|---|---|
| Name | Code | >90[a] | S(10) | $IC_{50}$ (nM) |
| **1** | **UNC-CA2-016** | 15 | 0.037 | 240 |
| **27** | **UNC-CA2-005** | 62 | 0.154 | 150 |
| **44** | **UNC-CA2-044** | 15 | 0.037 | 700 |
| **72** | **UNC-CA2-067** | 10 | 0.025 | 820 |
| **73** | **UNC-CA2-068** | 9 | 0.022 | 34 |
| **74** | **UNC-CA2-069** | 11 | 0.027 | 150 |
| **97** | **UNC-CA2-113** | 7 | 0.017 | 67 |
| **111** | **UNC-CA2-141** | 15 | 0.037 | 23 |
| **128** | **UNC-CA2-103** | 11 | 0.027 | 18 |

[a] Number of kinases inhibited above 90%.
[b] TLK2 enzyme assay result.

the negative control compound **129**, and the starting point compound **1** in an orthogonal assay measuring the conversion of ATP to ADP [61–63]. The results were consistent with both the weak and potent TLK2 binding of the five compounds in the enzyme assay (Fig. 13 and Table 13). The potent TLK2 activities of **97**, **117** and **128** in addition to their narrow spectrum kinome selectivity makes them attractive starting points for further optimization.

## 3. Discussion

TLK2 represents an attractive target for therapeutic development in a variety of cancer types and in "shock-and-kill" approaches for antiviral therapies. The published TLK2 inhibitors to date only offer compounds with moderate potency and poor or unknown kinome selectivity [19,64,65]. In the present study, we demonstrate optimization of a chemotype for increased potency and selectivity for the clinically important TLK2 kinase. Since we achieved selectivity over the closest human paralog TLK1, this work also provides important tool compounds for better characterization of the specific cellular functions of TLK2 [66,67].

The original target for the oxindole scaffold was receptor tyrosine kinases namely VEGFR and PDGFR [68]. However, the scaffold demonstrated varying affinities for a large portion of the kinome [21–24]. There have been a number of priority cancer targets including TRKA [69], CDK2 [70–72], PDK1 [73], and SRC [74], among others [75], inhibited by the oxindole scaffold. While the primary kinase targets were well defined, the oxindole chemotype has historically been considered as a broad-spectrum kinase inhibitor chemotype. However, a LRRK2 program at Novartis by Troxler et al., [76] suggested that the replacement of fluorine in the 5-position with a methoxy significantly improved kinome wide selectivity with the oxindole scaffold. This was supported by the narrow spectrum of the initial 5-methoxy substituted hit compound SU9516, when compared to the matched pair oxindoles GW5060033X and Sunitinib [21–24].

The two oxindole matched pairs in the literature (Fig. 1) demonstrated a tractable affinity to TLK2 [21–24]. We found several key structural features that could be tuned within the scaffold including: 1) The electronics of the oxindole head group and the internal hydrogen bond; 2) the electronics and sterics of the amide substitution pattern; and 3) formation of the key Lys491 interaction with the amide linker.

The use of conformational restriction has been an effective tool in drug discovery [77]. This methodology has been utilized to orient ATP competitive inhibitors in the preferred conformation. This can be used to not only increase potency, but also to enhance selectivity over other kinases/targets. There are several examples within kinase inhibitor design including cyclin G-associated kinase (GAK) [57,78], spleen tyrosine kinase (SYK) [79] and cardiac troponin I-interacting kinase (TNNI3K) [80,81] where addition or removal of a single nitrogen to alter the inhibitor conformation resulted in an increase by 60-160-fold on target. Another method employed in our EGFR inhibitor program involved fixing the pendent substituents with hydrogen bonds between an alcohol and a carbonyl [58]. There are also a number of other non-kinase examples including the development of adenosine A3 receptor antagonists [82], human histamine H4 receptor (hH4R) inhibitor agonists [83], and design of selective CB2 cannabinoid receptor agonists [84].

The adding or removing of a nitrogen has been proven to have a significant effect on activities across different systems not only by altered conformation, but also in reduced de-solvation energy potential and as a hydrogen bond donor/acceptor [85]. The oxindole scaffold has multiple potential contact points within the TLK2 ATP binding site. However, we found that that the most crucial nitrogen was on the pendant head group contained within the pyrrole/imidazole and which formed an interaction at the hinge with Glu548 and an addtional internal hydrogen bond with the carbonyl of the oxindole. This internal hydrogen bond pre-organizes the orientation of the molecule as an optimal ATP memetic (Fig. 14). The solvent exposed shell is a key modulator of activity, with differing profiles depending on the nitrogen location on the 'head group' 5-member ring. We can rationally explain these differences by modelling the first water network solvent shell [59,86,87]. Comparing Fig. 14D to 14E-F using WaterMap, both imidazoles are able to coordinate using the second nitrogen, while the pyrrole is not able to which leads to a 10–20 fold drop in potency on TLK2.

In addition to the conformation and head group nitrogen and oxindole hinge interactions our modelling highlights that to achieve a high affinity compound, a favorable fit into the hydrophobic back pocket is required. The key hydrogen bond interaction to the catalytic lysine (Lys491) affords a considerable boost in potency. The challenge is to maintain selectivity across the kinome, which was achieved in part by a series of cationic-pi interactions also donated by Lys491, and favorable fine-tuned π–π stacking interactions. This was demonstrated with a highlighted section of the 5-position substitution and the possibility to form a cationic- π interaction with Lys491. The small molecule crystal structures (Fig. 4 & Table S1) support the theoretical observations with the TLK2 ATP binding site.

## 4. Conclusions

Oxindole based kinase inhibitors are often considered to be promiscuous inhibitors across the kinome, this mainly derived from several well-known broad-spectrum inhibitors including sunitinib and GW506033X [88]. Here we demonstrate fine-tuning and optimization to derive a narrow kinome spectrum oxindole based TLK2 inhibitor utilizing cutting edge modelling to prospectively design potent and selective inhibitors.

The result was an inhibitor **128** (UNC-CA2-103) with 13-fold more potency against TLK2 ($IC_{50}$ = 18 nM) over the starting point **1** ($IC_{50}$ = 240 nM). This was achieved with an improvement overall kinome selectivity from **1** (S(10) = 0.037) to **128** (S(10) = 0.027), with

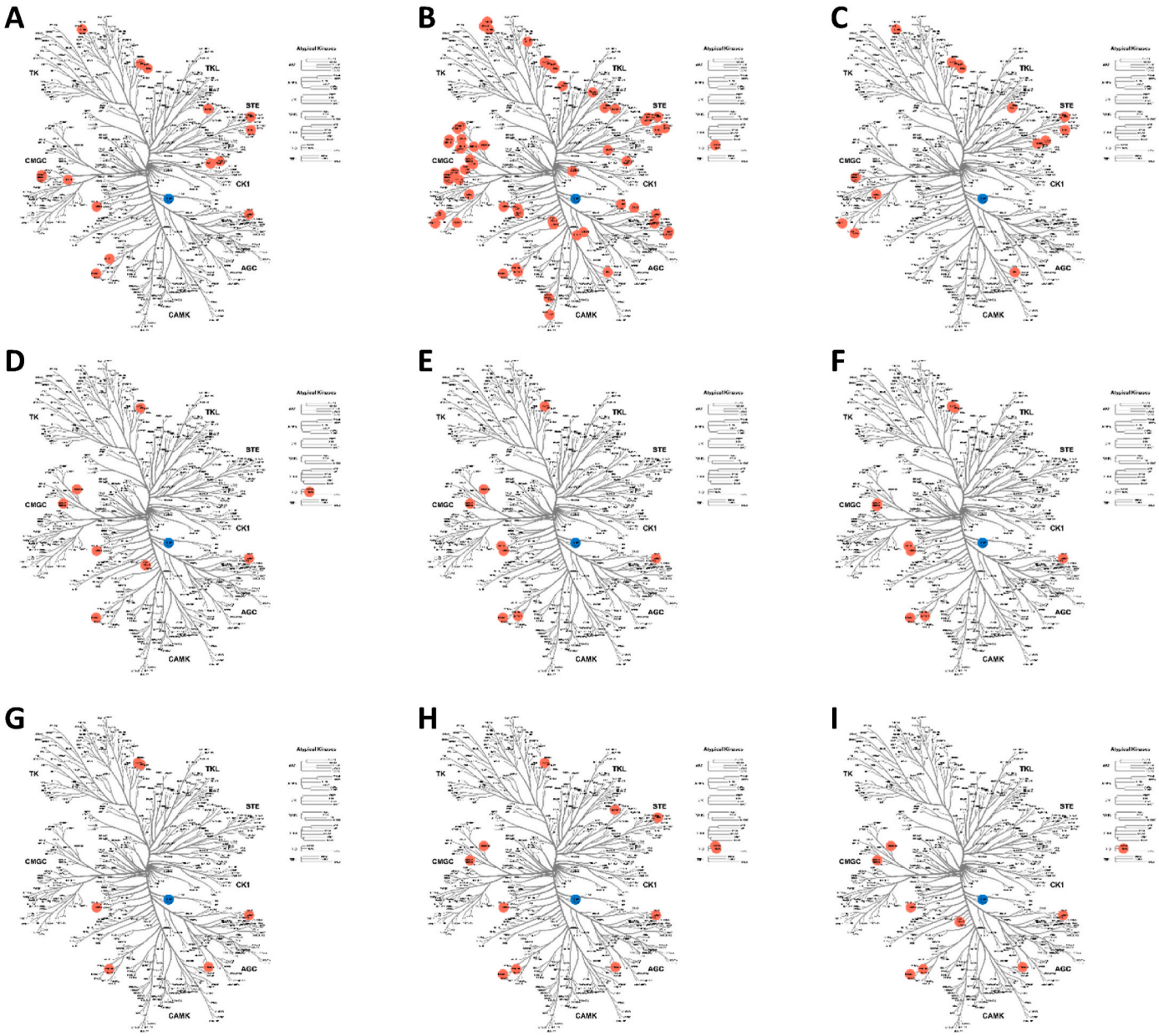


**Fig. 12.** Kinome tree image of KinomeScan data for A) **1**, B) **27**, C) **44**, D) **72**, E) **73**, F) **74**, G) **97**, H) **111**, I) **128**.

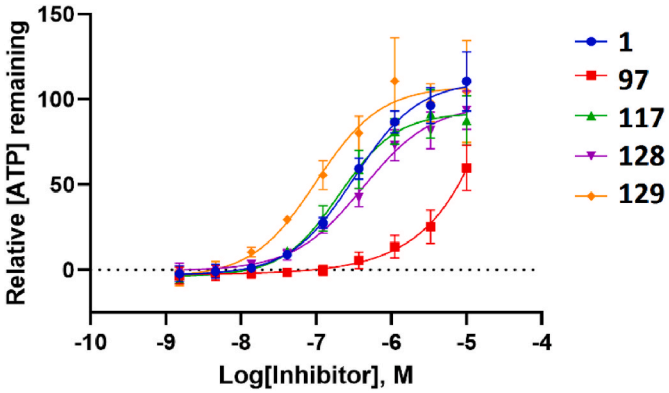


**Fig. 13.** TLK2 Kinase-Glo curves (n = 3) for **1**, **97**, **117**, **128** and **129**.

**Table 13**
TLK2 functional inhibition kinase-glo results.

| Name | TLK2 $IC_{50}$ (nM) | |
|---|---|---|
| | Enzyme | Kinase Glo |
| **1** | 240 | 280 |
| **97** | 67 | 450 |
| **117** | 15 | 97 |
| **128** | 18 | 250 |
| **129** | 2700 | 7800 |

concurrent selectivity over the sub-family member TLK1 (16% inhibition at 0.5 μM). In addition, we also identified several high potency TLK2 inhibitors including **96** ($IC_{50}$ = 9.1 nM) and **126** ($IC_{50}$ = 15 nM). However, both inhibitors **96** and **126** showed signs of increased kinome promiscuity FLT3 I = 75% and TRKC I = 57% at 0.5 μM and FLT3 I = 92% and TRKC I = 88% at 0.5 μM respectively. While two slightly weaker TLK2 inhibitors **73** ($IC_{50}$ = 34 nM) and **97** ($IC_{50}$ = 67 nM) both showed increased kinome wide selectivity S(10) = 0.022 and S

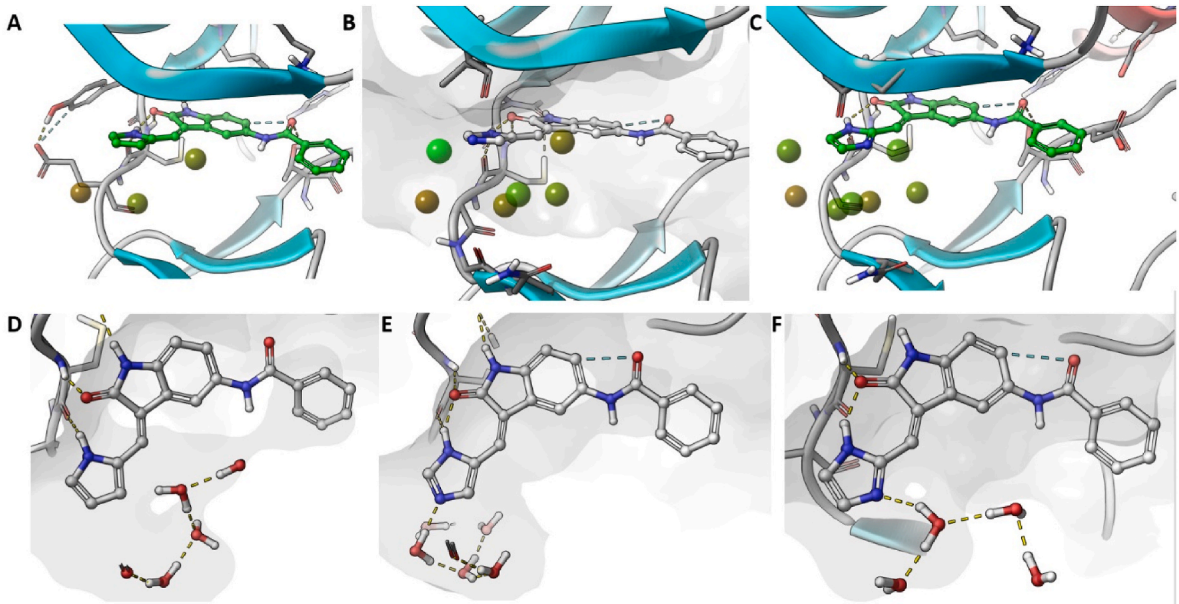


**Fig. 14.** Representative oxindoles with three key head groups showing first shell solvent front interactions using WaterMap A) **72**, B) **73**, C) **74**, D) **72**, E), **73** and F) **74** in TLK2 (PDB: 5O0Y). Waters are presented with two different representations balls A-C (green - low energy and red – higher energy) and full formulae D-F. WaterMap - green water is favorable and low energy, red water is unfavorable and higher energy.

(10) = 0.017, respectively.

The 3D-QSAR and water network modelling utilized in this work, has provided new insights into the development of selective chemical probes for TLK2 and beyond. The comprehensive data sets described here afford a more complete level of knowledge of the oxindole scaffold previously unavailable to the medicinal chemist's toolbox.

## 5. Experimental

### 5.1. Biology

The enzyme assays were performed as previously described for TLK2, TRKC, FLT3 and TLK1 at Reaction Biology Corporation (RBC) [24].

KinomeScan® assays were performed as previously described at EuroFins DiscoverX [21–23].

TLK2 ADP-Glo kinase activity assays: Recombinant human TLK2 (388-end) was purchased from SignalChem. Kinase reaction buffer consisted of 25 mM MOPS pH 7.2, 12.5 mM β-glycerol-phosphate, 25 mM $MgCL_2$, 5 mM ethylene glycol-bis(β-aminoethyl ether)-*N*,*N*,*N*′,*N*′-tetraacetic acid, 2 mM ethylenediaminetetraacetic acid, 0.25 mM dithiothreitol, 1 μM ATP, and 1 μM myelin basic protein (SignalChem). The indicated inhibitors were added to keep the final DMSO concentration in the kinase reaction constant at 1% of the total reaction volume. Kinase reactions were started by addition of 8 nM recombinant human TLK2 and incubation at 30 °C for 2 h. TLK2 kinase activity was determined using the ADP-Glo kinase assay (Promega) following manufacturer's protocol. Luminescence was measured using the PHERAstar microplate reader (BMG Labtech).

### 5.2. Molecular modelling

Ligand preparation: Structures of small molecules were parametrized and minimized using the LigPrep module of Schrodinger 2019-4 suite employing OPLS3e force field.

Protein preparation: The TLK2 kinase a crystal structure (PDB:5O0Y) co-crystallized with substrate analog (phosphothiophosphoric acid-adenylate ester) was downloaded from RCSB-databanks. The structure was hydrogen-bond optimized and minimized using standard protein preparation procedure of Schrödinger suite.

TLK2 Molecular docking: The ligand docking was performed using SP settings of Schrodinger docking protocol with softened vdw potential (scaling 0.6). The initial docking of resulted quite poor convergence, thus oxindole-indole scaffold can bind in several conformations. To ensure correct docking mode of the oxindole (2-indolone) scaffold to the kinase folds, structural inspection was done using LPDB module of the Schrödinger package with the oxindole as a query. This was done with four x-ray structures from the LPDB search (PDBs: 2X2K, 2X2M, 4QMO and 1PF8), which were then visual inspected. To further improve convergence of docking poses a hydrogen bond constraint to mainchain NH of hinge residue was required, as experimentally observed in the case of other oxindole containing scaffolds (NH of C507 in the case of TLK2). The grid box was centered using coordinate center of the core structure of corresponding x-ray ligand as template. Graphical illustrations were generated using, Maestro software of Schrödinger. Flexible ligand alignments were performed using a Bemis-Mucko method, enabling recognition of the largest common scaffolds using a favorable docking pose of structurally representative derivative as alignment template (**73**). Torsion angles of larger substituents, such as methoxy groups, were manually adjusted to fit template structures when needed.

Hydration site analysis: Hydration site analysis calculated with WaterMap (Schrödinger Release 2018-4: WaterMap, Schrödinger, LLC, New York, NY, 2018.). The structure of TLK2 (PDB:5O0Y) was prepared with Protein Preparation Wizard (as above). Water molecules were analyzed within 6 Å from the docked ligand and the 2 ns simulation was conducted with OPLS3e force field [89].

TLK2 3D-QSAR model: The model for the TLK2 kinase was constructed using the field based QSAR functionality of Schrödinger Maestro 2019-4. The models were constructed by defining 80% of compounds randomly as training sets and rest of the compounds were considered as test set. Grid spacing of 1.0 Å extended 3.0 beyond training set limits was used to the calculate field values. Subsequently, predicted versus measured affinities were plotted to identify outliers. The statistical metrics of models: R-square values with four PLS components were 0.79. The model shows acceptable internal predictivity (Q-square value 0.70), determined by leave-one-out (LOO) cross-validation. Stability value above 0.9 with four partial least squares regression (PLS) components let us to suggest that the quality and predictivity of the model inside the studied applicability domain was robust.

### 5.3. Crystallography

Each compound had a suitable crystal selected and mounted on a MITIGEN holder (MiTeGen, Ithaca, NY, USA) in perfluoroether oil on a Rigaku FRE+ diffractometer equipped with a Mo target, VHF Varimax confocal mirrors, an AFC12 goniometer and HyPix 6000 detector (**1**, **2**, **15**, **19**, **72** and **74**) or a Rigaku 007HF diffractometer equipped with a Cu target, HF Varimax confocal mirrors, an AFC11 goniometer and HyPix 6000 detector (**15**, **74**). The crystal was kept at a steady $T = 100(2)$ K during data collection. CrysAlisPro [90] was used to record images, process all data and apply empirical absorption corrections. Unit cell parameters were refined against all data. The structures were solved by the ShelXT [91] structure solution program using the using dual methods solution method and using Olex2 [92] as the graphical interface. The models were refined with version 2018/3 of ShelXL [91], using full matrix least squares minimization on $F^2$ minimization. All non-hydrogen atoms were refined anisotropically. Hydrogen atom positions were calculated geometrically and refined using the riding model, except for those bonded to N-atoms which were located in the difference map and refined with a riding model. Structure **72** crystallized as an ethanol solvate. The data for **72** were processed as a 2-component non-merohedral twin (rotation (UB1, UB2) = 179.9982° around [0.00 0.71 0.71] (reciprocal) or [−0.39 0.85 0.35] (direct) lattice vectors). CCDC deposit numbers: 2309069–2309077, see supporting information.

### 5.4. Chemistry

#### 5.4.1. General chemistry

All reactions were performed using flame-dried round-bottomed flasks or reaction vessels. Where appropriate, reactions were carried out under an inert atmosphere of nitrogen with dry solvents, unless otherwise stated. Yields refer to chromatographically and spectroscopically pure isolated yields. Reagents were purchased at the highest commercial quality and used without further purification. Reactions were monitored by thin-layer chromatography carried out on 0.25-mm. Merck silica gel plates ($60_{F\text{-}254}$) using ultraviolet light as a visualizing agent. NMR spectra were recorded on a Varian Inova 400 (Varian, Palo Alto, CA, USA), Inova 500 spectrometer (Varian, Palo Alto, CA, USA) or Bruker 600 spectrometer (Bruker, Billerica, MA, USA) and calibrated using residual undeuterated solvent as an internal reference ($CDCl_3$: $^1$H NMR = 7.26, $^{13}$C NMR = 77.16). The following abbreviations or combinations thereof were used to explain the multiplicities observed: s = singlet, d = doublet, t = triplet, q = quartet, m = multiplet, br = broad. Liquid chromatography (LC) and high-resolution mass spectra (HRMS) were recorded on a ThermoFisher hybrid LTQ FT (ICR 7T) (ThermoFisher, Waltham, MA USA). Compound spectra of **1**–**129** and mass spectrometry are included in the Supplementary Materials. All compounds were >98% pure by $^1$H/$^{13}$C NMR and LC-MS.

Mass spectrometry method: Samples were analysed with a ThermoFisher Q Exactive HF-X (ThermoFisher, Bremen, Germany) mass spectrometer coupled with a Waters Acquity H-class liquid chromatograph system. Samples were introduced *via* a heated electrospray source (HESI) at a flow rate of 0.6 mL/min. Electrospray source conditions were set as: spray voltage 3.0 kV, sheath gas (nitrogen) 60 arb, auxiliary gas (nitrogen) 20 arb, sweep gas (nitrogen) 0 arb, nebulizer temperature 375 degrees C, capillary temperature 380 degrees C, RF funnel 45 V. The mass range was set to 150–2000 *m/z*. All measurements were recorded at a resolution setting of 120000.

Separations were conducted on a Waters Acquity UPLC BEH C18 column (2.1 × 50 mM, 1.7 μM particle size). LC conditions were set at 100% water with 0.1% formic acid (A) ramped linearly over 9.8 min to 95% acetonitrile with 0.1% formic acid (B) and held until 10.2 min. At 10.21 min the gradient was switched back to 100%A and allowed to re-equilibrate until 11.25 min. Injection volume for all samples was 3 μL.

Xcalibur (ThermoFisher, Breman, Germany) was used to analyse the data. Solutions were analysed at 0.1 mg/mL or less based on responsiveness to the ESI mechanism. Molecular formula assignments were determined with Molecular Formula Calculator (v 1.2.3). All observed species were singly charged, as verified by unit *m/z* separation between mass spectral peaks corresponding to the $^{12}$C and $^{13}C^{12}C_{c\text{-}1}$ isotope for each elemental composition.

**3-[(3,5-Dimethyl-1H-pyrrol-2-yl)methylene]-1,3-dihydro-2H-indol-2-one** (SU5416/Semaxanib) (**10**) was consistent with commercial product and previous report [93,94]. **2-oxoindoline-5-sulfonyl chloride** (**49**) was prepared consistent with previous report [47]. **5-*iso*-propoxyindolin-2-one** (**56**) was prepared consistent with previous report [76].

### 5.5. General procedures

#### 5.5.1. Procedure A. Knoevenagel condensation

The oxindole (1.0 equiv), aldehyde (1.1 equiv), piperidine (2.4 equiv) were suspended in ethanol at reflux overnight. The solvent was removed and the resulting solid re-suspended DCM/EtOAc 1/1 and flushed through a plug of silica (DCM/EtOAc 1/1). The product was then purified by silica gel flash column chromatography (hexane:EtOAc) to afford the title compound.

#### 5.5.2. Procedure B. Friedel-crafts acylation

To a suspension of $AlCl_3$ (6.0 equiv) in $CH_2Cl_2$ was added the appropriate acyl chloride (3.0 equiv) and the slurry was stirred at room temperature for 30 min, followed by the addition of oxindole (1.0 equiv) in $CH_2Cl_2$. The resulting mixture was stirred at room temperature for 2 days. Upon completion, the solution was cooled to 0 °C before quenching the reaction with ice/water, followed extraction of the organics with $CH_2Cl_2$. The combined organics were washed with saturated solution of $NaHCO_3$, dried over $Na_2SO_3$ and the solvent was reduced *in vacuo* before purification by silica gel flash column chromatography (cyclohexane:EtOAc 9:1 to 1:1) to afford the title compound.

#### 5.5.3. Procedure C. Friedel-crafts acylation

The appropriate acyl chloride (3.0 equiv) was added to ground $AlCl_3$ (5.0 equiv) and the slurry was heated to 150 °C, then oxindole (1.0 equiv) was added portionwise. The resulting mixture was heated at 185 °C for 5 min. Upon completion, the mixture was cooled to 0 °C and was quenched with ice/water. The acylated product precipitated and was collected by filtration. Purification by silica gel flash column chromatography (cyclohexane:EtOAc 9:1 to 1:1) afforded the title compound.

#### 5.5.4. General procedure D. Sulphonamide coupling

To a solution of 2-oxoindoline-5-sulfonyl chloride (1.0 equiv) in THF the corresponding amine (1.1 equiv) and DIPEA (3.0 equiv) at room temperature, and the resulting mixture was stirred for 18 h at room temperature. Upon completion, the mixture was diluted with EtOAc and saturated solution of $NaHCO_3$ and layers were separated. The organics were further extracted from the aqueous with EtOAc and the combined organics were washed with brine, dried over $Na_2SO_4$, filtered and the solvent was reduced *in vacuo*. Purification by silica gel flash column chromatography (hexane:EtOAc or $CH_2Cl_2$:MeOH mixtures) afforded the desired compound.

#### 5.5.5. General procedure E. Mitsunobu reaction

A dry three-neck flask was charged with 5-hydroxyindolin-2-one (1.0 equiv), $PPh_3$ (1.4 equiv) and the appropriate alcohol (1.4 equiv) in anhydrous THF (0.25 M). The solution was cooled to 0 °C and diethyl azadicarboxylate (1.4 equiv) in PhMe was added dropwise. The resulting mixture was warmed to room temperature and stirred for 18 h. Upon completion, the solvent reduced *in vacuo*, before purification by silica gel flash column chromatography (hexane:EtOAc 8:2) to afford the title compound.

*5.5.6. General procedure F. Amide HATU coupling*

To a solution of amine (1.0 equiv) in THF, HATU (1.3 equiv), the corresponding carboxylic acid (1.1 equiv) and DIPEA (3.0 equiv) at room temperature, and the resulting mixture was stirred for 18 h at room temperature. Upon completion, the mixture was diluted with EtOAc and saturated solution of $NaHCO_3$ and layers were separated. The organics were further extracted from the aqueous with EtOAc and the combined organics were washed with brine, dried over $Na_2SO_4$, filtered and the solvent reduced *in vacuo*. Purification by silica gel flash column chromatography (hexane:EtOAc or $CH_2Cl_2$:MeOH mixtures) afforded the desired compound.

**(3Z)-3-[(1H-imidazole-5-yl)methylidene]-5-methoxy-2,3-dihydro-1H-indol-2-one (1)**: Compound **1** was prepared by procedure A to afford a purple solid (177 mg, 0.734 mmol, 80%). MP 210–212 °C; $^1$H NMR (400 MHz, DMSO-$d_6$) δ 13.81 (s, 1H), 10.82 (s, 1H), 8.02 (s, 1H), 7.88 (s, 1H), 7.61 (s, 1H), 7.36–7.35 (m, 1H), 6.80–6.76 (m, 2H), 3.76 (s, 3H). HRMS *m/z* $[M+H]^+$ calcd for $C_{13}H_{12}N_3O_2$: 242.0930, found 242.0918, LC $t_R$ = 2.94 min, >98% Purity. Consistent with previous report [93,94].

**(3Z)-5-methoxy-3-(1H-pyrrol-2-ylmethylidene)-2,3-dihydro-1H-indol-2-one (2)**: Compound **2** was prepared by procedure A to afford a dark orange solid (168 mg, 0.699 mmol, 76%). MP 220–222 °C; $^1$H NMR (400 MHz, DMSO-$d_6$) δ 13.16 (s, 1H), 10.84 (s, 1H), 7.56 (s, 1H), 7.52 (d, $J$ = 8.4 Hz, 1H), 7.29 (q, $J$ = 2.3 Hz, 1H), 6.75 (dt, $J$ = 3.6, 1.7 Hz, 1H), 6.58 (dd, $J$ = 8.4, 2.3 Hz, 1H), 6.45 (d, $J$ = 2.3 Hz, 1H), 6.34–6.29 (m, 1H), 3.76 (s, 3H). $^{13}$C NMR (100 MHz, DMSO-$d_6$) δ 169.8, 159.3, 140.3, 129.6, 124.7, 124.2, 119.6, 119.1, 117.9, 117.1, 111.1, 107.0, 96.1, 55.3. HRMS *m/z* $[M+H]^+$ calcd for $C_{14}H_{13}N_2O_2$: 241.0977, found 241.0961, LC $t_R$ = 4.38 min, >98% Purity.

**(3Z)-3-[(3,5-dimethyl-1H-pyrrol-2-yl)methylidene]-5-methoxy-2,3-dihydro-1H-indol-2-one (3)**: Compound **3** was prepared by procedure A to afford a red solid (200 mg, 0.745 mmol, 81%). MP 231–233 °C; $^1$H NMR (400 MHz, DMSO-$d_6$) δ 13.45 (s, 1H), 10.57 (s, 1H), 7.58 (s, 1H), 7.40 (d, $J$ = 2.4 Hz, 1H), 6.76 (d, $J$ = 8.4 Hz, 1H), 6.67 (dd, $J$ = 8.4, 2.4 Hz, 1H), 5.99 (d, $J$ = 2.5 Hz, 1H), 3.77 (s, 3H), 2.31 (s, 6H). $^{13}$C NMR (100 MHz, DMSO-$d_6$) δ 169.5, 154.8, 135.6, 132.0, 131.6, 126.9, 126.6, 123.7, 113.3, 112.5, 111.9, 109.6, 104.1, 55.6, 13.5, 11.4. HRMS *m/z* $[M+H]^+$ calcd for $C_{16}H_{17}N_2O_2$: 269.1290, found 269.1282, LC $t_R$ = 4.79 min, >98% Purity.

**(3Z)-5-methoxy-3-(1H-pyrazol-5-ylmethylidene)-2,3-dihydro-1H-indol-2-one (4)**: Compound **4** was prepared by procedure A to afford a red solid (160 mg, 0.663 mmol, 72%). MP 192–194 °C; $^1$H NMR (400 MHz, DMSO-$d_6$) δ 10.93 (s, 1H), 7.87 (s, 2H), 7.73 (s, 1H), 7.40 (d, $J$ = 2.2 Hz, 1H), 6.86–6.77 (m, 3H), 3.77 (s, 3H). $^{13}$C NMR (100 MHz, DMSO-$d_6$) δ 170.0, 154.8, 136.6, 134.5, 130.3, 126.0, 123.2, 114.9, 113.6, 111.0, 109.8, 106.3, 55.9. HRMS *m/z* $[M+H]^+$ calcd for $C_{13}H_{12}N_3O_2$: 242.0930, found 242.0920, LC $t_R$ = 3.85 min, >98% Purity.

**(3Z)-3-(1H-imidazole-2-ylmethylidene)-5-methoxy-2,3-dihydro-1H-indol-2-one (5)**: Compound **5** was prepared by procedure A to afford a red solid (164 mg, 0.680 mmol, 74%). MP > 300 °C; $^1$H NMR (400 MHz, DMSO-$d_6$) δ 10.97 (s, 1H), 7.86 (s, 1H), 7.55 (t, $J$ = 1.5 Hz, 2H), 7.34 (d, $J$ = 1.2 Hz, 1H), 6.82 (d, $J$ = 1.4 Hz, 2H), 3.77 (s, 3H). $^{13}$C NMR (100 MHz, DMSO-$d_6$) δ 168.9, 155.2, 143.7, 133.7, 132.6, 125.0, 124.7, 124.1, 120.6, 115.1, 110.5, 106.0, 55.6. HRMS *m/z* $[M+H]^+$ calcd for $C_{13}H_{12}N_3O_2$: 242.0930, found 242.0917, LC $t_R$ = 2.80 min, >98% Purity.

**(3Z)-5-methoxy-3-(pyridin-2-ylmethylidene)-2,3-dihydro-1H-indol-2-one (6)**: Compound **6** was prepared by procedure A to afford a dark red solid (176 mg, 0.698 mmol, 76%). MP 176–178 °C; $^1$H NMR (400 MHz, DMSO-$d_6$) δ 10.42 (s, 1H), 8.96–8.86 (m, 1H), 8.82 (d, $J$ = 2.7 Hz, 1H), 7.96 (td, $J$ = 7.6, 1.8 Hz, 1H), 7.88 (dt, $J$ = 7.8, 1.1 Hz, 1H), 7.56 (s, 1H), 7.47 (ddd, $J$ = 7.6, 4.7, 1.2 Hz, 1H), 6.88 (dd, $J$ = 8.4, 2.7 Hz, 1H), 6.77 (d, $J$ = 8.4 Hz, 1H), 3.77 (s, 3H). $^{13}$C NMR (100 MHz, DMSO- $d_6$) δ 169.3, 154.2, 153.2, 149.6, 137.3, 137.3, 133.7, 129.9, 128.6, 124.2, 122.3, 116.3, 114.0, 109.8, 55.3. HRMS *m/z* $[M+H]^+$ calcd for $C_{15}H_{13}N_2O_2$: 253.0977, found 253.0966, LC $t_R$ = 3.88 min, >98% Purity.

**(3Z)-5-methoxy-3-(pyridin-3-ylmethylidene)-2,3-dihydro-1H-indol-2-one (7)**: Compound **7** was prepared by procedure A to afford a red solid (104 mg, 0.412 mmol, 45%, ratio of E:Z - 50:50). MP 206–208 °C; (*Z*)-5-Methoxy-3-(pyridin-3-ylmethylene)indolin-2-one. $^1$H NMR (500 MHz, DMSO-$d_6$) δ 10.5 (d, $J$ = 6.0 Hz, 1H), 9.19 (dd, $J$ = 1.8, 1.1 Hz, 1H), 8.91 (dddd, $J$ = 8.1, 2.3, 1.6, 0.6 Hz, 1H), 8.58 (dd, $J$ = 4.8, 1.7 Hz, 1H), 7.84 (s, 1H), 7.49 (ddd, $J$ = 8.0, 4.9, 0.9 Hz, 1H), 7.41 (d, $J$ = 2.5 Hz, 1H), 6.82 (dd, $J$ = 8.4, 2.5 Hz, 1H), 6.74 (dd, $J$ = 8.4, 0.5 Hz, 1H), 3.77 (s, 3H). $^{13}$C NMR (125 MHz, DMSO-$d_6$) δ 167.1, 154.7, 152.4, 150.3, 137.9, 134.9, 133.0, 129.9, 129.3, 125.3, 123.2, 115.4, 110.1, 106.3, 55.6. (*E*)-5-Methoxy-3-(pyridin-3-ylmethylene)indolin-2-one. $^1$H NMR (500 MHz, DMSO-$d_6$) δ 10.5 (d, $J$ = 6.0 Hz, 2H), 8.862–8.857 (m, 1H), 8.65 (ddd, $J$ = 4.9, 1.7, 0.6 Hz, 1H), 8.12 (dddd, $J$ = 7.9, 2.4, 1.7, 0.8 Hz, 1H), 7.62 (s, 1H), 7.56 (ddd, $J$ = 7.9, 4.7, 0.5 Hz, 1H), 6.89–6.89 (m, 1H), 6.86 (dd, $J$ = 8.4, 2.5 Hz, 1H), 6.80 (dd, $J$ = 8.4, 0.5 Hz, 1H), 3.60 (s, 3H). $^{13}$C NMR (125 MHz, DMSO-$d_6$) δ 168.1, 154.0, 150.2, 149.7, 136.9, 136.3, 132.3, 130.5, 129.9, 123.6, 121.4, 115.6, 110.7, 108.9, 55.3. HRMS *m/z* $[M+H]^+$ calcd for $C_{15}H_{13}N_2O_2$: 253.0977, found 253.0966, LC $t_R$ = 3.10 min, >98% Purity.

**(3Z)-3-(1H-pyrazol-5-ylmethylidene)-2,3-dihydro-1H-indol-2-one (8)**: Compound **8** was prepared by procedure A to afford a bright yellow solid (156 mg, 0.739 mmol, 49%, ratio of E:Z - 33:67). MP 249–251 °C; (*Z*)-3-((1*H*-Pyrazol-5-yl)methylene)indolin-2-one. $^1$H NMR (600 MHz, DMSO-$d_6$) δ 10.39 (bs, 1H), 9.31 (d, $J$ = 7.6 Hz, 1H), 8.00 (s, 1H), 7.90 (s, 1H), 7.47 (s, 1H), 7.16 (td, $J$ = 7.6, 1.4 Hz, 1H), 6.96 (td, $J$ = 7.6, 1.1 Hz, 1H), 6.82 (d, $J$ = 8.5 Hz, 1H). $^{13}$C NMR (125 MHz, DMSO-$d_6$) δ 169.9, 141.5, 138.1, 137.0, 128.2, 126.9, 126.4, 126.1, 122.6, 121.28, 120.6, 108.7. (*E*)-3-((1*H*-Pyrazol-5-yl)methylene)indolin-2-one. $^1$H NMR (600 MHz, DMSO-$d_6$) δ 7.99 (s, 1H), 7.83 (s, 1H), 7.66 (d, $J$ = 6.9 Hz, 1H), 7.21–7.15 (m, 1H), 7.01 (td, $J$ = 7.6, 1.0 Hz, 1H), 6.89 (d, $J$ = 7.7 Hz, 1H). $^{13}$C NMR (125 MHz, DMSO-$d_6$) δ 168.6, 139.8, 139.0, 138.1, 127.9, 124.3, 123.9, 121.3, 120.6, 120.2, 119.2, 109.5. HRMS *m/z* $[M+H]^+$ calcd for $C_{12}H_{10}N_3O$: 212.0824, found 212.0814, LC $t_R$ = 2.82 min, >98% Purity.

**(3Z)-3-(1*H*-pyrrol-2-ylmethylidene)-2,3-dihydro-1H-indol-2-one (9)**: Compound **9** was prepared by procedure A to afford a dark orange solid (159 mg, 0.756 mmol, 67%). MP 218–220 °C; $^1$H NMR (400 MHz, DMSO-$d_6$) δ 13.34 (s, 1H), 10.89 (s, 1H), 7.74 (s, 1H), 7.63 (dt, $J$ = 7.4, 0.9 Hz, 1H), 7.35 (td, $J$ = 2.6, 1.4 Hz, 1H), 7.15 (td, $J$ = 7.6, 1.2 Hz, 1H), 6.99 (td, $J$ = 7.6, 1.1 Hz, 1H), 6.88 (dt, $J$ = 7.8, 0.9 Hz, 1H), 6.83 (dt, $J$ = 3.6, 1.7 Hz, 1H), 6.35 (dt, $J$ = 3.7, 2.3 Hz, 1H). $^{13}$C NMR (100 MHz, DMSO-$d_6$) δ 169.2, 139.0, 129.6, 126.9, 126.3, 125.6, 125.2, 121.2, 120.3, 118.5, 116.8, 111.4, 109.5. HRMS *m/z* $[M+H]^+$ calcd for $C_{13}H_{11}N_2O$: 211.0871, found 211.0865, LC $t_R$ = 4.47 min, >98% Purity.

**(3Z)-3-(1H-pyrazol-5-ylmethylidene)-2,3-dihydro-1H-indol-2-one (11)**: Compound **11** was prepared by procedure A to afford an orange solid (90 mg, 0.426 mmol, 38%). MP 190–192 °C; $^1$H NMR (600 MHz, DMSO-$d_6$) δ 13.56 (s, 1H), 10.52 (s, 1H), 7.94 (s, 1H), 7.72 (d, $J$ = 7.5 Hz, 1H), 7.48 (s, 1H), 7.27–7.24 (m, 1H), 7.00 (td, $J$ = 7.6, 1.1 Hz, 1H), 6.87 (d, $J$ = 7.7 Hz, 1H), 6.85–6.80 (m, 1H). $^{13}$C NMR (150 MHz, DMSO-$d_6$) δ 169.5, 146.3, 142.5, 140.4, 129.7, 126.2, 125.8, 125.0, 121.9, 121.0, 110.6, 109.4. HRMS *m/z* $[M+H]^+$ calcd for $C_{12}H_{10}N_3O$: 212.0824, found 212.0812, LC $t_R$ = 3.85 min, >98% Purity.

**(3Z)-3-(1H-imidazole-2-ylmethylidene)-2,3-dihydro-1H-indol-2-one (12)**: Compound **12** was prepared by procedure A to afford a bright yellow solid (195 mg, 0.923 mmol, 82% ratio of E:Z - 40:60 - not able to clearly distinguish *E*/Z isomers). MP > 300 °C; Major diastereoisomer. 3-((1*H*-Imidazole-2-yl)methylene)indolin-2-one. $^1$H NMR (600 MHz, DMSO-$d_6$) δ 10.52 (s, 1H), 9.40 (dd, $J$ = 7.7, 1.3 Hz, 1H), 7.45 (s, 2H), 7.39 (s, 1H), 7.24–7.22 (m, 1H), 7.00 (td, $J$ = 7.6, 1.1 Hz, 1H), 6.85 (d, $J$ = 7.7 Hz, 1H). $^{13}$C NMR (150 MHz, DMSO-$d_6$) δ 169.6, 143.4, 142.4, 129.6, 128.9, 127.1, 124.3, 121.8, 121.0, 120.9, 120.2, 109.1. Minor diastereoisomer. 3-((1*H*-Imidazole-2-yl)methylene)indolin-2-one. $^1$H NMR (600 MHz, DMSO-$d_6$) δ 14.10 (s, 1H), 7.83 (d, $J$ =

7.4 Hz, 1H), 7.80 (s, 1H), 7.55 (bs, 1H), 7.34 (s, 1H), 7.26–7.23 (m, 1H), 7.03 (td, $J = 7.6$, 1.0 Hz, 1H), 6.92 (d, $J = 7.8$ Hz, 1H). 13C NMR (150 MHz, DMSO-$d_6$) δ 168.9, 143.7, 140.1, 132.5, 127.1, 124.4, 124.0, 123.7, 122.0, 121.0, 120.7, 110.0. HRMS *m/z* $[M+H]^+$ calcd for $C_{12}H_{10}N_3O$: 212.0824, found 212.0813, LC $t_R = 2.60$ min, >98% Purity.

**(3Z)-3-(pyridin-2-ylmethylidene)-2,3-dihydro-1H-indol-2-one (13)**: Compound **13** was prepared by procedure A to afford a dark orange solid (160 mg, 0.720 mmol, 64%). MP 191–193 °C; $^1$H NMR (400 MHz, DMSO-$d_6$) δ 10.62 (s, 1H), 9.03–8.97 (m, 1H), 8.88 (ddd, $J = 4.8$, 1.8, 0.8 Hz, 1H), 7.94 (td, $J = 7.7$, 1.8 Hz, 1H), 7.86 (dt, $J = 7.9$, 1.1 Hz, 1H), 7.57 (s, 1H), 7.46 (ddd, $J = 7.5$, 4.7, 1.2 Hz, 1H), 7.28 (td, $J = 7.7$, 1.3 Hz, 1H), 6.98 (td, $J = 7.7$, 1.1 Hz, 1H), 6.87 (dt, $J = 7.7$, 0.9 Hz, 1H). $^{13}$C NMR (100 MHz, DMSO-$d_6$) δ 169.3, 153.2, 149.7, 143.6, 137.2, 133.7, 130.8, 129.3, 128.4, 127.9, 124.1, 121.5, 121.2, 109.6. HRMS *m/z* $[M+H]^+$ calcd for $C_{14}H_{11}N_2O$: 223.0871, found 223.0860, LC $t_R$ = 3.85 min, >98% Purity.

**(3Z)-3-(pyridin-3-ylmethylidene)-2,3-dihydro-1H-indol-2-one (14)**: Compound **14** was prepared by procedure A to afford a light yellow solid (45 mg, 0.203 mmol, 18%). MP 155–157 °C; $^1$H NMR (400 MHz, DMSO-$d_6$) δ 10.66 (s, 1H), 8.87 (dt, $J = 1.9$, 0.9 Hz, 1H), 8.65 (dd, $J = 4.9$, 1.6 Hz, 1H), 8.12 (dddd, $J = 7.9$, 2.4, 1.7, 0.8 Hz, 1H), 7.62 (s, 1H), 7.55 (ddd, $J = 7.9$, 4.8, 0.9 Hz, 1H), 7.37 (dd, $J = 7.8$, 1.1 Hz, 1H), 7.27–7.23 (m, 1H), 6.91–6.85 (m, 2H). $^{13}$C NMR (100 MHz, DMSO-$d_6$) δ 168.1, 150.1, 149.8, 143.2, 136.4, 132.1, 130.6, 130.6, 129.4, 123.7, 122.3, 121.3, 120.6, 110.3. HRMS *m/z* $[M+H]^+$ calcd for $C_{14}H_{11}N_2O$: 223.0871, found 223.0861, LC $t_R = 2.60$ min, >98% Purity.

**(3Z)-6-methoxy-3-(1H-pyrrol-2-ylmethylidene)-2,3-dihydro-1H-indol-2-one (15)**: Compound **15** was prepared by procedure A to afford an orange solid (137 mg, 0.570 mmol, 62%). MP 225–226 °C; $^1$H NMR (400 MHz, DMSO-$d_6$) δ 13.16 (s, 1H), 10.84 (s, 1H), 7.56 (s, 1H), 7.52 (d, $J = 8.4$ Hz, 1H), 7.29 (td, $J = 2.6$, 1.4 Hz, 1H), 6.75 (dt, $J = 3.6$, 1.7 Hz, 1H), 6.58 (dd, $J = 8.4$, 2.3 Hz, 1H), 6.45 (d, $J = 2.3$ Hz, 1H), 6.32 (dt, $J = 3.7$, 2.4 Hz, 1H), 3.76 (s, 3H). $^{13}$C NMR (100 MHz, DMSO-$d_6$) δ 169.8, 159.3, 140.3, 129.6, 124.7, 124.2, 119.6, 119.1, 117.9, 117.1, 111.1, 107.0, 96.1, 55.3. HRMS *m/z* $[M+H]^+$ calcd for $C_{14}H_{13}N_2O_2$: 241.0977, found 241.0962, LC $t_R = 4.41$ min, >98% Purity.

**(3Z)-3-[(3,5-dimethyl-1H-pyrrol-2-yl)methylidene]-6-methoxy-2,3-dihydro-1H-indol-2-one (16)**: Compound **16** was prepared by procedure A to afford an orange solid (200 mg, 0.745 mmol, 81%). MP 231–233 °C; $^1$H NMR (400 MHz, DMSO-$d_6$) δ 13.14 (s, 1H), 10.72 (s, 1H), 7.60 (d, $J = 8.4$ Hz, 1H), 7.40 (s, 1H), 6.56 (dd, $J = 8.4$, 2.3 Hz, 1H), 6.45 (d, $J = 2.3$ Hz, 1H), 5.96 (d, $J = 2.5$ Hz, 1H), 3.75 (s, 3H), 2.30 (s, 3H), 2.27 (s, 3H). $^{13}$C NMR (100 MHz, DMSO-$d_6$) δ 169.9, 158.5, 139.4, 134.4, 130.1, 126.5, 121.6, 119.1, 118.6, 113.1, 112.0, 106.7, 95.8, 55.2, 13.5, 11.3. HRMS *m/z* $[M+H]^+$ calcd for $C_{16}H_{17}N_2O_2$: 269.1290, found 269.1272, LC $t_R = 4.67$ min, >98% Purity.

**(3Z)-6-methoxy-3-(1H-pyrazol-5-ylmethylidene)-2,3-dihydro-1H-indol-2-one (17)**: Compound **17** was prepared by procedure A to afford an orange solid (189 mg, 0.783 mmol, 85%). MP 209–211 °C; $^1$H NMR (400 MHz, DMSO-$d_6$) δ 11.06 (s, 1H), 7.80 (s, 1H), 7.64 (dd, $J = 19.1$, 8.0 Hz, 3H), 6.85 (s, 1H), 6.62 (d, $J = 8.4$ Hz, 1H), 6.47 (s, 1H), 3.78 (s, 3H). $^{13}$C NMR (100 MHz, DMSO-$d_6$) δ 169.3, 160.8, 141.8, 140.2, 138.0, 125.0, 121.3, 118.6, 116.5, 110.7, 107.6, 96.5, 55.4. HRMS *m/z* $[M+H]^+$ calcd for $C_{13}H_{12}N_3O_2$: 242.0930, found 242.0917, LC $t_R = 3.54$ min, >98% Purity.

**(3Z)-3-(1H-imidazole-2-ylmethylidene)-6-methoxy-2,3-dihydro-1H-indol-2-one (18)**: Compound **18** was prepared by procedure A to afford an orange solid (126 mg, 0.522 mmol, 57%). MP > 300 °C; $^1$H NMR (600 MHz, DMSO-$d_6$) δ 13.94 (s, 1H), 11.33 (s, 1H), 7.73 (d, $J = 8.4$ Hz, 1H), 7.61 (s, 1H), 7.50 (s, 1H), 7.29 (s, 1H), 6.60 (dd, $J = 8.4$, 2.3 Hz, 1H), 6.48 (d, $J = 2.3$ Hz, 1H), 3.78 (s, 3H). $^{13}$C NMR (150 MHz, DMSO-$d_6$) δ 169.6, 160.6, 143.9, 141.7, 132.0, 123.8, 121.9, 121.5, 120.1, 116.7, 107.5, 96.4, 55.4. HRMS *m/z* $[M+H]^+$ calcd for $C_{13}H_{12}N_3O_2$: 242.0930, found 242.0916, LC $t_R = 2.82$ min, >98% Purity.

**(3Z)-6-methoxy-3-(pyridin-2-ylmethylidene)-2,3-dihydro-1H-indol-2-one (19)**: Compound **19** was prepared by procedure A to afford a mustard solid (151 mg, 0.599 mmol, 65%). MP 182–184 °C; δ $^1$H NMR (400 MHz, DMSO-$d_6$) δ 10.57 (s, 1H), 8.98 (d, $J = 8.6$ Hz, 1H), 8.89–8.78 (m, 1H), 7.92 (td, $J = 7.7$, 1.9 Hz, 1H), 7.81 (dt, $J = 8.0$, 1.1 Hz, 1H), 7.42 (ddd, $J = 7.6$, 4.7, 1.2 Hz, 1H), 7.39 (s, 1H), 6.55 (dd, $J = 8.7$, 2.5 Hz, 1H), 6.42 (d, $J = 2.4$ Hz, 1H), 3.79 (s, 3H). $^{13}$C NMR (100 MHz, DMSO-$d_6$) δ 170.0, 161.7, 153.6, 149.5, 145.5, 137.1, 130.4, 129.6, 128.9, 128.0, 123.7, 114. 6, 106.5, 96.0, 55.3. HRMS *m/z* $[M+H]^+$ calcd for $C_{15}H_{13}N_2O_2$: 253.0977, found 253.0970, LC $t_R$ = 3.85 min, >98% Purity.

**(Z)-6-methoxy-3-(pyridin-3-ylmethylene)indolin-2-one (20)** Compound **20** was prepared by procedure A to afford a mustard solid (93 mg, 0.369 mmol, 40%, ratio of E:Z - 28:72). MP 177–179 °C; (*Z*)-6-Methoxy-3-(pyridin-3-ylmethylene)indolin-2-one. $^1$H NMR (600 MHz, DMSO-$d_6$) δ 10.73 (bs, 1H), 8.84 (d, $J = 2.3$ Hz, 1H), 8.62 (dd, $J = 4.9$, 1.6 Hz, 1H), 8.08 (dt, $J = 7.9$, 2.1 Hz, 1H), 7.53 (dd, $J = 7.9$, 4.8 Hz, 1H), 7.43 (s, 1H), 7.32 (d, $J = 8.5$ Hz, 1H), 6.45–6.42 (m, 2H), 3.75 (s, 3H). 13C NMR (150 MHz, DMSO-$d_6$) δ 168.9, 161.5, 149.77, 149.75, 145.1, 136.2, 130.9, 129.0, 128.6, 123.7, 123.1, 113.4, 106.8, 96.7, 55.4. (*E*)-6-Methoxy-3-(pyridin-3-ylmethylene)indolin-2-one. $^1$H NMR (600 MHz, DMSO-$d_6$) δ 9.13 (d, $J = 2.2$ Hz, 1H), 8.82 (dt, $J = 8.1$, 2.0 Hz, 1H), 8.54 (dd, $J = 4.8$, 1.7 Hz, 1H), 7.62 (s, 1H), 7.62 (d, $J = 8.1$ Hz, 1H), 7.46 (dd, $J = 8.1$, 4.8 Hz, 1H), 6.57 (dd, $J = 8.4$, 2.4 Hz, 1H), 6.40 (d, $J = 2.3$ Hz, 1H), 3.78 (s, 3H). $^{13}$C NMR (150 MHz, DMSO-$d_6$) δ 167.7, 161.0, 152.1, 149.7, 142.7, 137.5, 130.2, 129.9, 128.6, 123.5, 121.5, 117.1, 106.9, 96.0, 55.4. HRMS *m/z* $[M+H]^+$ calcd for $C_{15}H_{13}N_2O_2$: 253.0977, found 253.0965, LC $t_R = 2.70$ min, >98% Purity.

**(Z)-3-(1H-imidazole-5-ylmethylidene)-5,6-dimethoxy-2,3-dihydro-1H-indol-2-one (21)**: Compound **21** was prepared by procedure A to afford a bright red solid (160 mg, 0.590 mmol, 76%, ratio of E:Z - 50:50). MP 222–224 °C; (*Z*)-3-((1H-Imidazole-5-yl)methylene)-5,6-dimethoxyindolin-2-one. $^1$H NMR (600 MHz, DMSO-$d_6$) δ 13.71 (bs, 1H), 7.94 (s, 1H), 7.68 (s, 1H), 7.56 (s, 1H), 7.38 (s, 1H), 6.53 (s, 1H), 3.77 (s, 3H), 3.77 (s, 3H). (*E*)-3-((1*H*-Imidazole-5-yl)methylene)-5,6-dimethoxyindolin-2-one. $^1$H NMR (600 MHz, DMSO-$d_6$) δ 10.14 (s, 1H), 9.20 (s, 1H), 7.97 (s, 1H), 7.81 (d, $J = 1.1$ Hz, 1H), 7.30 (s, 1H), 6.47 (s, 1H), 3.78 (s, 3H), 3.76 (s, 3H). $^{13}$C NMR (150 MHz, DMSO-$d_6$) δ 170.6, 150.0, 143.1, 137.9, 136.7, 125.1, 124.3, 122.2, 114.1, 113.1, 104.8, 94.6, 56.5, 55.6. HRMS *m/z* $[M+H]^+$ calcd for $C_{14}H_{14}N_3O_3$: 272.1035, found 272.1023, LC $t_R = 2.76$ min, >98% Purity.

**(3Z)-5,6-dimethoxy-3-(1H-pyrrol-2-ylmethylidene)-2,3-dihydro-1H-indol-2-one (22)**: Compound **22** was prepared by procedure A to afford a bright red solid (93 mg, 0.369 mmol, 40%). MP 167–169 °C; $^1$H NMR (400 MHz, DMSO-$d_6$) δ 13.27 (s, 1H), 10.65 (s, 1H), 7.61 (s, 1H), 7.35 (s, 1H), 7.29 (q, $J = 2.2$ Hz, 1H), 6.73 (dt, $J = 3.6$, 1.7 Hz, 1H), 6.52 (s, 1H), 6.32 (dt, $J = 4.0$, 2.4 Hz, 1H), 3.77 (d, $J = 2.2$ Hz, 6H). $^{13}$C NMR (100 MHz, DMSO-$d_6$) δ 169.6, 149.1, 144.4, 133.2, 129.7, 124.6, 124.4, 118.9, 117.9, 116.3, 111.1, 104.3, 95.4, 56.3, 55.8. HRMS *m/z* $[M+H]^+$ calcd for $C_{15}H_{15}N_2O_3$: 271.1083, found 271.1072, LC $t_R$ = 4.29 min, >98% Purity.

**(3Z)-3-[(3,5-dimethyl-1H-pyrrol-2-yl)methylidene]-5,6-dimethoxy-2,3-dihydro-1H-indol-2-one (23)**: Compound **23** was prepared by procedure A to afford a dark red solid (167 mg, 0.560 mmol, 72%). MP 282–285 °C; $^1$H NMR (400 MHz, DMSO-$d_6$) δ 13.28 (s, 1H), 10.53 (s, 1H), 7.45 (s, 1H), 7.42 (s, 1H), 6.51 (s, 1H), 5.96 (d, $J = 2.5$ Hz, 1H), 3.78 (s, 3H), 3.75 (s, 3H), 2.30 (s, 6H). 13C NMR (100 MHz, DMSO-$d_6$) δ $^{13}$C NMR (101 MHz, DMSO-$d_6$) δ 169.7, 148.4, 144.3, 134.3, 132.3, 130.1, 126.6, 121.9, 117.2, 114.0, 112.0, 104.3, 95.3, 56.6, 55.8, 13.5, 11.4. HRMS *m/z* $[M+H]^+$ calcd for $C_{22}H_{13}N_4O$: 349.1089, found 349.1088, LC $t_R = 4.61$ min, >98% Purity.

**(3Z)-5,6-dimethoxy-3-(1H-pyrazol-5-ylmethylidene)-2,3-dihydro-1H-indol-2-one (24)**: Compound **24** was prepared by procedure A to afford a dark red solid (160 mg, 0.590 mmol, 76%). MP 230–232 °C; $^1$H NMR (400 MHz, DMSO-$d_6$) δ 13.49 (s, 1H), 10.26 (s, 1H), 8.85 (s, 1H), 7.89 (d, $J = 2.3$ Hz, 1H), 7.29 (s, 1H), 6.75 (d, $J = 2.3$ Hz, 1H), 6.51 (s, 1H), 3.80 (s, 3H), 3.77 (s, 3H).$^{13}$C NMR (100 MHz, DMSO-$d_6$) δ

170.2, 150.9, 146.6, 143.2, 137.8, 129.7, 125.7, 122.6, 113.2, 112.6, 109.9, 94.9, 56.5, 55.6. HRMS *m/z* $[M+H]^+$ calcd for $C_{14}H_{14}N_3O_3$: 272.1035, found 272.1028, LC $t_R$ = 3.21 min, >98% Purity.

**(Z)-3-(1H-imidazole-2-ylmethylidene)-5,6-dimethoxy-2,3-dihydro-1H-indol-2-one (25)**: Compound **25** was prepared by procedure A to afford a dark red solid (95 mg, 0.350 mmol, 45%, ratio of E:Z - 44:56). MP > 300 °C; (*E*)-3-((1H-Imidazole-2-yl)methylene)-5,6-dimethoxyindolin-2-one. $^1$H NMR (500 MHz, DMSO-$d_6$) δ 10.28 (bs, 1H), 9.26 (s, 1H), 7.41 (s, 2H), 7.21 (s, 1H), 6.50 (s, 1H), 3.80 (s, 3H), 3.77 (s, 3H). $^{13}$C NMR (125 MHz, DMSO-$d_6$) δ 170.2, 151.1, 143.5, 143.2, 137.8, 132.1, 125.6, 117.5, 113.28, 113.26, 94.8, 56.5, 55.6. (*Z*)-3-((1H-Imidazole-2-yl)methylene)-5,6-dimethoxyindolin-2-one. $^1$H NMR (500 MHz, DMSO-$d_6$) δ 14.01 (bs, 1H), 7.69 (s, 1H), 7.56 (s, 1H), 7.50 (bs, 1H), 7.30 (bs, 1H), 6.54 (s, 1H), 3.78 (s, 3H), 3.77 (s, 3H). $^{13}$C NMR (125 MHz, DMSO-$d_6$) δ 169.4, 150.6, 144.7, 144.0, 134.5, 124.5, 122.2, 120.0, 115.1, 105.5, 95.5, 56.3, 55.8. HRMS *m/z* $[M+H]^+$ calcd for $C_{14}H_{14}N_3O_3$: 272.1035, found 272.1022, LC $t_R$ = 2.74 min, >98% Purity.

**(Z)-5-acetyl-3-(1H-pyrazol-5-ylmethylidene)-2,3-dihydro-1H-indol-2-one (26)**: Compound **26** was prepared by procedure A to afford a bright orange solid (154 mg, 0.608 mmol, 71%, *E*:Z ratio 32:68). MP 262–265 °C; (*Z*)-3-((1*H*-Pyrazol-5-yl)methylene)-5-acetylindolin-2-one. $^1$H NMR (500 MHz, DMSO-$d_6$) δ 10.80 (s, 1H), 10.12 (d, *J* = 1.8 Hz, 1H), 8.02 (s, 1H), 7.94 (d, *J* = 1.1 Hz, 1H), 7.82 (dd, *J* = 8.1, 1.9 Hz, 1H), 7.56 (s, 1H), 6.92 (d, *J* = 8.2 Hz, 1H), 2.57 (s, 3H). $^{13}$C NMR (150 MHz, DMSO-$d_6$) δ 196.8, 170.5, 145.4, 139.7, 137.0, 130.4, 128.9, 127.5, 122.7, 119.7, 119.4, 108.6, 26.5. (*E*)-3-((1*H*-Pyrazol-5-yl)methylene)-5-acetylindolin-2-one. $^1$H NMR (600 MHz, DMSO-$d_6$) δ 10.80 (s, 1H), 8.33 (d, *J* = 1.7 Hz, 1H), 8.06 (s, 1H), 8.01 (s, 1H), 7.85 (dd, *J* = 8.2, 1.7 Hz, 1H), 6.99 (d, *J* = 8.2 Hz, 1H), 2.58 (s, 3H). HRMS *m/z* $[M+H]^+$ calcd for $C_{14}H_{12}N_3O_2$: 254.0930, found 254.0918, LC $t_R$ = 2.74 min, >98% Purity.

**(3Z)-5-acetyl-3-(1H-pyrrol-2-ylmethylidene)-2,3-dihydro-1H-indol-2-one (27)**: Compound **27** was prepared by procedure A to afford a dark orange solid (117 mg, 0.467 mmol, 54%). MP 218–220 °C; $^1$H NMR (400 MHz, DMSO-$d_6$) δ 10.58 (s, 1H), 9.08–8.92 (m, 1H), 8.85 (ddd, *J* = 4.8, 1.9, 0.8 Hz, 1H), 7.92 (td, *J* = 7.7, 1.8 Hz, 1H), 7.84 (dt, *J* = 7.9, 1.1 Hz, 1H), 7.43 (ddd, *J* = 7.6, 4.7, 1.2 Hz, 1H), 7.25 (td, *J* = 7.6, 1.3 Hz, 1H), 6.95 (td, *J* = 7.7, 1.1 Hz, 1H), 6.84 (dt, *J* = 7.7, 0.8 Hz, 1H), 3.31 (s, 3H). $^{13}$C NMR (100 MHz, DMSO-$d_6$) δ 169.3, 153.2, 149.7, 143.6, 137.3, 133.7, 130.8, 129.3, 128.4, 127.9, 124.1, 121.5, 121.2, 109.6, 39.3. HRMS *m/z* $[M+H]^+$ calcd for $C_{15}H_{13}N_2O_2$: 253.0977, found 253.0963, LC $t_R$ = 3.99 min, >98% Purity.

**(3Z)-5-acetyl-3-[(3,5-dimethyl-1H-pyrrol-2-yl)methylidene]-2,3-dihydro-1H-indol-2-one (28)**: Compound **28** was prepared by procedure A to afford a dark orange solid (149 mg, 0.532 mmol, 62%). MP > 300 °C; δ $^1$H NMR (400 MHz, DMSO-$d_6$) δ 13.33 (s, 1H), 11.14 (s, 1H), 8.35 (d, *J* = 1.6 Hz, 1H), 7.82–7.68 (m, 2H), 6.96 (d, *J* = 8.2 Hz, 1H), 6.05 (d, *J* = 2.5 Hz, 1H), 2.59 (s, 3H), 2.35 (s, 3H), 2.33 (s, 3H). $^{13}$C NMR (100 MHz, DMSO-$d_6$) δ 197.0, 169.8, 141.8, 136.8, 133.1, 130.5, 126.9, 126.6, 125.9, 124.7, 118.5, 113.0, 111.3, 108.9, 26.7, 13.6, 11.5. HRMS *m/z* $[M+H]^+$ calcd for $C_{17}H_{17}N_2O_2$: 281.1290, found 281.1278, LC $t_R$ = 4.62 min, >98% Purity.

**(3Z)-5-acetyl-3-(1H-pyrazol-5-ylmethylidene)-2,3-dihydro-1H-indol-2-one (29)**: Compound **29** was prepared by procedure A to afford a mustard solid (33 mg, 0.130 mmol, 15%). MP 240–242 °C; $^1$H NMR (600 MHz, DMSO-$d_6$) δ 13.76 (s, 1H), 10.94 (s, 1H), 9.75 (s, 1H), 7.96 (s, 1H), 7.92 (dd, *J* = 8.2, 1.8 Hz, 1H), 7.56 (s, 1H), 6.97 (d, *J* = 8.1 Hz, 1H), 6.86 (s, 1H), 2.58 (s, 3H). $^{13}$C NMR (150 MHz, DMSO-$d_6$) δ 196.6, 170.0, 146.5, 146.2, 130.7, 130.1, 127.2, 127.0, 124.0, 121.8, 120.4, 111.0, 109.1, 26.5. HRMS *m/z* $[M+H]^+$ calcd for $C_{14}H_{12}N_3O_2$: 254.0930, found 254.0920, LC $t_R$ = 3.30 min, >98% Purity.

**(Z)-5-acetyl-3-(1H-imidazole-2-ylmethylidene)-2,3-dihydro-1H-indol-2-one (30)**: Compound **30** was prepared by procedure A to afford a bright yellow solid (134 mg, 0.529 mmol, 62%, *E*:Z ratio 47:53 - not able to distinguish E/Z isomers). MP > 300 °C; Major diastereoisomer. 3-((1*H*-Imidazole-2-yl)methylene)-5-acetylindolin-2-one. $^1$H NMR (600 MHz, DMSO-$d_6$) δ 10.94 (bs, 1H), 10.14 (d, *J* = 1.8 Hz, 1H), 7.91 (dd, *J* = 8.2, 1.9 Hz, 1H), 7.56 (bs, 1H), 7.48 (bs, 1H), 7.46 (s, 1H), 6.96 (d, *J* = 8.2 Hz, 1H), 2.58 (s, 3H). Minor diastereoisomer. 3-((1*H*-Imidazole-2-yl)methylene)-5-acetylindolin-2-one. $^1$H NMR (600 MHz, DMSO-$d_6$) δ 13.97 (bs, 1H), 10.95 (bs, 1H), 8.54 (d, *J* = 1.6 Hz, 1H), 8.06 (s, 1H), 7.88 (dd, *J* = 8.2, 1.7 Hz, 1H), 7.59 (d, *J* = 2.1 Hz, 1H), 7.39 (d, *J* = 1.3 Hz, 1H), 7.03 (d, *J* = 8.1 Hz, 1H), 2.60 (s, 3H). HRMS *m/z* $[M+H]^+$ calcd for $C_{14}H_{12}N_3O_2$: 254.0930, found 254.0917, LC $t_R$ = 2.86 min, >98% Purity.

**(3Z)-5-acetyl-3-(pyridin-2-ylmethylidene)-2,3-dihydro-1H-indol-2-one (31)**: Compound **31** was prepared by procedure A to afford a mustard solid (190 mg, 0.719 mmol, 63%). MP 250–252 °C; $^1$H NMR (400 MHz, DMSO-$d_6$) δ 11.00 (s, 1H), 9.77 (d, *J* = 1.8 Hz, 1H), 8.88 (dt, *J* = 4.8, 1.2 Hz, 1H), 7.96 (td, *J* = 7.6, 1.8 Hz, 1H), 7.93–7.80 (m, 2H), 7.62 (s, 1H), 7.49 (ddd, *J* = 7.5, 4.7, 1.3 Hz, 1H), 6.94 (d, *J* = 8.2 Hz, 1H), 2.55 (s, 3H). $^{13}$C NMR (100 MHz, DMSO-$d_6$) δ 196.4, 169.7, 152.9, 149.7, 147.6, 137.5, 134.9, 131.5, 130.6, 128.9, 128.9, 128.4, 124.6, 121.3, 109.5, 26.4. HRMS *m/z* $[M+H]^+$ calcd for $C_{16}H_{13}N_2O_2$: 265.0977, found 265.0966, LC $t_R$ = 3.72 min, >98% Purity.

**(3Z)-5-acetyl-3-(pyridin-3-ylmethylidene)-2,3-dihydro-1H-indol-2-one (32)**: Compound **32** was prepared by procedure A to afford a yellow solid (88 mg, 0.333 mmol, 39%, *E*:Z ratio 48:52 - not able to distinguish E/Z isomers). MP 209–211 °C; Major diastereoisomer. 5-Acetyl-3-(pyridin-3-ylmethylene)indolin-2-one. $^1$H NMR (600 MHz, DMSO-$d_6$) δ 11.10 (bs, 1H), 9.24 (d, *J* = 2.2 Hz, 1H), 8.93–8.91 (m, 2H), 8.61 (dd, *J* = 4.8, 1.7 Hz, 1H), 8.08 (s, 1H), 7.94–7.91 (m, 1H), 7.51 (dd, *J* = 8.1, 4.8 Hz, 1H), 6.94 (d, *J* = 8.2 Hz, 1H), 2.58 (s, 3H). Minor diastereoisomer. 5-Acetyl-3-(pyridin-3-ylmethylene)indolin-2-one. $^1$H NMR (600 MHz, DMSO-$d_6$) δ 11.08 (bs, 1H), 8.69 (dd, *J* = 4.8, 1.6 Hz, 1H), 8.38 (d, *J* = 1.6 Hz, 1H), 8.23–8.15 (m, 1H), 7.99 (d, *J* = 1.7 Hz, 1H), 7.94–7.91 (m, 1H), 7.73 (s, 1H), 7.59 (dd, *J* = 7.7, 5.0 Hz, 1H), 6.99 (d, *J* = 8.2 Hz, 1H), 2.42 (s, 3H). HRMS *m/z* $[M+H]^+$ calcd for $C_{16}H_{13}N_2O_2$: 265.0977, found 265.0967, LC $t_R$ = 2.46 min, >98% Purity.

**(3Z)-2-oxo-3-(1H-pyrrol-2-ylmethylidene)-2,3-dihydro-1H-indole-5-carboxylic acid (33)**: Compound **33** was prepared by procedure A to afford a dark orange solid (90 mg, 0.354 mmol, 42%, E/Z ratio 30:70). MP > 220 °C (decomp.); (*Z*)-3-((1*H*-pyrrol-2-yl)methylene)-2-oxoindoline-5-carboxylic acid. $^1$H NMR (600 MHz, DMSO-$d_6$) δ 13.28 (bs, 1H), 11.07 (bs, 1H), 8.18 (d, *J* = 1.5 Hz, 1H), 7.77 (dd, *J* = 8.0, 1.4 Hz, 1H), 7.77 (s, 1H), 7.34–7.33 (m, 1H), 6.88–6.85 (m, 1H), 6.83 (d, *J* = 8.0 Hz, 1H), 6.34 (dt, *J* = 3.7, 2.3 Hz, 1H). $^{13}$C NMR (125 MHz, DMSO-$d_6$) δ 170.3, 169.7, 140.1, 129.7 (s, 2C), 128.6, 126.1, 125.4, 124.1, 120.3, 119.5, 117.1, 111.3, 108.3. (*E*)-3-((1*H*-pyrrol-2-yl)methylene)-2-oxoindoline-5-carboxylic acid. $^1$H NMR (600 MHz, DMSO-$d_6$) δ 11.91 (bs, 1H), 10.58 (bs, 1H), 8.59 (d, *J* = 1.5 Hz, 1H), 7.81 (dd, *J* = 8.0, 1.4 Hz, 1H), 7.52 (s, 1H), 7.21–7.20 (m, 1H), 7.15–7.05 (m, 1H), 6.80 (d, *J* = 8.0 Hz, 1H), 6.42–6.41 (m, 1H). $^{13}$C NMR (125 MHz, DMSO-$d_6$) δ 170.3, 169.7142.6, 132.2, 129.8 (s, 2C), 127.6, 124.8, 124.0, 123.1, 120.9, 113.5, 111.5, 108.2. HRMS *m/z* $[M+H]^+$ calcd for $C_{14}H_{11}N_2O_3$: 255.0770, found 255.0762, LC $t_R$ = 3.79 min, >98% Purity.

**(3Z)-3-(1H-imidazole-5-ylmethylidene)-2-oxo-2,3-dihydro-1H-indole-5-carboxylic acid (34)**: Compound **34** was prepared by procedure A to afford a yellow solid (104 mg, 0.408 mmol, 48%). MP > 300 °C; $^1$H NMR (600 MHz, DMSO-$d_6$) δ 10.75 (s, 1H), 9.90 (s, 1H), 8.25 (s, 1H), 8.07 (s, 1H), 7.96 (s, 1H), 7.83 (dd, *J* = 8.1, 1.7 Hz, 1H), 7.54 (s, 1H), 6.89 (d, *J* = 8.1 Hz, 1H). $^{13}$C NMR (150 MHz, DMSO-$d_6$) δ 170.3, 167.9, 145.3, 138.3, 130.6, 129.8, 128.2, 126.6, 124.4, 123.9, 122.4, 120.6, 108.6. HRMS *m/z* $[M+H]^+$ calcd for $C_{13}H_{10}N_3O_3$: 256.0722, found 256.0716, LC $t_R$ = 2.46 min, >98% Purity.

**(3Z)-3-(1H-imidazole-2-ylmethylidene)-2-oxo-2,3-dihydro-1H-indole-5-carboxylic acid (35)**: Compound **35** was prepared by procedure A to afford a yellow solid (113 mg, 0.443 mmol, 52%). MP > 260 °C (decomp.); $^1$H NMR (600 MHz, DMSO-$d_6$) δ 14.34 (s, 1H), 8.15

(d, $J = 1.4$ Hz, 1H), 7.83 (dd, $J = 8.0$, 1.4 Hz, 1H), 7.57 (s, 1H), 7.53 (s, 1H), 7.36–7.25 (m, 1H), 6.81 (d, $J = 7.9$ Hz, 1H). $^{13}$C NMR (150 MHz, DMSO-$d_6$) δ 174.4, 169.3, 143.9, 137.0, 134.7, 132.2, 130.5, 128.2, 125.0, 123.0, 122.8, 120.5, 108.8. HRMS *m/z* $[M+H]^+$ calcd for $C_{13}H_{10}N_3O_3$: 256.0722, found 256.0714, LC $t_R$ = 2.46 min, >98% Purity.

**5-butyrylindolin-2-one** (**36**): Compound **36** was prepared by procedure B to afford a colourless solid (901 mg, 4.431 mmol, 59%). MP 130–132 °C; $^1$H NMR (400 MHz, DMSO-$d_6$) δ 10.73 (s, 1H), 7.89–7.82 (m, 1H), 7.82–7.76 (m, 1H), 6.89 (d, $J = 8.1$ Hz, 1H), 3.54 (s, 2H), 2.90 (t, $J = 7.2$ Hz, 2H), 1.61 (h, $J = 7.3$ Hz, 2H), 0.91 (t, $J = 7.4$ Hz, 3H). $^{13}$C NMR (100 MHz, DMSO-$d_6$) δ 198.5, 176.8, 148.2, 130.4, 129.0, 126.1, 124.1, 108.7, 39.4, 35.5, 17.6, 13.7. HRMS *m/z* $[M+H]^+$ calcd for $C_{12}H_{14}NO_2$: 204.1025, found 204.1017, LC $t_R$ = 3.18 min, >98% Purity.

**5-benzoylindolin-2-one** (**37**): Compound **37** was prepared by procedure C to afford a colourless solid (1.319 g, 5.555 mmol, 74%). MP 186–188 °C; $^1$H NMR (400 MHz, DMSO-$d_6$) δ 10.81 (s, 1H), 7.73–7.59 (m, 5H), 7.57–7.51 (m, 2H), 6.95 (d, $J = 8.6$ Hz, 1H), 3.57 (s, 2H). $^{13}$C NMR (100 MHz, DMSO-$d_6$) δ 194.7, 176.7, 148.3, 138.0, 131.9, 131.3, 130.0, 129.2 (s, 2C), 128.4 (s, 2C), 126.2, 126.0, 108.7, 35.6. HRMS *m/z* $[M+H]^+$ calcd for $C_{15}H_{12}NO_2$: 238.0868, found 238.0858, LC $t_R$ = 3.36 min, >98% Purity.

**5-(4-fluorobenzoyl)indolin-2-one** (**38**): Compound **38** was prepared by procedure B to afford a colourless/light green solid (571 mg, 2.237 mmol, 30%). MP 155–157 °C; $^1$H NMR (400 MHz, DMSO-$d_6$) δ 10.86 (s, 1H), 7.76–7.55 (m, 3H), 7.51 (td, $J = 7.4$, 1.7 Hz, 1H), 7.40–7.31 (m, 2H), 6.95 (d, $J = 8.6$ Hz, 1H), 3.57 (s, 2H). 13C NMR (100 MHz, DMSO-$d_6$) δ 191.4, 176. 8, 158.8 (d, $J = 247.6$ Hz), 149.3, 132.8 (d, $J = 8.2$ Hz), 131.2, 130.0 (d, $J = 14.9$ Hz), 129.9, 127.20 (d, $J = 16.1$ Hz), 126.5, 125.5, 124.7 (d, $J = 3.4$ Hz), 116.1 (d, $J = 21.4$ Hz), 109.0, 35.5. HRMS *m/z* $[M+H]^+$ calcd for $C_{15}H_{11}FNO_2$: 256.0774, found 256.0763, LC $t_R$ = 3.40 min, >98% Purity.

**5-(furan-2-carbonyl)indolin-2-one** (**39**): Compound **39** was prepared by procedure B to afford a beige solid (836 mg, 3.579 mmol, 49%). Consistent with previous report [95].

**(3Z)-5-butanoyl-3-(1H-pyrrol-2-ylmethylidene)-2,3-dihydro-1H-indol-2-one** (**40**): Compound **40** was prepared by procedure A to afford a mustard solid (43 mg, 0.153 mmol, 31%). MP 153–155 °C; $^1$H NMR (400 MHz, DMSO-$d_6$) δ 13.22 (s, 1H), 11.23 (s, 1H), 8.30 (d, $J = 1.6$ Hz, 1H), 7.99 (s, 1H), 7.82 (dd, $J = 8.2$, 1.7 Hz, 1H), 7.40 (q, $J = 1.8$, 1.3 Hz, 1H), 6.97 (d, $J = 8.2$ Hz, 1H), 6.92 (dt, $J = 3.6$, 1.7 Hz, 1H), 6.39 (dt, $J = 3.7$, 2.3 Hz, 1H), 2.99 (t, $J = 7.2$ Hz, 2H), 1.66 (h, $J = 7.3$ Hz, 2H), 0.95 (t, $J = 7.4$ Hz, 3H). $^{13}$C NMR (100 MHz, DMSO-$d_6$) δ 198.8, 169.6, 142.6, 130.6, 129.6, 127.8, 127.5, 126.5, 125.3, 121.3, 118.6, 115.6, 111.8, 109.2, 17.6 (s, 2C), 13.8. HRMS *m/z* $[M+H]^+$ calcd for $C_{17}H_{17}N_2O_2$: 281.1290, found 281.1286, LC $t_R$ = 4.85 min, >98% Purity.

**(3Z)-5-butanoyl-3-(1H-imidazole-5-ylmethylidene)-2,3-dihydro-1H-indol-2-one** (**41**): Compound **41** was prepared by procedure A to afford a bright yellow solid (58 mg, 0.207 mmol, 42%). MP > 300 °C; $^1$H NMR (600 MHz, DMSO-$d_6$) δ 10.52 (s, 1H), 10.36 (d, $J = 1.9$ Hz, 1H), 8.53 (s, 1H), 7.75–7.61 (m, 3H), 7.51 (s, 1H), 6.85 (d, $J = 8.1$ Hz, 1H), 2.96 (t, $J = 7.3$ Hz, 2H), 1.74–1.68 (m, 2H), 0.99 (t, $J = 7.4$ Hz, 3H). $^{13}$C NMR (150 MHz, DMSO-$d_6$) δ 174.3, 170.5, 165.8, 156.3, 148.0, 145.3, 130.8, 124.3, 122.2, 121.8, 114.0, 111.9, 108.1, 48.6, 25.6, 14.0. HRMS *m/z* $[M+H]^+$ calcd for $C_{16}H_{16}N_3O_2$: 282.1243, found 282.1233, LC $t_R$ = 3.36 min, >98% Purity.

**(3Z)-5-butanoyl-3-(1H-imidazole-2-ylmethylidene)-2,3-dihydro-1H-indol-2-one** (**42**): Compound **42** was prepared by procedure A to afford a bright yellow solid (77 mg, 0.274 mmol, 56%). MP > 300 °C; $^1$H NMR (600 MHz, DMSO-$d_6$) δ 13.98 (s, 1H), 11.48 (s, 1H), 8.56 (d, $J = 1.6$ Hz, 1H), 8.08 (s, 1H), 7.89 (dd, $J = 8.2$, 1.7 Hz, 1H), 7.59 (d, $J = 2.1$ Hz, 1H), 7.39 (d, $J = 1.1$ Hz, 1H), 7.02 (d, $J = 8.2$ Hz, 1H), 3.03 (t, $J = 7.2$ Hz, 2H), 1.65 (q, $J = 7.3$ Hz, 2H), 0.96 (t, $J = 7.4$ Hz, 3H). $^{13}$C NMR (150 MHz, DMSO-$d_6$) δ 199.0, 169.4, 143.6, 143.5, 132.9, 131.1, 129.2, 125.9, 124.1, 122.6, 121.2, 120.8, 109.9, 40.1, 17.6, 13.8. HRMS *m/z* $[M+H]^+$ calcd for $C_{16}H_{16}N_3O_2$: 282.1243, found 282.1236, LC $t_R$ = 3.29 min, >98% Purity.

**(3Z)-5-benzoyl-3-(1H-pyrrol-2-ylmethylidene)-2,3-dihydro-1H-indol-2-one** (**43**): Compound **43** was prepared by procedure A to afford a red solid (29 mg, 0.092 mmol, 22%). MP 232–234 °C; $^1$H NMR (400 MHz, DMSO-$d_6$) δ 13.21 (s, 1H), 11.29 (s, 1H), 8.10 (d, $J = 1.6$ Hz, 1H), 7.97 (s, 1H), 7.78–7.70 (m, 2H), 7.69–7.64 (m, 1H), 7.61–7.53 (m, 3H), 7.41 (q, $J = 1.8$, 1.2 Hz, 1H), 7.03 (d, $J = 8.1$ Hz, 1H), 6.93 (dt, $J = 3.6$, 1.7 Hz, 1H), 6.38 (dt, $J = 3.7$, 2.3 Hz, 1H). $^{13}$C NMR (100 MHz, DMSO-$d_6$) δ 195.1, 169.6, 142.6, 138.0, 132.1, 130.4, 130.0, 129.6, 129.4 (s, 2C), 128.5 (s, 2C), 128.1, 126.6, 125.4, 121.6, 119.9, 115.2, 111.8, 109.1. HRMS *m/z* $[M+H]^+$ calcd for $C_{20}H_{15}N_2O_2$: 315.1134, found 315.1120, LC $t_R$ = 4.90 min, >98% Purity.

**(3Z)-5-benzoyl-3-(1H-imidazole-5-ylmethylidene)-2,3-dihydro-1H-indol-2-one** (**44**): Compound **44** was prepared by procedure A to afford a dark orange solid (24 mg, 0.076 mmol, 24%). MP 255–257 °C; $^1$H NMR (400 MHz, DMSO-$d_6$) δ 10.86 (s, 1H), 9.96 (s, 1H), 7.95 (d, $J = 1.0$ Hz, 1H), 7.78–7.71 (m, 4H), 7.69–7.55 (m, 5H), 6.99 (d, $J = 8.1$ Hz, 1H). $^{13}$C NMR (100 MHz, DMSO-$d_6$) δ 194.9, 170.3, 145.6, 138.3, 137.8, 136.9, 131.7, 131.3, 129.9, 129.5, 129.3 (s, 2C), 128.6, 128.2 (s, 2C), 126.6, 122.34, 120.6, 108.9. HRMS *m/z* $[M+H]^+$ calcd for $C_{19}H_{14}N_3O_2$: 316.1086, found 316.1076, LC $t_R$ = 3.51 min, >98% Purity.

**(3Z)-5-[(4-fluorophenyl)carbonyl]-3-(1H-pyrrol-2-ylmethylidene)-2,3-dihydro-1H-indol-2-one** (**45**): Compound **45** was prepared by procedure A to afford a dark orange solid (37 mg, 0.111 mmol, 28%). MP 242–244 °C; $^1$H NMR (400 MHz, DMSO-$d_6$) δ 13.19 (s, 1H), 11.35 (s, 1H), 8.14 (d, $J = 1.6$ Hz, 1H), 7.98 (s, 1H), 7.65 (ddd, $J = 13.9$, 5.5, 2.7 Hz, 1H), 7.62–7.51 (m, 2H), 7.46–7.30 (m, 3H), 7.02 (d, $J = 8.1$ Hz, 1H), 6.94 (dt, $J = 3.7$, 1.7 Hz, 1H), 6.39 (dt, $J = 4.1$, 2.3 Hz, 1H). $^{13}$C NMR (100 MHz, DMSO-$d_6$) δ 191.7, 169.6, 159.0 (d, $J = 248.1$ Hz), 143.5, 132.9 (d, $J = 8.2$ Hz), 130.4, 130.2 (d, $J = 3.0$ Hz), 130.0, 129.6, 128.3, 127.3 (d, $J = 15.7$ Hz), 126.8, 125.7, 124.7 (d, $J = 3.4$ Hz), 121.8, 119.3, 116.2 (d, $J = 21.4$ Hz), 114.9, 111.8, 109.3. HRMS *m/z* $[M+H]^+$ calcd for $C_{20}H_{14}N_2O_2F$: 333.1039, found 333.1035, LC $t_R$ = 4.88 min, >98% Purity.

**(3Z)-5-[(4-fluorophenyl)carbonyl]-3-(1H-imidazole-5-ylmethylidene)-2,3-dihydro-1H-indol-2-one** (**46**): Compound **46** was prepared by procedure A to afford a bright yellow solid (51 mg, 0.153 mmol, 39%). MP > 300 °C; $^1$H NMR (600 MHz, DMSO-$d_6$) δ 10.04 (d, $J = 1.6$ Hz, 1H), 7.98 (d, $J = 39.4$ Hz, 1H), 7.75 (s, 1H), 7.70 (dd, $J = 8.2$, 1.9 Hz, 1H), 7.66 (tdd, $J = 7.5$, 5.3, 1.8 Hz, 1H), 7.53 (dd, $J = 7.2$, 1.9 Hz, 1H), 7.50 (d, $J = 5.3$ Hz, 1H), 7.42 (s, 1H), 7.39 (d, $J = 3.9$ Hz, 1H), 7.37 (d, $J = 7.5$ Hz, 1H), 6.94 (d, $J = 8.2$ Hz, 1H). $^{13}$C NMR (150 MHz, DMSO-$d_6$) δ 192.1, 173.7, 170.8, 158.9 (d, $J = 246.5$ Hz), 145.3, 137.1, 132.1 (d, $J = 8.5$ Hz), 129.9, 129.8 (d, $J = 3.6$ Hz, 2C), 129.6, 129.6, 128.2 (d, $J = 16.6$ Hz, 2C), 128.1, 124.5 (d, $J = 3.5$ Hz), 123.6, 115.9 (d, $J = 21.5$ Hz), 108.6. HRMS *m/z* $[M+H]^+$ calcd for $C_{19}H_{13}N_3O_2F$: 334.0992, found 334.0979, LC $t_R$ = 3.57 min, >98% Purity.

**(Z)-3-((1H-pyrrol-2-yl)methylene)-5-(furan-2-carbonyl)indolin-2-one** (**47**): Compound **47** was prepared by procedure A to afford a yellow solid (19 mg, 0.062 mmol, 14%). MP > 220 °C (decomp.); $^1$H NMR (600 MHz, DMSO-$d_6$) δ 13.82 (s, 1H), 8.53 (s, 1H), 8.13 (s, 1H), 8.08 (d, $J = 1.6$ Hz, 1H), 7.83 (s, 1H), 7.78 (dd, $J = 8.2$, 1.7 Hz, 1H), 7.37 (d, $J = 3.5$ Hz, 1H), 7.33 (s, 1H), 6.95 (d, $J = 8.1$ Hz, 1H), 6.91–6.80 (m, 1H), 6.78 (dd, $J = 3.6$, 1.7 Hz, 1H), 6.34 (d, $J = 3.0$ Hz, 1H). $^{13}$C NMR (150 MHz, DMSO-$d_6$) δ 180.6, 174.2, 165.6, 151.9, 147.6, 133.6, 130.0, 129.2, 126.6, 125.4, 119.8, 118.9, 116.2, 115.5, 114.1, 112.4, 111.3, 109.9. HRMS *m/z* $[M+H]^+$ calcd for $C_{18}H_{13}N_2O_3$: 305.0926, found 305.0920, LC $t_R$ = 4.44 min, >98% Purity.

**(3Z)-5-[(furan-2-yl)carbonyl]-3-(1H-imidazole-2-ylmethylidene)-2,3-dihydro-1H-indol-2-one** (**48**): Compound **48** was prepared by procedure A to afford a yellow solid (23 mg, 0.075 mmol, 17%). MP > 270 °C (decomp.); $^1$H NMR (600 MHz, DMSO-$d_6$) δ 10.73 (s, 2H), 10.55 (s, 1H), 8.53 (s, 1H), 8.09 (d, $J = 1.6$ Hz, 1H), 7.81 (dd, $J = 8.1$, 2.0 Hz, 1H), 7.73 (d, $J = 3.6$ Hz, 1H), 7.53 (s, 1H), 7.36 (s, 1H), 6.96 (d, $J = 8.1$ Hz, 1H), 6.85 (dd, $J = 3.5$, 1.7 Hz, 1H). $^{13}$C NMR (150 MHz,

DMSO-$d_6$) δ 180.4, 173.9, 165.5, 151.6, 147.5, 131.8, 129.7, 129.2, 127.6, 122.5, 120.1, 117.3, 114.9, 114.0, 112.4, 111.2, 108.6. HRMS *m/z* $[M+H]^+$ calcd for $C_{17}H_{12}N_3O_3$: 306.0879, found 306.0867, LC $t_R$ = 2.96 min, >98% Purity.

***N,N*-dimethyl-2-oxoindoline-5-sulfonamide** (**50**): Compound **50** was prepared by procedure D to afford a beige solid (447 mg, 1.985 mmol, 55%). MP 198–200 °C; $^1$H NMR (400 MHz, DMSO-$d_6$) δ 10.82 (s, 1H), 7.67–7.46 (m, 2H), 7.04–6.96 (m, 1H), 3.60 (s, 2H), 2.57 (s, 6H). $^{13}$C NMR (100 MHz, DMSO-$d_6$) δ 176.4, 148.0, 128.4, 126.9, 126.9, 123.7, 109.1, 37.6 (s, 2C), 35.7. HRMS *m/z* $[M+H]^+$ calcd for $C_{10}H_{13}N_2O_3S$: 241.0649, found 241.0633.

**5-((4-methylpiperazin-1-yl)sulfonyl)indolin-2-one** (**51**): Compound **51** was prepared by procedure D to afford a beige/brown solid (496 mg, 1.679 mmol, 39%). MP 170–172 °C; HRMS *m/z* $[M+H]^+$ calcd for $C_{13}H_{18}N_3O_3S$: 296.1069, found 296.1054. Consistent with previous report [96].

**(3Z)-*N,N*-dimethyl-2-oxo-3-(1H-pyrrol-2-ylmethylidene)-2,3-dihydro-1H-indole-5-sulfonamide** (**52**): Compound **52** was prepared by procedure A to afford an orange solid (54 mg, 0.170 mmol, 41%). MP 258–260 °C; $^1$H NMR (400 MHz, DMSO-$d_6$) δ 13.23 (s, 1H), 11.33 (s, 1H), 8.11 (s, 1H), 8.05 (d, *J* = 1.7 Hz, 1H), 7.53 (dd, *J* = 8.2, 1.8 Hz, 1H), 7.44 (q, *J* = 2.3 Hz, 1H), 7.09 (d, *J* = 8.2 Hz, 1H), 6.94 (dt, *J* = 3.7, 1.7 Hz, 1H), 6.41 (dt, *J* = 4.1, 2.3 Hz, 1H), 2.61 (s, 6H). $^{13}$C NMR (100 MHz, DMSO-$d_6$) δ 169.3, 142.1, 129.6, 128.9, 127.1, 127.1, 126.6, 125.9, 122.0, 117.9, 114.7, 112.0, 109.5, 37.7 (2C, s). HRMS *m/z* $[M+H]^+$ calcd for $C_{15}H_{16}N_3O_3S$: 318.0912, found 318.0897, LC $t_R$ = 4.10 min, >98% Purity.

**(3Z)-3-(1H-imidazole-5-ylmethylidene)-*N,N*-dimethyl-2-oxo-2,3-dihydro-1H-indole-5-sulfonamide** (**53**): Compound **53** was prepared by procedure A to afford an orange solid (52 mg, 0.217 mmol, 52%). MP 275–277 °C; $^1$H NMR (400 MHz, DMSO-$d_6$) δ 12.81 (s, 1H), 10.87 (s, 1H), 9.92 (d, *J* = 1.9 Hz, 1H), 8.07 (t, *J* = 0.9 Hz, 1H), 8.02 (d, *J* = 1.1 Hz, 1H), 7.62 (d, *J* = 0.7 Hz, 1H), 7.58 (dd, *J* = 8.2, 2.0 Hz, 1H), 7.04–6.99 (m, 1H), 2.65 (s, 6H). $^{13}$C NMR (100 MHz, DMSO-$d_6$) δ 170.0, 145.1, 138.3, 136.9, 129.4, 128.4, 127.14, 127.09, 125.9, 123.0, 120.1, 108.9, 37.8. HRMS *m/z* $[M+H]^+$ calcd for $C_{14}H_{15}N_4O_3S$: 319.0865, found 319.0850, LC $t_R$ = 2.54 min, >98% Purity.

**(3Z)-5-[(4-methylpiperazin-1-yl)sulfonyl]-3-(1H-pyrrol-2-ylmethylidene)-2,3-dihydro-1H-indol-2-one** (**54**): Compound **54** was prepared by procedure A to afford a bright yellow solid (82 mg, 0.220 mmol, 65%). MP > 260 °C (decomp.); $^1$H NMR (400 MHz, DMSO-$d_6$) δ 13.23 (s, 1H), 11.35 (s, 1H), 8.09 (s, 1H), 8.02 (d, *J* = 1.7 Hz, 1H), 7.51 (dd, *J* = 8.2, 1.8 Hz, 1H), 7.44 (q, *J* = 2.2 Hz, 1H), 7.09 (d, *J* = 8.1 Hz, 1H), 6.95 (dt, *J* = 3.6, 1.7 Hz, 1H), 6.41 (dt, *J* = 4.0, 2.3 Hz, 1H), 2.89 (t, *J* = 4.7 Hz, 4H), 2.36 (t, *J* = 4.9 Hz, 4H), 2.13 (s, 3H). $^{13}$C NMR (100 MHz, DMSO-$d_6$) δ 169.3, 142.2, 129.6, 129.0, 127.2, 127.2, 126.6, 125.9, 122.1, 117.8, 114.6, 112.0, 109.5, 53.5, 45.8 (s, 2C), 45.3 (s, 2C). HRMS *m/z* $[M+H]^+$ calcd for $C_{18}H_{21}N_4O_3S$: 373.1334, found 373.1326, LC $t_R$ = 3.10 min, >98% Purity.

**(3Z)-3-(1H-imidazole-5-ylmethylidene)-5-[(4-methylpiperazin-1-yl)sulfonyl]-2,3-dihydro-1H-indol-2-one** (**55**): Compound **55** was prepared by procedure A to afford a bright yellow solid (67 mg, 0.228 mmol, 67%). MP > 260 °C (decomp.); $^1$H NMR (600 MHz, DMSO-$d_6$) δ 10.85 (s, 1H), 9.96 (d, *J* = 1.9 Hz, 1H), 7.97 (s, 1H), 7.94 (s, 1H), 7.59 (s, 1H), 7.52 (dd, *J* = 8.1, 2.0 Hz, 1H), 6.99 (d, *J* = 8.1 Hz, 1H), 2.95 (s, 4H), 2.36 (d, *J* = 5.2 Hz, 4H), 2.12 (s, 3H). $^{13}$C NMR (150 MHz, DMSO-$d_6$) δ 170.2, 144.7, 140.9, 137.0, 129.9, 127.8, 127.7, 127.0, 125.6, 123.4, 118.5, 108.6, 53.7 (s, 2C), 45.9 (s, 2C), 45.3. HRMS *m/z* $[M+H]^+$ calcd for $C_{17}H_{20}N_5O_3S$: 374.1287, found 374.1276, LC $t_R$ = 2.29 min, >98% Purity.

**(Z)-3-((1H-pyrrol-2-yl)methylene)-5-isopropoxyindolin-2-one** (**57**): Compound **57** was prepared by procedure A to afford a red solid (48 mg, 0.179 mmol, 68%). MP 149–151 °C; $^1$H NMR (400 MHz, DMSO-$d_6$) δ 13.39 (s, 1H), 10.68 (s, 1H), 7.76 (s, 1H), 7.34 (td, *J* = 2.6, 1.3 Hz, 1H), 7.31 (d, *J* = 2.3 Hz, 1H), 6.79 (dt, *J* = 3.6, 1.7 Hz, 1H), 6.75 (d, *J* = 8.3 Hz, 1H), 6.70 (dd, *J* = 8.4, 2.3 Hz, 1H), 6.35 (dt, *J* = 3.6, 2.3 Hz, 1H), 4.54 (p, *J* = 6.0 Hz, 1H), 1.26 (s, 3H), 1.25 (s, 3H). $^{13}$C NMR (100 MHz, DMSO-$d_6$) δ 169.3, 152.8, 132.9, 129.5, 126.6, 126.2, 125.5, 120.1, 117.4, 115.4, 111.4, 110.0, 107.0, 70.1, 22.0 (s, 2C). HRMS *m/z* $[M+H]^+$ calcd for $C_{16}H_{17}N_2O_2$: 269.1290, found 269.1283, LC $t_R$ = 4.97 min, >98% Purity.

**(3Z)-3-(1H-imidazole-5-ylmethylidene)-5-(propan-2-yloxy)-2,3-dihydro-1H-indol-2-one** (**58**): Compound **58** was prepared by procedure A to afford an orange solid (37 mg, 0.137 mmol, 53%). MP 211–213 °C; $^1$H NMR (400 MHz, DMSO-$d_6$) δ 13.79 (s, 1H), 10.81 (s, 1H), 8.01 (s, 1H), 7.87 (s, 1H), 7.59 (s, 1H), 7.36–7.34 (m, 1H), 6.76 (d, *J* = 3.0 Hz, 2H), 4.57–4.51 (m, 1H), 1.27 (s, 3H), 1.25 (s, 3H). $^{13}$C NMR (100 MHz, DMSO-$d_6$) δ $^{13}$C NMR (100 MHz, DMSO-$d_6$) δ 169.1, 153.0, 139.5, 138.1, 133.6, 128.1, 125.4, 123.1, 120.6, 116.5, 110.3, 107.7, 70.1, 22.0. HRMS *m/z* $[M+H]^+$ calcd for $C_{15}H_{16}N_3O_2$: 270.1243, found 270.1230, LC $t_R$ = 3.42 min, >98% Purity.

**(3Z)-3-(1H-imidazole-2-ylmethylidene)-5-(propan-2-yloxy)-2,3-dihydro-1H-indol-2-one** (**59**): Compound **59** was prepared by procedure A to afford a bright orange solid (44 mg, 0.163 mmol, 62%). MP 256–258 °C; $^1$H NMR (400 MHz, DMSO-$d_6$) δ 10.30 (s, 1H), 9.17 (d, *J* = 2.6 Hz, 1H), 7.85 (s, 1H), 7.55–7.34 (m, 3H), 6.79 (d, *J* = 1.4 Hz, 2H), 4.59 (p, *J* = 6.0 Hz, 1H), 1.30–1.25 (m, 6H). $^{13}$C NMR (100 MHz, DMSO-$d_6$) δ 169.0, 153.2, 143.7, 133.7, 132.5, 125.0, 124.7, 124.2, 120.6, 117.4, 110.6, 108.3, 69.9, 22.0 (s, 2C). HRMS *m/z* $[M+H]^+$ calcd for $C_{15}H_{16}N_3O_2$: 270.1243, found 270.1230, LC $t_R$ = 3.29 min, >98% Purity.

***N*-(2-oxoindolin-5-yl)butyramide** (**60**): Compound **60** was prepared by procedure F to afford a colourless solid (552 mg, 2.531 mmol, 75%). MP 165–167 °C; $^1$H NMR (600 MHz, DMSO-$d_6$) δ 10.26 (s, 1H), 9.70 (s, 1H), 7.55–7.47 (m, 1H), 7.32 (dd, *J* = 8.3, 2.0 Hz, 1H), 6.71 (d, *J* = 8.3 Hz, 1H), 3.44 (s, 2H), 2.23 (t, *J* = 7.3 Hz, 2H), 1.59 (h, *J* = 7.4 Hz, 2H), 0.90 (t, *J* = 7.4 Hz, 3H). $^{13}$C NMR (150 MHz, DMSO-$d_6$) δ 176.3, 170.6, 139.1, 133.5, 126.0, 118.4, 116.5, 108.8, 38.3, 36.1, 18.7, 13.6. HRMS *m/z* $[M+H]^+$ calcd for $C_{12}H_{15}N_2O_2$: 219.1134, found 219.1125, LC $t_R$ = 2.51 min, >98% Purity.

**2-ethyl-*N*-(2-oxoindolin-5-yl)butanamide** (**61**): Compound **61** was prepared by procedure F to afford a colourless solid (590 mg, 2.395 mmol, 71%). MP 228–230 °C; $^1$H NMR (400 MHz, DMSO-$d_6$) δ 10.26 (s, 1H), 9.68 (s, 1H), 7.54 (d, *J* = 2.0 Hz, 1H), 7.33 (dd, *J* = 8.4, 2.1 Hz, 1H), 6.72 (d, *J* = 8.3 Hz, 1H), 3.45 (s, 2H), 2.16 (tt, *J* = 9.4, 5.1 Hz, 1H), 1.59–1.48 (m, 2H), 1.47–1.36 (m, 2H), 0.84 (t, *J* = 7.4 Hz, 6H). $^{13}$C NMR (100 MHz, DMSO-$d_6$) δ $^{13}$C NMR (100 MHz, DMSO-$d_6$) δ 176.3, 173.4, 139.2, 133.3, 126.0, 118.69, 116.8, 108.8, 49.8, 36.0, 25.3 (s, 2C), 11.9 (s, 2C). HRMS *m/z* $[M+H]^+$ calcd for $C_{14}H_{19}N_2O_2$: 247.1447, found 247.1436, LC $t_R$ = 3.06 min, >98% Purity.

***N*-(2-oxoindolin-5-yl)cyclohexanecarboxamide** (**62**): Compound **62** was prepared by procedure F to afford a colourless solid (780 mg, 2.632 mmol, 78%). MP 223–225 °C; $^1$H NMR (600 MHz, DMSO-$d_6$) δ 10.25 (s, 1H), 9.62 (s, 1H), 7.57–7.45 (m, 1H), 7.33 (dd, *J* = 8.4, 2.1 Hz, 1H), 6.70 (d, *J* = 8.3 Hz, 1H), 3.44 (s, 2H), 2.27 (tt, *J* = 11.7, 3.3 Hz, 1H), 2.03–1.67 (m, 4H), 1.68–1.60 (m, 1H), 1.39 (qd, *J* = 13.4, 12.9, 3.7 Hz, 2H), 1.29–1.13 (m, 3H). $^{13}$C NMR (150 MHz, DMSO-$d_6$) δ 176.3, 173.8, 139.0, 133.6, 125.9, 118.4, 116.5, 108.8, 44.8, 36.0, 29.2 (s, 2C), 25.42, 25.26 (s, 2C). HRMS *m/z* $[M+H]^+$ calcd for $C_{15}H_{19}N_2O_2$: 259.1447, found 259.1435, LC $t_R$ = 3.25 min, >98% Purity.

***N*-(2-oxoindolin-5-yl)benzamide** (**63**): Compound **63** was prepared by procedure F to afford a colourless solid (647 mg, 2.565 mmol, 76%). MP 115–117 °C; $^1$H NMR (600 MHz, DMSO-$d_6$) δ 10.37 (s, 1H), 10.14 (s, 1H), 7.99–7.90 (m, 2H), 7.67 (d, *J* = 2.0 Hz, 1H), 7.59–7.55 (m, 1H), 7.55–7.44 (m, 3H), 6.79 (d, *J* = 8.3 Hz, 1H), 3.49 (s, 2H). $^{13}$C NMR (150 MHz, DMSO-$d_6$) 176.4, 165.2, 139.8, 135.1, 133.2, 131.4, 128.4 (s, 2C), 127.6 (s, 2C), 125.9, 119.9, 117.8, 108.8, 36.1. HRMS *m/z* $[M+H]^+$ calcd for $C_{15}H_{13}N_2O_2$: 253.0977, found 253.0967, LC $t_R$ = 2.93 min, >98% Purity.

***N*-(2-oxoindolin-5-yl)furan-2-carboxamide** (**64**): Compound **55** was prepared by procedure F to afford a beige solid (605 mg, 2.498 mmol, 74%). $^1$H NMR (600 MHz, DMSO-$d_6$) δ 10.35 (s, 1H), 10.07 (s,

1H), 7.90 (d, $J = 1.6$ Hz, 1H), 7.64 (d, $J = 2.2$ Hz, 1H), 7.49 (dd, $J = 8.4$, 2.1 Hz, 1H), 7.29 (d, $J = 3.4$ Hz, 1H), 6.78 (d, $J = 8.3$ Hz, 1H), 6.68 (dd, $J = 3.5$, 1.7 Hz, 1H), 3.49 (s, 2H). $^{13}$C NMR (150 MHz, DMSO-$d_6$) δ 176.4, 156.0, 147.7, 145.5, 139.9, 132.4, 126.0, 120.0, 117.8, 114.3, 112.1, 108.8, 36.1. HRMS *m/z* $[M+H]^+$ calcd for $C_{13}H_{11}N_2O_3$: 243.0770, found 243.0759, LC $t_R = 2.51$ min, >98% Purity.

***N*-[(3Z)-2-oxo-3-(1H-pyrrol-2-ylmethylidene)-2,3-dihydro-1H-indol-5-yl] butanamide (65)**: Compound **65** was prepared by procedure A to afford a bright yellow solid (85 mg, 0.288 mmol, 63%). MP 260–262 °C; $^1$H NMR (400 MHz, DMSO-$d_6$) δ 13.34 (s, 1H), 10.80 (s, 1H), 9.74 (s, 1H), 7.95 (d, $J = 2.0$ Hz, 1H), 7.59 (s, 1H), 7.35 (q, $J = 2.2$ Hz, 1H), 7.17 (dd, $J = 8.3$, 2.0 Hz, 1H), 6.92 (dt, $J = 3.5$, 1.6 Hz, 1H), 6.80 (d, $J = 8.3$ Hz, 1H), 6.35 (dt, $J = 3.7$, 2.3 Hz, 1H), 2.27 (t, $J = 7.3$ Hz, 2H), 1.62 (h, $J = 7.4$ Hz, 2H), 0.93 (t, $J = 7.4$ Hz, 3H). $^{13}$C NMR (100 MHz, DMSO-$d_6$) δ 170.7, 169.3, 134.8, 133.5, 129.5, 126.1, 125.7, 125.1, 120.7, 118.8, 117.0, 111.4, 110.5, 109.4, 38.2, 18.7, 13.7. HRMS *m/z* $[M+H]^+$ calcd for $C_{17}H_{18}N_3O_2$: 296.1399, found 296.1392, LC $t_R = 4.14$ min, >98% Purity.

**2-ethyl-*N*-[(3Z)-2-oxo-3-(1H-pyrrol-2-ylmethylidene)-2,3-dihydro-1H-indol-5-yl] butanamide (66)**: Compound **66** was prepared by procedure A to afford a yellow solid (86 mg, 0.266 mmol, 66%). MP > 300 °C; $^1$H NMR (400 MHz, DMSO-$d_6$) δ 13.32 (s, 1H), 10.79 (s, 1H), 9.72 (s, 1H), 8.02–7.92 (m, 1H), 7.60 (s, 1H), 7.33 (td, $J = 2.6$, 1.4 Hz, 1H), 7.16 (dd, $J = 8.3$, 2.0 Hz, 1H), 6.90 (dt, $J = 3.6$, 1.7 Hz, 1H), 6.83–6.73 (m, 1H), 6.33 (dt, $J = 3.7$, 2.3 Hz, 1H), 2.18 (tt, $J = 9.4$, 5.1 Hz, 1H), 1.55 (ddq, $J = 13.2$, 9.0, 7.4 Hz, 2H), 1.48–1.35 (m, 2H), 0.86 (t, $J = 7.4$ Hz, 6H). $^{13}$C NMR (100 MHz, DMSO-$d_6$) δ 173.5, 169.3, 134.9, 133.3, 129.5, 126.2, 125.7, 125.1, 120.7, 119.1, 117.0, 111.4, 110.8, 109.4, 49.8, 25.3 (2C, s), 11.9 (2C, s). HRMS *m/z* $[M+H]^+$ calcd for $C_{19}H_{22}N_3O_2$: 324.1712, found 324.1702, LC $t_R = 4.56$ min, >98% Purity.

**2-ethyl-*N*-[(3Z)-3-(1H-imidazole-5-ylmethylidene)-2-oxo-2,3-dihydro-1H-indol-5-yl] butanamide (67)**: Compound **67** was prepared by procedure A to afford a yellow solid (70 mg, 0.216 mmol, 53%). MP 285–287 °C; $^1$H NMR (600 MHz, DMSO-$d_6$) δ 13.74 (s, 1H), 9.84 (s, 1H), 8.02 (s, 1H), 7.98 (s, 1H), 7.85 (d, $J = 22.8$ Hz, 1H), 7.71 (s, 1H), 7.24 (dd, $J = 8.2$, 2.0 Hz, 1H), 6.82 (d, $J = 8.2$ Hz, 1H), 2.21 (tt, $J = 9.5$, 5.0 Hz, 1H), 1.56 (dddd, $J = 13.5$, 7.3, 5.8, 1.9 Hz, 2H), 1.44 (ddd, $J = 13.0$, 7.3, 5.2 Hz, 2H), 0.87 (t, $J = 7.4$ Hz, 6H). $^{13}$C NMR (150 MHz, DMSO-$d_6$) δ 174.4, 173.6, 140.3, 135.8, 133.5, 132.5, 124.4, 121.2, 120.4, 120.0, 111.5, 109.6, 108.2, 49.7, 25.3 (s, 2C), 11.9 (s, 2C). HRMS *m/z* $[M+H]^+$ calcd for $C_{18}H_{21}N_4O_2$: 325.1665, found 325.1660, LC $t_R = 3.29$ min, >98% Purity.

**2-ethyl-*N*-[(3Z)-3-(1H-imidazole-2-ylmethylidene)-2-oxo-2,3-dihydro-1H-indol-5-yl] butanamide (68)**: Compound **68** was prepared by procedure A to afford a yellow solid (74 mg, 0.228 mmol, 56%). MP > 300 °C; $^1$H NMR (600 MHz, DMSO-$d_6$) δ 14.06 (s, 1H), 11.08 (s, 1H), 9.80 (s, 1H), 7.99 (s, 1H), 7.56 (d, $J = 4.2$ Hz, 2H), 7.46–7.27 (m, 2H), 6.86 (d, $J = 8.2$ Hz, 1H), 2.20 (tt, $J = 9.8$, 5.0 Hz, 1H), 1.56 (dq, $J = 15.5$, 7.6 Hz, 2H), 1.45 (dq, $J = 13.2$, 6.7, 6.0 Hz, 2H), 0.87 (t, $J = 7.5$ Hz, 6H). $^{13}$C NMR (150 MHz, DMSO-$d_6$) δ 173.7, 169.0, 143.4, 135.9, 133.8, 132.6, 124.0, 123.8, 123.7, 121.1, 120.9, 112.0, 110.0, 49.8, 25.3, 11.9. HRMS *m/z* $[M+H]^+$ calcd for $C_{18}H_{21}N_4O_2$: 325.1665, found 325.1656, LC $t_R = 3.24$ min, >98% Purity.

***N*-[(3Z)-2-oxo-3-(1H-pyrrol-2-ylmethylidene)-2,3-dihydro-1H-indol-5-yl] cyclohexanecarboxamide (69)**: Compound **69** was prepared by procedure A to afford a yellow solid (71 mg, 0.274 mmol, 71%). MP > 300 °C; $^1$H NMR (400 MHz, DMSO-$d_6$) δ 13.37–13.27 (m, 1H), 10.78 (s, 1H), 9.66 (s, 1H), 7.96 (d, $J = 1.9$ Hz, 1H), 7.57 (s, 1H), 7.33 (td, $J = 2.6$, 1.3 Hz, 1H), 7.14 (dd, $J = 8.3$, 2.0 Hz, 1H), 6.89 (dt, $J = 3.7$, 1.7 Hz, 1H), 6.78 (d, $J = 8.3$ Hz, 1H), 6.33 (dt, $J = 3.7$, 2.3 Hz, 1H), 2.33–2.25 (m, 1H), 1.76 (td, $J = 13.9$, 3.4 Hz, 4H), 1.64 (d, $J = 11.3$ Hz, 1H), 1.41 (qd, $J = 13.6$, 13.1, 3.5 Hz, 2H), 1.31–1.14 (m, 3H). $^{13}$C NMR (100 MHz, DMSO-$d_6$) δ 173.9, 169.3, 134.8, 133.6, 129.5, 126.1, 125.7, 125.0, 120.6, 118.8, 117.0, 111.4, 110.6, 109.4, 44.7, 29.2 (2C, s), 25.4, 25.3 (2C, s). HRMS *m/z* $[M+H]^+$ calcd for $C_{20}H_{22}N_3O_2$: 336.1712, found 336.1703, LC $t_R = 4.71$ min, >98% Purity.

***N*-[(3Z)-3-(1H-imidazole-5-ylmethylidene)-2-oxo-2,3-dihydro-1H-indol-5-yl] cyclohexanecarboxamide (70)**: Compound **70** was prepared by procedure A to afford a yellow solid (89 mg, 0.265 mmol, 68%). >300 °C; $^1$H NMR (400 MHz, DMSO-$d_6$) δ 13.70 (s, 1H), 10.89 (s, 1H), 9.71 (s, 1H), 8.00 (d, $J = 8.4$ Hz, 2H), 7.70 (s, 2H), 7.21 (d, $J = 8.3$ Hz, 1H), 6.81 (d, $J = 8.3$ Hz, 1H), 2.31 (tt, $J = 11.7$, 3.4 Hz, 1H), 2.08–1.67 (m, 4H), 1.65 (dd, $J = 10.5$, 4.0 Hz, 1H), 1.42 (qd, $J = 13.7$, 13.1, 3.5 Hz, 2H), 1.35–1.06 (m, 3H). $^{13}$C NMR (100 MHz, DMSO-$d_6$) δ 173.9, 168.9, 146.2, 139.5, 138.6, 135.5, 133.8, 128.0, 124.3, 123.7, 119.8, 111.2, 109.7, 44.7, 29.2 (2C, s), 25.4, 25.3 (2C, s). HRMS *m/z* $[M+H]^+$ calcd for $C_{19}H_{21}N_4O_2$: 337.1665, found 337.1657, LC $t_R = 3.47$ min, >98% Purity.

***N*-[(3Z)-3-(1H-imidazole-2-ylmethylidene)-2-oxo-2,3-dihydro-1H-indol-5-yl] cyclohexanecarboxamide (71)**: Compound **71** was prepared by procedure A to afford a yellow solid (81 mg, 0.241 mmol, 62%). MP > 300 °C; $^1$H NMR (600 MHz, DMSO-$d_6$) δ 14.05 (s, 1H), 11.07 (s, 1H), 9.74 (s, 1H), 7.98 (d, $J = 2.0$ Hz, 1H), 7.56 (d, $J = 2.1$ Hz, 1H), 7.51 (s, 1H), 7.38 (dd, $J = 8.4$, 2.0 Hz, 1H), 7.34 (t, $J = 1.2$ Hz, 1H), 6.85 (d, $J = 8.3$ Hz, 1H), 2.31 (tt, $J = 11.7$, 3.5 Hz, 1H), 1.78 (ddt, $J = 23.2$, 12.4, 3.3 Hz, 4H), 1.68–1.63 (m, 1H), 1.42 (qd, $J = 12.5$, 3.2 Hz, 2H), 1.27 (qt, $J = 12.4$, 3.1 Hz, 2H), 1.20 (tt, $J = 12.5$, 3.2 Hz, 1H). $^{13}$C NMR (150 MHz, DMSO-$d_6$) δ 174.0, 168.9, 143.4, 135.7, 134.1, 132.6, 123.8, 123.8, 123.8, 120.9, 120.8, 111.6, 110.0, 44.8, 29.2 (2C, s), 25.4, 25.3 (2C, s). HRMS *m/z* $[M+H]^+$ calcd for $C_{19}H_{21}N_4O_2$: 337.1665, found 337.1652, LC $t_R = 2.88$ min, >98% Purity.

***N*-[(3Z)-2-oxo-3-(1H-pyrrol-2-ylmethylidene)-2,3-dihydro-1H-indol-5-yl] benzamide (72)**: Compound **55** was prepared by procedure A to afford a mustard solid (60 mg, 0.182 mmol, 46%). MP 254–256 °C; $^1$H NMR (400 MHz, DMSO-$d_6$) δ 13.34 (s, 1H), 10.87 (s, 1H), 10.17 (s, 1H), 8.08 (d, $J = 1.9$ Hz, 1H), 8.03–7.94 (m, 2H), 7.65 (s, 1H), 7.62–7.50 (m, 3H), 7.43–7.33 (m, 2H), 6.92 (dt, $J = 3.6$, 1.7 Hz, 1H), 6.87 (d, $J = 8.3$ Hz, 1H), 6.36 (dt, $J = 3.7$, 2.3 Hz, 1H). $^{13}$C NMR (100 MHz, DMSO-$d_6$) δ 169.3, 165.1, 135.4, 135.0, 133.1, 131.4, 129.5, 128.4 (s, 2C), 127.5 (s, 2C), 126.2, 125.8, 125.1, 120.7, 120.3, 116.9, 112.0, 111.5, 109.4. HRMS *m/z* $[M+H]^+$ calcd for $C_{20}H_{16}N_3O_2$: 330.1242, found 330.1234, LC $t_R = 4.45$ min, >98% Purity.

***N*-[(3Z)-3-(1H-imidazole-5-ylmethylidene)-2-oxo-2,3-dihydro-1H-indol-5-yl] benzamide (73)**: Compound **73** was prepared by procedure A to afford an orange solid (78 mg, 0.236 mmol, 60%, *E*:Z ratio 43:57 - not able to distinguish E/Z isomers). MP > 300 °C; Major diastereoisomer. *N*-(3-((1*H*-imidazole-5-yl)methylene)-2-oxoindolin-5-yl) benzamide. $^1$H NMR (600 MHz, DMSO-$d_6$) δ 10.25 (bs, 1H), 10.19 (bs, 1H), 8.11 (d, $J = 2.1$ Hz, 1H), 8.01–7.95 (m, 3H), 7.84 (s, 1H), 7.74 (s, 1H), 7.55–7.49 (m, 3H), 7.45 (dd, $J = 8.3$, 2.0 Hz, 1H), 6.89 (d, $J = 8.3$ Hz, 1H). Minor diastereoisomer. *N*-(3-((1*H*-imidazole-5-yl)methylene)-2-oxoindolin-5-yl)benzamide. $^1$H NMR (600 MHz, DMSO-$d_6$) δ 10.32 (bs, 1H), 9.31 (bs, 1H), 8.00–7.98 (m, 1H), 7.81 (s, 1H), 7.59–7.55 (m, 2H), 7.53–7.50 (m, 3H), 7.49 (s, 1H), 7.40 (dd, $J = 8.2$, 2.2 Hz, 1H), 6.79 (d, $J = 8.2$ Hz, 1H). HRMS *m/z* $[M+H]^+$ calcd for $C_{19}H_{15}N_4O_2$: 331.1195, found 331.1181, LC $t_R = 3.20$ min, >98% Purity.

***N*-[(3Z)-3-(1H-imidazole-2-ylmethylidene)-2-oxo-2,3-dihydro-1H-indol-5-yl] benzamide (74)**: Compound **74** was prepared by procedure A to afford an orange solid (89 mg, 0.269 mmol, 68%). MP > 300 °C; $^1$H NMR (400 MHz, DMSO-$d_6$) δ 11.14 (s, 1H), 10.22 (s, 1H), 8.11 (d, $J = 2.0$ Hz, 1H), 7.98 (dd, $J = 7.0$, 1.9 Hz, 2H), 7.62–7.51 (m, 6H), 7.35 (d, $J = 1.4$ Hz, 1H), 6.93 (d, $J = 8.4$ Hz, 1H). $^{13}$C NMR (100 MHz, DMSO-$d_6$) δ 169.0, 165.3, 143.4, 136.4, 134.9, 133.6, 132.6, 131.5, 128.4 (s, 2C), 127.6 (s, 2C), 124.0, 123.8, 123.7, 122.3, 120.9, 113.3, 109.9. HRMS *m/z* $[M+H]^+$ calcd for $C_{19}H_{15}N_4O_2$: 331.1195, found 331.1186, LC $t_R = 3.23$ min, >98% Purity.

***N*-[(3Z)-2-oxo-3-(1H-pyrrol-2-ylmethylidene)-2,3-dihydro-1H-indol-5-yl] furan-2-carboxamide (75)**: Compound **75** was prepared by procedure A to afford an orange solid (74 mg, 0.232 mmol, 56%). MP 226–228 °C; $^1$H NMR (600 MHz, DMSO-$d_6$) δ 13.38 (s, 1H), 10.94 (s,

1H), 10.13 (s, 1H), 8.01 (d, $J$ = 2.0 Hz, 1H), 7.94 (d, $J$ = 1.7 Hz, 1H), 7.64 (s, 1H), 7.39 (dd, $J$ = 8.3, 2.0 Hz, 1H), 7.37 (t, $J$ = 1.9 Hz, 1H), 7.33 (d, $J$ = 3.5 Hz, 1H), 6.91 (dd, $J$ = 3.6, 1.4 Hz, 1H), 6.87 (d, $J$ = 8.3 Hz, 1H), 6.71 (dd, $J$ = 3.5, 1.8 Hz, 1H), 6.36 (dd, $J$ = 3.7, 2.4 Hz, 1H). $^{13}$C NMR (150 MHz, DMSO-$d_6$) δ 174.0, 169.4, 156.1, 147.7, 145.5, 135.8, 132.3, 129.5, 126.2, 125.8, 125.2, 120.6, 120.3, 117.0, 114.2, 112.1, 111.5, 109.5. HRMS $m/z$ [M+H]$^+$ calcd for $C_{18}H_{14}N_3O_3$: 320.1035, found 320.1018, LC $t_R$ = 3.90 min, >98% Purity.

***N*-[(3Z)-3-(1H-imidazole-2-ylmethylidene)-2-oxo-2,3-dihydro-1H-indol-5-yl] furan-2-carboxamide** (**76**): Compound **76** was prepared by procedure A to afford an orange solid (72 mg, 0.225 mmol, 54%). MP > 300 °C; $^1$H NMR (600 MHz, DMSO-$d_6$) δ 14.06 (s, 1H), 11.14 (s, 1H), 10.14 (s, 1H), 8.06 (d, $J$ = 2.0 Hz, 1H), 7.94 (dd, $J$ = 1.7, 0.8 Hz, 1H), 7.59 (s, 1H), 7.58–7.52 (m, 2H), 7.35 (t, $J$ = 1.1 Hz, 1H), 7.31 (dd, $J$ = 3.5, 0.8 Hz, 1H), 6.91 (d, $J$ = 8.3 Hz, 1H), 6.71 (dd, $J$ = 3.5, 1.7 Hz, 1H). $^{13}$C NMR (150 MHz, DMSO-$d_6$) δ $^{13}$C NMR (150 MHz, DMSO) δ 169.0, 156.2, 147.6, 145.6, 143.4, 136.5, 132.9, 132.6, 124.1, 123.9, 123.6, 122.3, 121.0, 114.4, 113.3, 112.1, 110.0. HRMS $m/z$ [M+H]$^+$ calcd for $C_{17}H_{13}N_4O_3$: 321.0988, found 321.0979, LC $t_R$ = 2.35 min, >98% Purity.

**4-cyano-*N*-(2-oxoindolin-5-yl)benzamide** (**77**): Compound **77** was prepared by procedure F to afford a colourless solid (786 mg, 2.835 mmol, 84%). MP > 240 °C (decomp.); $^1$H NMR (600 MHz, DMSO-$d_6$) δ 10.36 (s, 1H), 10.35 (s, 1H), 8.08 (d, $J$ = 8.1 Hz, 2H), 8.01 (d, $J$ = 8.3 Hz, 2H), 7.66 (d, $J$ = 2.1 Hz, 1H), 7.52 (dd, $J$ = 8.3, 2.1 Hz, 1H), 6.80 (d, $J$ = 8.3 Hz, 1H), 3.50 (s, 2H). $^{13}$C NMR (150 MHz, DMSO-$d_6$) δ 176.3, 163.7, 140.1, 139.1, 132.7, 132.4 (s, 2C), 128.4 (s, 2C), 126.0, 120.0, 118.4, 117.8, 113.7, 108.9, 36.1. HRMS $m/z$ [M+H]$^+$ calcd for $C_{16}H_{12}N_3O_2$: 278.0929, found 278.0920, LC $t_R$ = 2.90 min, >98% Purity.

**3-cyano-*N*-(2-oxoindolin-5-yl)benzamide** (**78**): Compound **78** was prepared by procedure F to afford a colourless solid (814 mg, 2.936 mmol, 87%). MP 214–216 °C; $^1$H NMR (600 MHz, DMSO-$d_6$) δ 10.36 (s, 1H), 10.30 (s, 1H), 8.37 (t, $J$ = 1.7 Hz, 1H), 8.23 (dt, $J$ = 7.9, 1.4 Hz, 1H), 8.04 (dt, $J$ = 7.7, 1.4 Hz, 1H), 7.74 (t, $J$ = 7.8 Hz, 1H), 7.66 (d, $J$ = 2.1 Hz, 1H), 7.51 (dd, $J$ = 8.4, 2.1 Hz, 1H), 6.81 (d, $J$ = 8.3 Hz, 1H), 3.50 (s, 2H). $^{13}$C NMR (150 MHz, DMSO-$d_6$) δ 176.4, 163.2, 140.1, 136.0, 134.8, 132.7, 132.4, 131.2, 129.8, 126.1, 120.0, 118.4, 117.7, 111.5, 108.9, 36.1. HRMS $m/z$ [M+H]$^+$ calcd for $C_{16}H_{12}N_3O_2$: 278.0929, found 278.0919, LC $t_R$ = 2.92 min, >98% Purity.

**2-cyano-*N*-(2-oxoindolin-5-yl)benzamide** (**79**): Compound **79** was prepared by procedure F to afford a colourless solid (664 mg, 2.395 mmol, 71%). MP 218–220 °C; $^1$H NMR (600 MHz, DMSO-$d_6$) δ 10.53 (s, 1H), 10.18 (s, 1H), 8.23 (s, 1H), 7.91 (ddd, $J$ = 33.5, 5.4, 3.1 Hz, 1H), 7.85 (q, $J$ = 7.8 Hz, 2H), 7.77 (t, $J$ = 7.5 Hz, 1H), 7.26–7.19 (m, 2H), 6.93 (d, $J$ = 8.2 Hz, 1H), 3.55 (s, 2H). $^{13}$C NMR (150 MHz, DMSO-$d_6$) δ 176.5, 167.3, 143.7, 134.6, 133.6, 132.5, 131.6, 127.8, 127.2, 126.4, 124.7, 124.0, 123.3, 122.8, 109.1, 35.9. HRMS $m/z$ [M+H]$^+$ calcd for $C_{16}H_{12}N_3O_2$: 278.0929, found 278.0921, LC $t_R$ = 3.08 min, >98% Purity.

**4-methoxy-*N*-(2-oxoindolin-5-yl)benzamide** (**80**): Compound **80** was prepared by procedure F to afford a colourless solid (738 mg, 2.614 mmol, 77%). MP 125–127 °C; $^1$H NMR (600 MHz, DMSO-$d_6$) δ 10.33 (s, 1H), 9.96 (s, 1H), 7.97–7.91 (m, 2H), 7.68–7.64 (m, 1H), 7.51 (dd, $J$ = 8.4, 2.2 Hz, 1H), 7.08–7.01 (m, 2H), 6.79 (d, $J$ = 8.3 Hz, 1H), 3.83 (s, 3H), 3.49 (s, 2H). $^{13}$C NMR (100 MHz, DMSO-$d_6$) δ $^{13}$C NMR (151 MHz, DMSO) δ 176.4, 164.6, 161.8, 139.6, 133.3, 129.5 (s, 2C), 127.1, 125.9, 120.0, 117.9, 113.6 (s, 2C), 108.8, 55.4, 36.1. HRMS $m/z$ [M+H]$^+$ calcd for $C_{16}H_{15}N_2O_3$: 283.1083, found 283.1072, LC $t_R$ = 3.01 min, >98% Purity.

**3-methoxy-*N*-(2-oxoindolin-5-yl)benzamide** (**81**): Compound **81** was prepared by procedure F to afford a colourless solid (820 mg, 2.905 mmol, 86%). MP 125–127 °C; $^1$H NMR (600 MHz, DMSO-$d_6$) δ 10.34 (s, 1H), 10.08 (s, 1H), 7.65 (s, 1H), 7.52 (dq, $J$ = 7.8, 1.8, 1.2 Hz, 2H), 7.48–7.46 (m, 1H), 7.43 (t, $J$ = 7.9 Hz, 1H), 7.14 (ddd, $J$ = 8.2, 2.6, 1.0 Hz, 1H), 6.79 (d, $J$ = 8.3 Hz, 1H), 3.83 (s, 3H), 3.50 (s, 2H). $^{13}$C NMR (150 MHz, DMSO-$d_6$) δ 176.4, 164.9, 159.2, 139.8, 136.5, 133.1, 129.5, 125.9, 120.0, 119.8, 117.9, 117.1, 112.8, 108.8, 55.3, 36.1. HRMS $m/z$ [M+H]$^+$ calcd for $C_{16}H_{15}N_2O_3$: 283.1083, found 283.1073, LC $t_R$ = 3.08 min, >98% Purity.

**2-methoxy-*N*-(2-oxoindolin-5-yl)benzamide** (**82**): Compound **82** was prepared by procedure F to afford a colourless oil (676 mg, 2.395 mmol, 71%). $^1$H NMR (600 MHz, DMSO-$d_6$) δ 10.33 (s, 1H), 9.98 (s, 1H), 7.65 (d, $J$ = 2.0 Hz, 1H), 7.63 (dd, $J$ = 7.5, 1.8 Hz, 1H), 7.49 (tdd, $J$ = 8.8, 6.9, 2.0 Hz, 2H), 7.17 (d, $J$ = 8.4 Hz, 1H), 7.06 (td, $J$ = 7.5, 0.9 Hz, 1H), 6.77 (d, $J$ = 8.3 Hz, 1H), 3.89 (s, 3H), 3.49 (s, 2H). $^{13}$C NMR (150 MHz, DMSO-$d_6$) δ 176.4, 164.1, 156.5, 139.6, 133.2, 132.0, 129.7, 126.1, 125.0, 120.5, 119.2, 117.0, 112.0, 108.9, 55.9, 36.1. HRMS $m/z$ [M+H]$^+$ calcd for $C_{16}H_{15}N_2O_3$: 283.1083, found 283.1072, LC $t_R$ = 3.21 min, >98% Purity.

**4-fluoro-*N*-(2-oxoindolin-5-yl)benzamide** (**83**): Compound **83** was prepared by procedure F to afford a colourless solid (812 mg, 3.005 mmol, 89%). MP 150–152 °C; $^1$H NMR (600 MHz, DMSO-$d_6$) δ 10.38 (s, 1H), 10.17 (s, 1H), 8.04–7.99 (m, 2H), 7.65 (d, $J$ = 2.0 Hz, 1H), 7.50 (dd, $J$ = 8.4, 2.1 Hz, 1H), 7.35 (t, $J$ = 8.8 Hz, 2H), 6.80 (d, $J$ = 8.3 Hz, 1H), 3.49 (s, 2H). $^{13}$C NMR (150 MHz, DMSO-$d_6$) δ 176.4, 164.1, 164.0 (d, $J$ = 248.8 Hz), 139.9, 133.1, 131.5 (d, $J$ = 3.0 Hz), 130.3 (d, $J$ = 9.0 Hz, 2C), 126.0, 120.1, 117.9, 115.3 (d, $J$ = 21.8 Hz, 2C), 108.8, 36.1. HRMS $m/z$ [M+H]$^+$ calcd for $C_{15}H_{12}FN_2O_2$: 271.0883, found 271.0872, LC $t_R$ = 3.09 min, >98% Purity.

**3-fluoro-*N*-(2-oxoindolin-5-yl)benzamide** (**84**): Compound **84** was prepared by procedure F to afford a colourless solid (830 mg, 3.071 mmol, 91%). MP 89–91 °C; $^1$H NMR (600 MHz, DMSO-$d_6$) δ 10.40 (s, 1H), 10.23 (s, 1H), 7.80 (dd, $J$ = 7.8, 1.3 Hz, 1H), 7.75 (dt, $J$ = 9.8, 2.1 Hz, 1H), 7.66 (d, $J$ = 2.0 Hz, 1H), 7.57 (td, $J$ = 8.0, 5.8 Hz, 1H), 7.52 (dd, $J$ = 8.4, 2.1 Hz, 1H), 7.43 (td, $J$ = 8.5, 2.6 Hz, 1H), 6.80 (d, $J$ = 8.3 Hz, 1H), 3.50 (s, 2H). $^{13}$C NMR (150 MHz, DMSO-$d_6$) δ 176.4, 163.7 (d, $J$ = 2.3 Hz), 161.9 (d, $J$ = 244.2 Hz), 140.0, 137.4 (d, $J$ = 6.8 Hz), 132.9, 130.6 (d, $J$ = 8.1 Hz), 126.0, 123.8 (d, $J$ = 2.7 Hz), 120.1, 118.3 (d, $J$ = 21.2 Hz), 117.9, 114.4 (d, $J$ = 22.9 Hz), 108.8, 36.1. HRMS $m/z$ [M+H]$^+$ calcd for $C_{15}H_{12}FN_2O_2$: 271.0883, found 271.0873, LC $t_R$ = 3.12 min, >98% Purity.

**2-fluoro-*N*-(2-oxoindolin-5-yl)benzamide** (**85**): Compound **85** was prepared by procedure F to afford a colourless solid (438 mg, 1.621 mmol, 48%). MP 85–87 °C; $^1$H NMR (600 MHz, DMSO-$d_6$) δ 10.36 (s, 1H), 10.26 (s, 1H), 7.74–7.59 (m, 2H), 7.56 (d, $J$ = 9.0 Hz, 1H), 7.48 (d, $J$ = 8.2 Hz, 1H), 7.33 (t, $J$ = 9.8 Hz, 2H), 6.79 (t, $J$ = 6.5 Hz, 1H), 3.49 (s, 2H). $^{13}$C NMR (150 MHz, DMSO-$d_6$) δ 176.4, 162.4, 158.9 (d, $J$ = 248.2 Hz), 139.9, 133.0, 132.3 (d, $J$ = 8.2 Hz), 129.9 (d, $J$ = 2.8 Hz), 126.1, 125.21 (d, $J$ = 15.3 Hz), 124.6 (d, $J$ = 3.1 Hz), 119.2, 117.0, 116.2 (d, $J$ = 21.8 Hz), 108.9, 36.1. HRMS $m/z$ [M+H]$^+$ calcd for $C_{15}H_{12}FN_2O_2$: 271.0883, found 271.0866, LC $t_R$ = 3.14 min, >98% Purity.

***N*-(2-oxoindolin-5-yl)-4-(trifluoromethyl)benzamide** (**86**): Compound **86** was prepared by procedure F to afford a colourless solid (897 mg, 2.801 mmol, 83%). MP 140–142 °C; $^1$H NMR (400 MHz, DMSO-$d_6$) δ 10.39 (s, 1H), 10.34 (s, 1H), 7.84 (dd, $J$ = 8.0, 1.3 Hz, 1H), 7.78 (t, $J$ = 7.5 Hz, 1H), 7.75–7.63 (m, 2H), 7.60 (d, $J$ = 2.0 Hz, 1H), 7.43 (dd, $J$ = 8.4, 2.1 Hz, 1H), 6.79 (d, $J$ = 8.3 Hz, 1H). $^{13}$C NMR (100 MHz, DMSO-$d_6$) δ 176.4, 165.2, 139.9, 136.4 (q, $J$ = 2.2 Hz), 133.0, 131.2 (d, $J$ = 272.0 Hz), 128.5, 126.3 (m, 1C), 126.2, 125.8 (d, $J$ = 31.3 Hz), 125.2, 122.5, 119.1, 116.9, 108.9, 36.1. HRMS $m/z$ [M+H]$^+$ calcd for $C_{16}H_{12}F_3N_2O_2$: 321.0851, found 321.0841, LC $t_R$ = 3.69 min, >98% Purity.

***N*-(2-oxoindolin-5-yl)-2-(trifluoromethyl)benzamide** (**87**): Compound **87** was prepared by procedure F to afford a colourless solid (778 mg, 2.429 mmol, 72%). MP > 240 °C (decomp.); $^1$H NMR (400 MHz, DMSO-$d_6$) δ 10.39 (s, 1H), 10.34 (s, 1H), 7.84 (dd, $J$ = 7.9, 1.2 Hz, 1H), 7.81–7.75 (m, 1H), 7.73–7.64 (m, 2H), 7.60 (d, $J$ = 2.0 Hz, 1H), 7.44 (dd, $J$ = 8.4, 2.1 Hz, 1H), 6.79 (d, $J$ = 8.3 Hz, 1H), 3.50 (s, 2H). $^{13}$C NMR (100 MHz, DMSO-$d_6$) δ 176.4, 165.2, 139.9, 136.5 (q, $J$ = 2.4 Hz), 133.0, 132.6, 129.9, 128.5, 126.3 (q, $J$ = 4.5 Hz), 126.2, 125.8 (d, $J$ = 31.3 Hz), 123.8 (d, $J$ = 273.9 Hz), 119.1, 116.9, 108.9, 36.1. HRMS $m/z$ [M+H]$^+$ calcd for $C_{16}H_{12}F_3N_2O_2$: 321.0851, found 321.0839, LC $t_R$ =

3.23 min, >98% Purity.

**4-cyano-*N*-[(3Z)-3-(1H-imidazole-5-ylmethylidene)-2-oxo-2,3-dihydro-1H-indol-5-yl] benzamide (88)**: Compound **88** was prepared by procedure A to afford a red/orange solid (68 mg, 0.191 mmol, 53%, *E*:Z ratio 50:50 - not able to distinguish E/Z isomers). MP > 300 °C; Diastereoisomer 1. *N*-(3-((1*H*-imidazole-5-yl)methylene)-2-oxoindolin-5-yl)-4-cyanobenzamide. $^1$H NMR (600 MHz, DMSO-$d_6$) δ 10.50 (s, 1H), 9.48 (d, $J$ = 2.2 Hz, 1H), 8.14–8.12 (m, 2H), 8.05–8.02 (m, 2H), 7.60 (s, 1H), 7.58 (s, 1H), 7.35 (bs, 1H), 6.94 (d, $J$ = 8.3 Hz, 1H). Diastereoisomer 2. *N*-(3-((1*H*-imidazole-5-yl)methylene)-2-oxoindolin-5-yl)-4-cyanobenzamide. $^1$H NMR (600 MHz, DMSO-$d_6$) δ 10.55 (s, 1H), 10.46 (s, 1H), 8.14–8.12 (m, 2H), 8.12–8.10 (m, 1H), 8.05–8.02 (m, 2H), 7.56 (s, 2H), 7.52 (bs, 1H), 7.41 (s, 1H), 7.39 (bs, 1H), 6.86 (d, $J$ = 8.3 Hz, 1H). HRMS *m/z* [M+H]$^+$ calcd for $C_{20}H_{14}N_5O_2$: 356.1148, found 356.1138, LC $t_R$ = 3.13 min, >98% Purity.

**3-cyano-*N*-[(3Z)-3-(1H-imidazole-5-ylmethylidene)-2-oxo-2,3-dihydro-1H-indol-5-yl] benzamide (89)**: Compound **89** was prepared by procedure A to afford a red/orange solid (73 mg, 0.205 mmol, 73%, *E*:Z ratio 43:57 - not able to distinguish E/Z isomers). MP > 250 °C (decomp.); Major diastereoisomer. *N*-(3-((1*H*-imidazole-5-yl)methylene)-2-oxoindolin-5-yl)-3-cyanobenzamide. $^1$H NMR (600 MHz, DMSO-$d_6$) δ 12.94 (bs, 1H), 10.55 (s, 1H), 9.48 (d, $J$ = 2.2 Hz, 1H), 8.43 (s, 1H), 8.29–8.26 (m, 1H), 8.07 (tt, $J$ = 7.9, 1.4 Hz, 2H), 7.78–7.74 (m, 1H), 7.58 (m, 1H), 7.58–7.56 (m, 1H), 7.41 (s, 1H), 6.86 (d, $J$ = 8.3 Hz, 1H). Minor diastereoisomer. *N*-(3-((1*H*-imidazole-5-yl)methylene)-2-oxoindolin-5-yl)-3-cyanobenzamide. $^1$H NMR (600 MHz, DMSO-$d_6$) δ 14.06 (bs, 1H), 11.18 (bs, 1H), 10.45 (s, 1H), 8.43–8.42 (m, 1H), 8.29–8.26 (m, 1H), 8.10 (d, $J$ = 2.1 Hz, 1H), 8.06–7.98 (m, 1H), 7.78–7.74 (m, 1H), 7.60 (s, 1H), 7.57–7.56 (m, 1H), 7.41 (s, 1H), 7.36 (s, 1H), 6.95 (d, $J$ = 8.3 Hz, 1H). HRMS *m/z* [M+H]$^+$ calcd for $C_{20}H_{14}N_5O_2$: 356.1148, found 356.1142, LC $t_R$ = 3.13 min, >98% Purity.

**3-cyano-*N*-[(3Z)-3-(1H-imidazole-2-ylmethylidene)-2-oxo-2,3-dihydro-1H-indol-5-yl] benzamide (90)**: Compound **90** was prepared by procedure A to afford a yellow/mustard solid (69 mg, 0.194 mmol, 54%). MP > 250 °C (decomp.); $^1$H NMR (600 MHz, DMSO-$d_6$) δ 13.70 (s, 1H), 11.02 (s, 1H), 10.40 (s, 1H), 8.42 (t, $J$ = 1.7 Hz, 1H), 8.27 (dt, $J$ = 8.0, 1.5 Hz, 1H), 8.13 (d, $J$ = 2.0 Hz, 1H), 8.07 (dt, $J$ = 7.7, 1.4 Hz, 1H), 8.03 (s, 1H), 7.79 (d, $J$ = 3.7 Hz, 1H), 7.76 (d, $J$ = 7.8 Hz, 1H), 7.73 (s, 1H), 7.43 (dd, $J$ = 8.4, 2.0 Hz, 1H), 6.91 (d, $J$ = 8.3 Hz, 1H). $^{13}$C NMR (150 MHz, DMSO-$d_6$) δ 169.1, 163.3, 139.7, 138.9, 136.4, 135.9, 134.9, 133.0, 132.4, 131.2, 129.9, 128.1, 124.4, 123.0, 121.2, 120.0, 118.4, 112.6, 111.5, 109.8. HRMS *m/z* [M+H]$^+$ calcd for $C_{20}H_{14}N_5O_2$: 356.1148, found 356.1140, LC $t_R$ = 3.18 min, >98% Purity.

**2-cyano-*N*-[(3Z)-3-(1H-imidazole-2-ylmethylidene)-2-oxo-2,3-dihydro-1H-indol-5-yl] benzamide (91)**: Compound **91** was prepared by procedure A to afford an orange solid (76 mg, 0.214 mmol, 59%, *E*:Z ratio 25:75 - not able to distinguish E/Z isomers). MP > 300 °C; (*Z*)-*N*-(3-((1*H*-imidazole-2-yl)methylene)-2-oxoindolin-5-yl)-2-cyanobenzamide. $^1$H NMR (600 MHz, DMSO-$d_6$) δ 13.28 (bs, 1H), 11.07 (bs, 1H), 8.18 (s, 1H), 7.78–7.77 (m, 1H), 7.77 (s, 1H), 7.33 (s, 1H), 6.87 (s, 1H), 6.82 (d, $J$ = 8.0 Hz, 1H), 6.35–6.34 (m, 1H). (*E*)-*N*-(3-((1*H*-imidazole-2-yl) methylene)-2-oxoindolin-5-yl)-2-cyanobenzamide. $^1$H NMR (600 MHz, DMSO-$d_6$) δ 11.91 (bs, 1H), 10.59 (bs, 1H), 8.59 (s, 1H), 7.81 (dd, $J$ = 8.0, 1.4 Hz, 1H), 7.52 (s, 1H), 7.20 (s, 1H), 7.10 (s, 1H), 6.80 (d, $J$ = 8.0 Hz, 1H), 6.41 (s, 1H). HRMS *m/z* [M+H]$^+$ calcd for $C_{20}H_{14}N_5O_2$: 356.1148, found 356.1135, LC $t_R$ = 2.45 min, >98% Purity.

***N*-[(3Z)-3-(1H-imidazole-5-ylmethylidene)-2-oxo-2,3-dihydro-1H-indol-5-yl]-4-methoxybenzamide (92)**: Compound **92** was prepared by procedure A to afford a yellow solid (70 mg, 0.194 mmol, 55%). MP 275–277 °C; $^1$H NMR (600 MHz, DMSO-$d_6$) δ 13.69 (s, 1H), 10.91 (s, 1H), 10.04 (s, 1H), 8.10 (s, 1H), 8.00 (s, 1H), 7.99–7.95 (m, 2H), 7.74 (s, 2H), 7.43 (dd, $J$ = 8.3, 2.0 Hz, 1H), 7.09–7.05 (m, 2H), 6.87 (d, $J$ = 8.3 Hz, 1H), 3.84 (s, 3H). $^1$H NMR (400 MHz, DMSO-$d_6$) δ $^{13}$C NMR (150 MHz, DMSO-$d_6$) δ 176.3, 168.9, 164.6, 161.8, 136.0, 133.5, 129.4 (s, 2C), 127.0, 124.4, 121.3, 120.4, 119.9, 117.8, 113.6 (s, 2C), 112.7, 109.6, 108.7, 55.4. HRMS *m/z* [M+H]$^+$ calcd for $C_{20}H_{17}N_4O_3$: 361.1301, found 361.1291, LC $t_R$ = 2.74 min, >98% Purity.

***N*-[(3Z)-3-(1H-imidazole-2-ylmethylidene)-2-oxo-2,3-dihydro-1H-indol-5-yl]-4-methoxybenzamide (93)**: Compound **93** was prepared by procedure A to afford a bright orange solid (91 mg, 0.253 mmol, 71%). MP > 300 °C; $^1$H NMR (400 MHz, DMSO-$d_6$) δ 11.14 (s, 1H), 10.06 (s, 1H), 8.10 (d, $J$ = 2.0 Hz, 1H), 8.02–7.94 (m, 2H), 7.66–7.49 (m, 3H), 7.36 (s, 1H), 7.12–7.04 (m, 2H), 6.95–6.87 (m, 1H), 3.84 (s, 3H). $^{13}$C NMR (100 MHz, DMSO-$d_6$) δ 169.0, 164.7, 161.8, 143.4, 136.2, 133.8, 132.6, 129.5 (2C, s), 126.9, 123.9, 123.8, 123.8, 122.3, 120.9, 113.6 (2C, s), 113.2, 109.9, 55.4. HRMS *m/z* [M+H]$^+$ calcd for $C_{20}H_{17}N_4O_3$: 361.1301, found 361.1292, LC $t_R$ = 3.25 min, >98% Purity.

***N*-[(3Z)-3-(1H-imidazole-5-ylmethylidene)-2-oxo-2,3-dihydro-1H-indol-5-yl]-3-methoxybenzamide (94)**: Compound **94** was prepared by procedure A to afford a yellow solid (98 mg, 0.272 mmol, 70%). MP 138–140 °C; $^1$H NMR (400 MHz, DMSO-$d_6$) δ 13.71 (s, 1H), 10.99 (s, 1H), 10.18 (s, 1H), 8.12 (d, $J$ = 2.0 Hz, 1H), 8.03 (s, 1H), 7.78 (s, 1H), 7.72 (s, 1H), 7.58–7.55 (m, 1H), 7.52 (dd, $J$ = 2.7, 1.5 Hz, 1H), 7.48–7.44 (m, 1H), 7.44–7.41 (m, 1H), 7.16 (ddd, $J$ = 8.2, 2.6, 1.0 Hz, 1H), 6.89 (d, $J$ = 8.4 Hz, 1H), 3.85 (s, 3H). $^{13}$C NMR (100 MHz, DMSO-$d_6$) δ 169.1, 164.9, 159.2, 139.7, 138.8, 136.3, 136.2, 133.3, 129.6, 128.1, 124.3, 122.9, 121.4, 120.1, 119.8, 117.2, 112.8, 109.7, 55.3. HRMS *m/z* [M+H]$^+$ calcd for $C_{20}H_{17}N_4O_3$: 361.1301, found 361.1288, LC $t_R$ = 2.78 min, >98% Purity.

***N*-[(3Z)-3-(1H-imidazole-2-ylmethylidene)-2-oxo-2,3-dihydro-1H-indol-5-yl]-3-methoxybenzamide (95)**: Compound **95** was prepared by procedure A to afford a red solid (55 mg, 0.153 mmol, 43%, *E*:Z ratio 37:63 - not able to distinguish E/Z isomers). MP > 300 °C; Major diastereoisomer. *N*-(3-((1*H*-imidazole-2-yl)methylene)-2-oxoindolin-5-yl)-3- methoxybenzamide. 1H NMR (600 MHz, DMSO-$d_6$) δ 12.90 (bs, 1H), 11.15 (bs, 1H), 10.53 (s, 1H), 10.21 (s, 1H), 9.44 (d, $J$ = 2.2 Hz, 1H), 7.58–7.40 (m, 5H), 7.40 (s, 1H), 7.15 (tdd, $J$ = 8.2, 2.7, 0.9 Hz, 1H), 6.85 (d, $J$ = 8.2 Hz, 1H), 3.85 (s, 3H). Minor diastereoisomer. *N*-(3-((1*H*-imidazole-2-yl)methylene)-2-oxoindolin-5-yl)-3- methoxybenzamide. 1H NMR (600 MHz, DMSO-$d_6$) δ 14.07 (s, 1H), 10.19 (s, 1H), 8.10 (d, $J$ = 2.0 Hz, 1H), 7.60 (s, 1H), 7.58–7.40 (m, 5H), 7.35 (d, $J$ = 1.2 Hz, 1H), 7.17–7.14 (m, 1H), 6.93 (d, $J$ = 8.3 Hz, 1H), 3.84 (s, 3H). HRMS *m/z* [M+H]$^+$ calcd for $C_{20}H_{17}N_4O_3$: 361.1301, found 361.1291, LC $t_R$ = 3.28 min, >98% Purity.

***N*-[(3Z)-3-(1H-imidazole-5-ylmethylidene)-2-oxo-2,3-dihydro-1H-indol-5-yl]-2-methoxybenzamide (96)**: Compound **96** was prepared by procedure A to afford a mustard/yellow solid (59 mg, 0.164 mmol, 46%). MP > 250 °C (decomp.); $^1$H NMR (600 MHz, DMSO-$d_6$) δ 13.70 (s, 1H), 10.94 (d, $J$ = 74.7 Hz, 1H), 10.44 (s, 1H), 8.21–7.99 (m, 6H), 7.76 (s, 2H), 7.52–7.39 (m, 1H), 6.90 (d, $J$ = 8.3 Hz, 1H), 3.34 (s, 3H). $^{13}$C NMR (150 MHz, DMSO-$d_6$) δ 206.5, 169.0, 163.8, 139.7, 139.0, 136.5, 132.9, 132.5 (s, 2C) 128.4 (s, 2C) 124.5, 123.0, 121.3, 120.1, 118.4, 113.8, 112.6, 109.7, 30.7. HRMS *m/z* [M+H]$^+$ calcd for $C_{20}H_{17}N_4O_3$: 361.1301, found 361.1290, LC $t_R$ = 2.96 min, >98% Purity.

***N*-[(3Z)-3-(1H-imidazole-2-ylmethylidene)-2-oxo-2,3-dihydro-1H-indol-5-yl]-2-methoxybenzamide (97)**: Compound **97** was prepared by procedure A to afford a bright red solid (49 mg, 0.136 mmol, 38%). MP > 300 °C; $^1$H NMR (600 MHz, DMSO-$d_6$) δ 14.08 (s, 1H), 11.13 (s, 1H), 10.08 (s, 1H), 8.07 (d, $J$ = 2.0 Hz, 1H), 7.74 (dd, $J$ = 7.6, 1.8 Hz, 1H), 7.68 (dd, $J$ = 8.4, 2.0 Hz, 1H), 7.65 (s, 1H), 7.57 (d, $J$ = 2.2 Hz, 1H), 7.53–7.51 (m, 1H), 7.36 (t, $J$ = 1.2 Hz, 1H), 7.20 (dd, $J$ = 8.5, 0.9 Hz, 1H), 7.09 (td, $J$ = 7.5, 1.0 Hz, 1H), 6.91 (d, $J$ = 8.4 Hz, 1H), 3.96 (s, 3H). $^{13}$C NMR (150 MHz, DMSO-$d_6$) δ 169.0, 163.9, 156.6, 143.5, 136.2, 133.7, 132.6, 132.3, 130.0, 124.2, 124.2, 124.0, 123.7, 121.3, 120.9, 120.6, 112.3, 112.1, 110.0, 56.0. HRMS *m/z* [M+H]$^+$ calcd for $C_{20}H_{17}N_4O_3$: 361.1301, found 361.1290, LC $t_R$ = 2.84 min, >98% Purity.

**4-fluoro-*N*-[(3Z)-3-[(1H-imidazole-5-yl)methylidene]-2-oxo-2,3-dihydro-1H-indol-5-yl] benzamide (98)**: Compound **98** was prepared by procedure A to afford a yellow/orange solid (57 mg, 0.164

mmol, 44%). MP > 250 °C (decomp.); $^1$H NMR (600 MHz, DMSO-$d_6$) δ 13.72 (s, 1H), 11.00 (s, 1H), 10.22 (s, 1H), 8.12 (s, 1H), 8.07–8.04 (m, 2H), 8.03 (s, 1H), 7.75 (d, $J$ = 32.5 Hz, 2H), 7.48–7.39 (m, 1H), 7.39–7.36 (m, 2H), 6.89 (d, $J$ = 8.3 Hz, 1H). $^{13}$C NMR (150 MHz, DMSO-$d_6$) δ 169.1, 164.1, 164.0 (d, $J$ = 250.0 Hz), 139.7, 138.8, 136.3, 133.3, 131.4 (d, $J$ = 2.8 Hz), 130.3 (d, $J$ = 8.9 Hz, 2C), 128.1, 124.4, 122.9, 121.4, 120.2, 115.4 (d, $J$ = 21.8 Hz, 2C), 112.8, 109.7. HRMS $m/z$ [M+H]$^+$ calcd for $C_{19}H_{14}FN_4O_2$: 349.1101, found 349.1092, LC $t_R$ = 2.80 min, >98% Purity.

**4-fluoro-*N*-[(3Z)-3-[(1H-imidazole-2-yl)methylidene]-2-oxo-2,3-dihydro-1H-indol-5-yl]benzamide (99)**: Compound **99** was prepared by procedure A to afford an orange solid (87 mg, 0.250 mmol, 68%). MP > 300 °C (decomp.); $^1$H NMR (400 MHz, DMSO-$d_6$) δ 11.15 (s, 1H), 10.23 (s, 1H), 8.14–8.01 (m, 3H), 7.59 (s, 1H), 7.56 (dd, $J$ = 8.4, 2.0 Hz, 1H), 7.45–7.27 (m, 3H), 6.93 (d, $J$ = 8.3 Hz, 1H). $^{13}$C NMR (100 MHz, DMSO-$d_6$) δ 169.0, 164.2, 164.0 (d, $J$ = 249.0 Hz), 143.4, 136.4, 133.5, 132.6, 131.3 (d, $J$ = 3.0 Hz), 130.3, 130.2, 124.0, 123.8 (2C, d, $J$ = 19.9 Hz), 122.3, 121.0, 115.3 (2C, d, $J$ = 21.8 Hz), 113.3, 109.9. HRMS $m/z$ [M+H]$^+$ calcd for $C_{19}H_{14}FN_4O_2$: 349.1101, found 349.1091, LC $t_R$ = 2.74 min, >98% Purity.

**3-fluoro-*N*-[(3Z)-3-[(1H-imidazole-5-yl)methylidene]-2-oxo-2,3-dihydro-1H-indol-5-yl]benzamide (100)**: Compound **100** was prepared by procedure A to afford an orange solid (67 mg, 0.192 mmol, 52%). MP > 300 °C; $^1$H NMR (600 MHz, DMSO-$d_6$) δ 13.71 (s, 1H), 11.00 (s, 1H), 10.28 (s, 1H), 8.12 (s, 1H), 8.03 (s, 1H), 7.84 (dt, $J$ = 7.8, 1.2 Hz, 1H), 7.83–7.75 (m, 2H), 7.73 (s, 1H), 7.60 (td, $J$ = 8.0, 5.8 Hz, 1H), 7.50–7.38 (m, 2H), 6.90 (d, $J$ = 8.3 Hz, 1H). $^{13}$C NMR (150 MHz, DMSO-$d_6$) δ 169.1, 163.8 (d, $J$ = 2.7 Hz), 162.0 (d, $J$ = 244.4 Hz), 139.7, 138.9, 137.2 (d, $J$ = 6.8 Hz), 136.4, 133.1, 130.6 (d, $J$ = 8.1 Hz), 128.1, 124.4, 123.8 (d, $J$ = 2.6 Hz), 123.0, 121.4, 120.1, 118.4 (d, $J$ = 21.1 Hz), 114.4 (d, $J$ = 22.8 Hz), 112.8, 109.8. HRMS $m/z$ [M+H]$^+$ calcd for $C_{19}H_{14}FN_4O_2$: 349.1101, found 349.1090, LC $t_R$ = 2.80 min, >98% Purity.

**3-fluoro-*N*-[(3Z)-3-[(1H-imidazole-2-yl)methylidene]-2-oxo-2,3-dihydro-1H-indol-5-yl]benzamide (101)**: Compound **101** was prepared by procedure A to afford a yellow solid (75 mg, 0.215 mmol, 58%, *E*:Z ratio 35:65), MP > 210 °C (decomp.); (*Z*)-*N*-(3-((1*H*-imidazole-2-yl)methylene)-2-oxoindolin-5-yl)-3-fluorobenzamide. $^1$H NMR (600 MHz, DMSO-$d_6$) δ 10.54 (s, 1H), 10.32 (s, 1H), 9.46 (d, $J$ = 2.2 Hz, 1H), 7.86–7.83 (m, 1H), 7.81–7.77 (m, 1H), 7.59–7.56 (m, 1H), 7.53 (dd, $J$ = 8.3, 2.2 Hz, 1H), 7.47–7.42 (m, 2H), 7.41 (s, 1H), 6.85 (d, $J$ = 8.3 Hz, 1H). (*E*)-*N*-(3-((1*H*-imidazole-2-yl)methylene)-2-oxoindolin-5-yl)-3-fluorobenzamide. $^1$H NMR (600 MHz, DMSO-$d_6$) δ 14.06 (s, 1H), 10.29 (s, 1H), 8.10 (d, $J$ = 2.0 Hz, 1H), 7.86–7.83 (m, 1H), 7.81–7.77 (m, 1H), 7.60 (s, 1H), 7.59–7.56 (m, 1H), 7.47–7.42 (m, 2H), 7.35 (s, 1H), 6.94 (d, $J$ = 8.3 Hz, 1H). HRMS $m/z$ [M+H]$^+$ calcd for $C_{19}H_{14}FN_4O_2$: 349.1101, found 349.1088, LC $t_R$ = 3.33 min, >98% Purity.

**2-fluoro-*N*-[(3Z)-3-[(1H-imidazole-2-yl)methylidene]-2-oxo-2,3-dihydro-1H-indol-5-yl]benzamide (102)**: Compound **102** was prepared by procedure A to afford an orange solid (48 mg, 0.138 mmol, 37%). MP > 300 °C; $^1$H NMR (400 MHz, DMSO-$d_6$) δ 11.15 (s, 1H), 10.33 (s, 1H), 8.09 (d, $J$ = 2.0 Hz, 1H), 7.69 (td, $J$ = 7.4, 1.8 Hz, 1H), 7.62–7.57 (m, 2H), 7.54 (dd, $J$ = 8.4, 2.0 Hz, 1H), 7.45–7.22 (m, 3H), 6.92 (d, $J$ = 8.3 Hz, 1H). $^{13}$C NMR (100 MHz, DMSO-$d_6$) δ 169.0, 162.5, 158.9 (d, $J$ = 248.8 Hz), 143.4, 136.4, 133.4, 132.5 (d, $J$ = 8.4 Hz), 129.9 (d, $J$ = 3.0 Hz), 125.0, 124.9, 124.6 (d, $J$ = 3.4 Hz), 124.1, 123.9, 123.6, 121.5, 121.1–120.9 (m), 116.2 (d, $J$ = 22.0 Hz), 112.4, 110.1. HRMS $m/z$ [M+H]$^+$ calcd for $C_{19}H_{14}FN_4O_2$: 349.1101, found 349.1084, LC $t_R$ = 2.83 min, >98% Purity.

***N*-[(3Z)-3-[(1H-imidazole-5-yl)methylidene]-2-oxo-2,3-dihydro-1H-indol-5-yl]-4-(trifluoromethyl)benzamide (103)**: Compound **100** was prepared by procedure A to afford a yellow solid (58 mg, 0.146 mmol, 47%). MP > 300 °C; $^1$H NMR (600 MHz, DMSO-$d_6$) δ 13.71 (s, 1H), 11.01 (s, 1H), 10.44 (s, 1H), 8.17 (d, $J$ = 8.0 Hz, 2H), 8.14 (d, $J$ = 2.0 Hz, 1H), 8.03–8.02 (m, 1H), 7.93 (d, $J$ = 8.2 Hz, 2H), 7.80 (s, 1H), 7.73 (s, 1H), 7.43 (dd, $J$ = 8.3, 2.0 Hz, 1H), 6.91 (d, $J$ = 8.3 Hz, 1H). $^{13}$C NMR (150 MHz, DMSO-$d_6$) δ 169.1, 164.0, 139.7, 138.9, 138.7, 136.4, 133.0, 131.3 (q, $J$ = 32.8, 31.9 Hz), 128.5 (s, 2C), 128.1, 125.5 (dd, $J$ = 4.9, 2.2 Hz, 2C), 124.9, 124.4, 123.0 (d, $J$ = 6.1 Hz), 121.4, 120.1, 112.8, 109.8. HRMS $m/z$ [M+H]$^+$ calcd for $C_{20}H_{14}F_3N_4O_2$: 399.1069, found 399.1058, LC $t_R$ = 3.25 min, >98% Purity.

**(Z)-*N*-(3-((1H-imidazole-2-yl)methylene)-2-oxoindolin-5-yl)-4-(trifluoromethyl)benzamide (104)**: Compound **104** was prepared by procedure A to afford a yellow solid (51 mg, 0.128 mmol, 41%, *E*:Z ratio 34:66 - not able to distinguish E/Z isomers). MP > 210 °C (decomp.); Major diastereoisomer. *N*-(3-((1*H*-imidazole-2-yl)methylene)-2-oxoindolin-5-yl)-4- (trifluoromethyl)benzamide. $^1$H NMR (600 MHz, DMSO-$d_6$) δ 12.87 (bs, 1H), 10.55 (bs, 1H), 10.48 (s, 1H), 9.48 (d, $J$ = 2.2 Hz, 1H), 8.18–8.17 (m, 2H), 7.92–7.91 (m, 2H), 7.61–7.56 (m, 2H), 7.41 (s, 1H), 6.86 (d, $J$ = 8.3 Hz, 1H). Minor diastereoisomer. *N*-(3-((1*H*-imidazole-2-yl)methylene)-2-oxoindolin-5-yl)-4- (trifluoromethyl)benzamide. $^1$H NMR (600 MHz, DMSO-$d_6$) δ 14.06 (bs, 1H), 11.16 (bs, 1H), 10.45 (s, 1H), 8.18–8.17 (m, 2H), 7.97–7.92 (m, 2H), 7.61 (s, 1H), 7.46 (bs, 2H), 7.35 (s, 1H), 6.95 (d, $J$ = 8.3 Hz, 1H). HRMS $m/z$ [M+H]$^+$ calcd for $C_{20}H_{14}F_3N_4O_2$: 399.1069, found 399.1058, LC $t_R$ = 3.20 min, >98% Purity.

***N*-[(3Z)-3-[(1H-imidazole-5-yl)methylidene]-2-oxo-2,3-dihydro-1H-indol-5-yl]-2-(trifluoromethyl)benzamide (105)**: Compound **105** was prepared by procedure A to afford a yellow solid (46 mg, 0.116 mmol, 37%, *E*:Z ratio 38:62 - not able to distinguish E/Z isomers). MP 225–227 °C; Major Diastereoisomer. *N*-(3-((1*H*-imidazole-5-yl)methylene)-2-oxoindolin-5-yl)-2- (trifluoromethyl)benzamide. $^1$H NMR (600 MHz, DMSO-$d_6$) δ 10.47 (bs, 1H), 10.42 (bs, 1H), 9.29 (d, $J$ = 2.1 Hz, 1H), 7.88 (s, 2H), 7.86–7.68 (m, 4H), 7.60 (dd, $J$ = 8.3, 2.2 Hz, 1H), 7.50 (s, 1H), 6.82 (d, $J$ = 8.3 Hz, 1H). Minor Diastereoisomer. *N*-(3-((1*H*-imidazole-5-yl)methylene)-2-oxoindolin-5-yl)-2- (trifluoromethyl)benzamide. $^1$H NMR (600 MHz, DMSO-$d_6$) δ 10.53 (bs, 1H), 8.09 (d, $J$ = 2.0 Hz, 1H), 8.00 (s, 1H), 7.95 (s, 1H), 7.86–7.68 (m, 5H), 7.34 (dd, $J$ = 8.3, 2.0 Hz, 1H), 6.89 (d, $J$ = 8.3 Hz, 1H). HRMS $m/z$ [M+H]$^+$ calcd for $C_{20}H_{14}F_3N_4O_2$: 399.1069, found 399.1058, LC $t_R$ = 2.89 min, >98% Purity.

***N*-[(3Z)-3-[(1H-imidazole-2-yl)methylidene]-2-oxo-2,3-dihydro-1H-indol-5-yl]-2-(trifluoromethyl)benzamide (106)**: Compound **106** was prepared by procedure A to afford a yellow solid (56 mg, 0.141 mmol, 45%, *E*:Z ratio 34:66 - not able to distinguish E/Z isomers). MP > 300 °C; Major diastereoisomer. *N*-(3-((1*H*-imidazole-2-yl)methylene)-2-oxoindolin-5-yl)-2- (trifluoromethyl)benzamide. $^1$H NMR (600 MHz, DMSO-$d_6$) δ 12.93 (bs, 1H), 10.54 (bs, 1H), 10.50 (bs, 1H), 9.45 (d, $J$ = 2.1 Hz, 1H), 7.87–7.83 (m, 1H), 7.81–7.77 (m, 1H), 7.73–7.68 (m, 3H), 7.50 (s, 1H), 7.41 (s, 1H), 7.36 (s, 1H), 6.85 (d, $J$ = 8.3 Hz, 1H). Minor diastereoisomer. *N*-(3-((1*H*-imidazole-2-yl)methylene)-2-oxoindolin-5-yl)-2- (trifluoromethyl)benzamide. $^1$H NMR (600 MHz, DMSO-$d_6$) δ 14.07 (bs, 1H), 11.17 (bs, 1H), 10.51 (bs, 1H), 8.04 (d, $J$ = 2.0 Hz, 1H), 7.81–7.77 (m, 1H), 7.70–7.68 (m, 3H), 7.58–7.57 (m, 2H), 7.52 (d, $J$ = 2.0 Hz, 1H), 7.37–7.34 (m, 1H), 6.93 (d, $J$ = 8.3 Hz, 1H). HRMS $m/z$ [M+H]$^+$ calcd for $C_{20}H_{14}F_3N_4O_2$: 399.1069, found 399.1057, LC $t_R$ = 2.86 min, >98% Purity.

***N*-(2-oxoindolin-5-yl)thiophene-2-carboxamide (107)**: Compound **107** was prepared by procedure F to afford a red solid (514 mg, 1.991 mmol, 59%). MP 105–107 °C; $^1$H NMR (600 MHz, DMSO-$d_6$) δ 10.34 (s, 1H), 10.10 (s, 1H), 7.97 (dd, $J$ = 3.7, 1.1 Hz, 1H), 7.82 (dd, $J$ = 5.0, 1.1 Hz, 1H), 7.63–7.57 (m, 1H), 7.46 (dd, $J$ = 8.4, 2.1 Hz, 1H), 7.21 (dd, $J$ = 5.0, 3.7 Hz, 1H), 6.79 (d, $J$ = 8.3 Hz, 1H), 3.50 (s, 2H). $^{13}$C NMR (150 MHz, DMSO-$d_6$) δ 176.3, 159.6, 140.3, 139.9, 132.6, 131.5, 128.7, 128.0, 126.1, 120.1, 117.9, 108.9, 36.1. HRMS $m/z$ [M+H]$^+$ calcd for $C_{13}H_{11}N_2O_2S$: 259.0541, found 259.0532, LC $t_R$ = 2.84 min, >98% Purity.

**3-methoxy-*N*-(2-oxoindolin-5-yl)thiophene-2-carboxamide (108)**: Compound **108** was prepared by procedure F to afford a beige solid (662 mg, 2.296 mmol, 68%). MP 75–77 °C; $^1$H NMR (600 MHz, DMSO-$d_6$) δ 10.37 (s, 1H), 9.14 (s, 1H), 7.80 (d, $J$ = 5.5 Hz, 1H), 7.59–7.55 (m, 1H), 7.43 (dd, $J$ = 8.3, 2.2 Hz, 1H), 7.18 (d, $J$ = 5.6 Hz,

1H), 6.77 (d, $J = 8.3$ Hz, 1H), 4.06 (s, 3H), 3.48 (s, 2H). $^{13}$C NMR (150 MHz, DMSO-$d_6$) δ 176.3, 159.1, 156.7, 139.8, 132.2, 130.4, 126.2, 119.6, 117.4, 117.1, 115.6, 108.9, 59.5, 36.0. HRMS *m/z* [M+H]$^+$ calcd for $C_{14}H_{13}N_2O_3S$: 289.0647, found 289.0637, LC $t_R = 3.05$ min, >98% Purity.

**3-ethoxy-*N*-(2-oxoindolin-5-yl)thiophene-2-carboxamide** (**109**): Compound **109** was prepared by procedure F to afford a beige solid (796 mg, 2.633 mmol, 78%). MP 98–100 °C; $^1$H NMR (600 MHz, DMSO-$d_6$) δ 10.33 (s, 1H), 9.20 (s, 1H), 7.78 (d, $J = 5.5$ Hz, 1H), 7.56–7.51 (m, 1H), 7.39 (dd, $J = 8.4$, 2.1 Hz, 1H), 7.16 (d, $J = 5.5$ Hz, 1H), 6.78 (d, $J = 8.3$ Hz, 1H), 4.33 (q, $J = 7.0$ Hz, 2H), 3.49 (s, 2H), 1.45 (t, $J = 7.0$ Hz, 3H). $^{13}$C NMR (150 MHz, DMSO-$d_6$) δ 176.3, 159.0, 155.8, 139.8, 132.3, 130.4, 126.4, 119.0, 117.5, 116.9, 115.9, 109.1, 68.0, 36.1, 14.8. HRMS *m/z* [M+H]$^+$ calcd for $C_{15}H_{15}N_2O_3S$: 303.0803, found 303.0795, LC $t_R = 3.56$ min, >98% Purity.

**3-fluoro-*N*-(2-oxoindolin-5-yl)thiophene-2-carboxamide** (**110**): Compound **110** was prepared by procedure F to afford a beige solid (532 mg, 1.926 mmol, 57%). MP 101–103 °C; HRMS *m/z* [M+H]$^+$ calcd for $C_{13}H_{10}FN_2O_2S$: 277.0447, found 277.0438, LC $t_R = 3.35$ min, >98% Purity.

***N*-(2-oxoindolin-5-yl)thieno [3,2-*b*] thiophene-2-carboxamide** (**111**): Compound **111** was prepared by procedure F to afford a beige solid (366 mg, 1.164 mmol, 69%). MP 125–127 °C; HRMS *m/z* [M+H]$^+$ calcd for $C_{15}H_{11}N_2O_2S_2$: 315.0262, found 315.0251, LC $t_R = 3.45$ min, >98% Purity.

**2-fluoro-*N*-(2-oxoindolin-5-yl)-5-(trifluoromethyl)benzamide** (**112**): Compound **112** was prepared by procedure F to afford a beige solid (651 mg, 1.925 mmol, 57%). MP 96–97 °C; $^1$H NMR (600 MHz, DMSO-$d_6$) δ 10.46 (s, 1H), 10.38 (s, 1H), 8.03 (dd, $J = 6.2$, 2.5 Hz, 1H), 7.97 (dt, $J = 7.7$, 3.2 Hz, 1H), 7.65–7.54 (m, 2H), 7.46 (dd, $J = 8.3$, 2.1 Hz, 1H), 6.81 (d, $J = 8.3$ Hz, 1H), 3.50 (s, 2H). $^{13}$C NMR (150 MHz, DMSO-$d_6$) δ 176.4, 162.0–160.0 (m, 1C), 140.1, 132.6, 129.6 (dd, $J = 9.6$, 3.9 Hz), 127.3 (p, $J = 3.9$ Hz), 126.2, 126.1 (d, $J = 17.0$ Hz), 125.4 (qd, $J = 32.8$, 3.2 Hz), 124.5, 122.7, 119.4, 117.7 (d, $J = 23.5$ Hz), 117.2, 109.0, 36.1. HRMS *m/z* [M+H]$^+$ calcd for $C_{16}H_{11}F_4N_2O_2$: 339.0757, found 339.0740, LC $t_R = 3.80$ min, >98% Purity.

***N*-(2-oxoindolin-5-yl)benzo [*d*] [1,3] dioxole-4-carboxamide** (**113**): Compound **113** was prepared by procedure F to afford a beige solid (750 mg, 2.531 mmol, 75%). MP 105–107 °C; $^1$H NMR (600 MHz, DMSO-$d_6$) δ 10.38 (s, 1H), 9.70 (s, 1H), 7.60 (d, $J = 2.0$ Hz, 1H), 7.47 (dd, $J = 8.4$, 2.0 Hz, 1H), 7.22 (d, $J = 8.1$ Hz, 1H), 7.10 (d, $J = 7.7$ Hz, 1H), 6.96 (t, $J = 7.9$ Hz, 1H), 6.78 (d, $J = 8.3$ Hz, 1H), 6.15 (s, 2H), 3.49 (s, 2H). $^{13}$C NMR (150 MHz, DMSO-$d_6$) δ 176.3, 161.8, 147.8, 145.2, 139.9, 132.7, 126.1, 121.7, 121.1, 119.4, 117.7, 117.2, 110.9, 108.90, 101.7, 36.1. HRMS *m/z* [M+H]$^+$ calcd for $C_{16}H_{13}N_2O_4$: 297.0875, found 297.0865, LC $t_R = 3.18$ min, >98% Purity.

***N*-(2-oxoindolin-5-yl)thiazole-2-carboxamide** (**114**): Compound **114** was prepared by procedure F to afford a beige solid (735 mg, 2.835 mmol, 84%). MP 108–110 °C; $^1$H NMR (600 MHz, DMSO-$d_6$) δ 10.71 (s, 1H), 10.39 (s, 1H), 8.38 (s, 1H), 7.68 (d, $J = 2.0$ Hz, 1H), 7.57 (dd, $J = 8.4$, 2.1 Hz, 1H), 7.53 (s, 1H), 6.79 (d, $J = 8.4$ Hz, 1H), 3.50 (s, 2H). $^{13}$C NMR (150 MHz, DMSO-$d_6$) δ 176.4, 155.1, 152.9, 142.5, 140.4, 131.8, 128.3, 126.1, 120.3, 117.8, 108.9, 36.0. HRMS *m/z* [M+H]$^+$ calcd for $C_{12}H_{10}N_3O_2S$: 260.0494, found 260.0484, LC $t_R = 2.72$ min, >98% Purity.

***N*-(2-oxoindolin-5-yl)oxazole-2-carboxamide** (**115**): Compound **115** was prepared by procedure F to afford a beige solid (345 mg, 1.418 mmol, 70%). MP 87–89 °C; $^1$H NMR (600 MHz, DMSO-$d_6$) δ 10.65 (s, 1H), 10.39 (s, 1H), 8.13–8.07 (m, 2H), 7.72 (d, $J = 2.0$ Hz, 1H), 7.63 (dd, $J = 8.4$, 2.1 Hz, 1H), 6.80 (d, $J = 8.4$ Hz, 1H), 3.49 (s, 2H). $^{13}$C NMR (150 MHz, DMSO-$d_6$) δ 176.8, 164.6, 157.9, 144.4, 140.7, 132.4, 126.7, 126.5, 120.7, 118.3, 109.3, 36.5. HRMS *m/z* [M+H]$^+$ calcd for $C_{12}H_{10}N_3O_3$: 244.0722, found 244.0709, LC $t_R = 2.25$ min, >98% Purity.

***N*-(2-oxoindolin-5-yl)isothiazole-5-carboxamide** (**116**): Compound **116** was prepared by procedure A to afford a beige solid (328 mg, 1.265 mmol, 75%). MP 178–180 °C; $^1$H NMR (400 MHz, DMSO-$d_6$) δ 10.47 (s, 1H), 10.38 (s, 1H), 8.71 (d, $J = 1.8$ Hz, 1H), 8.09 (d, $J = 1.8$ Hz, 1H), 7.61 (d, $J = 2.0$ Hz, 1H), 7.47 (dd, $J = 8.4$, 2.1 Hz, 1H), 6.82 (d, $J = 8.3$ Hz, 1H), 3.51 (s, 2H). $^{13}$C NMR (100 MHz, DMSO-$d_6$) δ 176.33, 163.32, 159.18, 157.40, 140.49, 131.77, 126.22, 123.87, 120.32, 117.97, 108.97, 36.03. HRMS *m/z* [M+H]$^+$ calcd for $C_{12}H_{10}N_3O_2S$: 260.0494, found 260.0485, LC $t_R = 2.57$ min, >98% Purity.

***N*- [(3Z)-3- [(1H-imidazole-5-yl)methylidene] -2-oxo-2,3-dihydro-1H-indol-5-yl] thiophene-2-carboxamide** (**117**): Compound **117** was prepared by procedure A to afford an orange solid (89 mg, 0.265 mmol, 68%). MP > 300 °C; $^1$H NMR (600 MHz, DMSO-$d_6$) δ 13.71 (s, 1H), 11.00 (s, 1H), 10.22 (s, 1H), 8.06 (d, $J = 2.0$ Hz, 1H), 8.03 (s, 1H), 8.01–8.00 (m, 1H), 7.84 (dd, $J = 5.0$, 1.1 Hz, 1H), 7.80 (s, 1H), 7.71 (s, 1H), 7.39 (dd, $J = 8.3$, 2.0 Hz, 1H), 7.23 (dd, $J = 5.0$, 3.7 Hz, 1H), 6.90 (d, $J = 8.3$ Hz, 1H). $^{13}$C NMR (150 MHz, DMSO -$d_6$) δ 169.1, 159.7, 140.2, 139.7, 138.8, 136.3, 132.8, 131.6, 128.8, 128.1 (s, 2C), 124.5, 123.0, 121.4, 120.1, 112.9, 109.8. HRMS *m/z* [M+H]$^+$ calcd for $C_{17}H_{13}N_4O_2S$: 337.0759, found 327.0721, LC $t_R = 2.78$ min, >98% Purity.

***N*- [(3Z)-3- [(1H-imidazole-2-yl)methylidene] -2-oxo-2,3-dihydro-1H-indol-5-yl] thiophene-2-carboxamide** (**118**): Compound **118** was prepared by procedure A to afford an orange solid (92 mg, 0.274 mmol, 71%, *E*:Z ratio 34:66 - not able to distinguish E/Z isomers). MP > 300 °C; Major diastereoisomer. *N*-(3-((1*H*-imidazole-2-yl)methylene)-2-oxoindolin-5-yl)thiophene-2- carboxamide. $^1$H NMR (600 MHz, DMSO-$d_6$) δ 12.94 (bs, 1H), 10.55 (bs, 1H), 10.26 (bs, 1H), 9.42 (d, $J = 2.2$ Hz, 1H), 8.05 (d, $J = 3.9$ Hz, 1H), 7.83 (dd, $J = 5.0$, 1.1 Hz, 1H), 7.49 (dd, $J = 8.3$, 2.2 Hz, 1H), 7.50–7.44 (bs, 2H), 7.41 (s, 1H), 7.22 (dd, $J = 5.0$, 3.7 Hz, 1H), 6.85 (d, $J = 8.3$ Hz, 1H). Minor diastereoisomer. *N*-(3-((1*H*-imidazole-2-yl)methylene)-2-oxoindolin-5-yl)thiophene-2- carboxamide. $^1$H NMR (600 MHz, DMSO-$d_6$) δ 14.07 (bs, 1H), 11.16 (bs, 1H), 10.22 (bs, 1H), 8.06 (d, $J = 2.0$ Hz, 1H), 8.01 (dd, $J = 3.8$, 1.2 Hz, 1H), 7.85 (dd, $J = 5.0$, 1.1 Hz, 1H), 7.62 (s, 1H), 7.57 (d, $J = 2.1$ Hz, 1H), 7.52 (dd, $J = 8.4$, 2.1 Hz, 1H), 7.36 (bt, $J = 1.2$ Hz, 1H), 7.23 (dd, $J = 5.0$, 3.7 Hz, 1H), 6.93 (d, $J = 8.3$ Hz, 1H). HRMS *m/z* [M+H]$^+$ calcd for $C_{17}H_{13}N_4O_2S$: 337.0759, found 337.0753, LC $t_R = 3.07$ min, >98% Purity.

**(Z)-*N*-(3-((1H-imidazole-5-yl)methylene)-2-oxoindolin-5-yl)-3-methoxythiophene-2-carboxamide** (**119**): Compound **119** was prepared by procedure A to afford an orange solid (45 mg, 0.123 mmol, 35%). MP 268–270 °C; $^1$H NMR (400 MHz, DMSO-$d_6$) δ 13.72 (s, 1H), 10.99 (s, 1H), 9.20 (s, 1H), 8.03 (s, 1H), 7.96 (d, $J = 2.0$ Hz, 1H), 7.84–7.80 (m, 2H), 7.69 (s, 1H), 7.50–7.47 (m, 1H), 7.20 (d, $J = 5.6$ Hz, 1H), 6.87 (d, $J = 8.3$ Hz, 1H), 4.09 (s, 3H). $^{13}$C NMR (100 MHz, DMSO-$d_6$) δ 169.1, 159.2, 156.8, 139.7, 138.7, 136.2, 132.5, 130.5, 128.1, 124.6, 123.1, 120.7, 120.0, 117.1, 115.5, 112.3, 109.7, 59.6. HRMS *m/z* [M+H]$^+$ calcd for $C_{18}H_{15}N_4O_3S$: 367.0865, found 367.0854, LC $t_R = 2.78$ min, >98% Purity.

**3-ethoxy-*N*- [(3Z)-3- [(1H-imidazole-5-yl)methylidene] -2-oxo-2,3-dihydro-1H-indol-5-yl] thiophene-2-carboxamide** (**120**): Compound **120** was prepared by procedure A to afford an orange solid (52 mg, 0.137 mmol, 41%, *E*:Z ratio 28:72 - not able to distinguish E/Z isomers). MP Decomp. >250 °C; Major diastereoisomer. *N*-(3-((1*H*-imidazole-5-yl)methylene)-2-oxoindolin-5-yl)-3-ethoxythiophene- 2-carboxamide. $^1$H NMR (600 MHz, DMSO-$d_6$) δ 12.74 (bs, 1H), 10.39 (bs, 1H), 9.32 (s, 1H), 9.23 (bs, 1H), 7.96–7.95 (m, 2H), 7.87 (dd, $J = 8.3$, 2.2 Hz, 1H), 7.81 (d, $J = 5.5$ Hz, 1H), 7.51 (s, 1H), 7.21 (d, $J = 5.5$ Hz, 1H), 6.81 (d, $J = 8.3$ Hz, 1H), 4.41–4.37 (m, 2H), 1.59 (t, $J = 6.9$ Hz, 3H). Minor diastereoisomer. *N*-(3-((1*H*-imidazole-5-yl)methylene)-2-oxoindolin-5-yl)-3-ethoxythiophene- 2-carboxamide. $^1$H NMR (600 MHz, DMSO-$d_6$) δ 13.73 (bs, 1H), 10.99 (bs, 1H), 9.25 (s, 1H), 8.02 (d, $J = 14.3$ Hz, 2H), 7.83 (s, 1H), 7.81–7.79 (m, 1H), 7.71 (s, 1H), 7.37 (dd, $J = 8.4$, 2.1 Hz, 1H), 7.19 (d, $J = 5.5$ Hz, 1H), 6.89 (d, $J = 8.3$ Hz, 1H), 4.39–4.35 (m, 2H), 1.47 (t, $J = 7.0$ Hz, 3H). HRMS *m/z* [M+H]$^+$ calcd for $C_{19}H_{17}N_4O_3S$: 381.1021, found 381.1007, LC $t_R = 3.03$ min, >98% Purity.

**3-fluoro-*N*-[(3Z)-3-[(1H-imidazole-5-yl)methylidene]-2-oxo-2,3-dihydro-1H-indol-5-yl]thiophene-2-carboxamide (121)**: Compound **121** was prepared by procedure A to afford an orange solid (37 mg, 0.104 mmol, 29%). MP > 300 °C; $^1$H NMR (400 MHz, DMSO-$d_6$) δ 13.69 (s, 1H), 11.00 (s, 1H), 9.83–9.72 (m, 1H), 8.03 (s, 1H), 7.98 (d, $J$ = 2.0 Hz, 1H), 7.86 (dd, $J$ = 5.5, 4.0 Hz, 1H), 7.81 (s, 1H), 7.70 (s, 1H), 7.38 (dd, $J$ = 8.3, 2.0 Hz, 1H), 7.16 (d, $J$ = 5.5 Hz, 1H), 6.88 (d, $J$ = 8.3 Hz, 1H). $^{13}$C NMR (100 MHz, DMSO-$d_6$) δ 169.10, 157.67, 156.86, 154.22, 139.70, 138.82, 136.49, 132.43, 129.77 (d, $J$ = 9.9 Hz), 128.08, 124.46, 123.10, 121.51, 119.97, 118.30 (d, $J$ = 26.4 Hz), 113.03, 109.72. HRMS $m/z$ [M+H]$^+$ calcd for $C_{17}H_{12}FN_4O_2S$: 355.0665, found 355.0652, LC $t_R$ = 2.68 min, >98% Purity.

**(Z)-*N*-(3-((1H-imidazole-5-yl)methylene)-2-oxoindolin-5-yl)thieno[3,2-*b*]thiophene-2-carboxamide (122)**: Compound **122** was prepared by procedure A to afford a light orange solid (45 mg, 0.110 mmol, 36%). MP > 250 °C (decomp.); $^1$H NMR (600 MHz, DMSO-$d_6$) δ 13.68 (s, 1H), 10.95 (s, 1H), 10.34 (s, 1H), 8.34 (s, 1H), 8.09 (d, $J$ = 2.0 Hz, 1H), 8.01 (s, 1H), 7.89 (d, $J$ = 5.2 Hz, 1H), 7.78 (s, 1H), 7.54 (d, $J$ = 5.2 Hz, 1H), 7.40 (dd, $J$ = 8.2, 2.0 Hz, 1H), 6.90 (d, $J$ = 8.3 Hz, 1H). $^{13}$C NMR (150 MHz, DMSO-$d_6$) δ 169.0, 160.1, 142.0, 141.6, 139.4, 138.5, 136.3, 132.7, 131.8, 124.5, 121.4 (s, 2C), 121.2, 120.6, 120.4 (s, 2C), 120.3, 112.7, 109.7. HRMS $m/z$ [M+H]$^+$ calcd for $C_{19}H_{13}N_4O_2S_2$: 393.0480, found 393.0468, LC $t_R$ = 3.08 min, >98% Purity.

**2-fluoro-*N*-[(3Z)-3-[(1H-imidazole-5-yl)methylidene]-2-oxo-2,3-dihydro-1H-indol-5-yl]-5-(trifluoromethyl)benzamide (123)**: Compound **123** was prepared by procedure A to afford an orange solid (21 mg, 0.062 mmol, 21%). MP 202–204 °C; $^1$H NMR (600 MHz, DMSO-$d_6$) δ 13.73 (s, 1H), 10.99 (s, 1H), 10.75 (s, 1H), 8.22 (s, 1H), 8.03 (s, 1H), 7.85 (d, $J$ = 2.3 Hz, 1H), 7.79–7.75 (m, 2H), 7.35 (dd, $J$ = 9.4, 5.8 Hz, 2H), 6.91 (d, $J$ = 8.4 Hz, 1H). $^{13}$C NMR (150 MHz, DMSO) δ 169.1, 164.6, 154.3, 139.7, 139.0, 136.1, 133.3, 128.9, 128.1, 126.7, 125.3, 124.6, 123.5, 123.0, 121.7, 121.4, 120.1, 119.8, 111.4, 110.1. HRMS $m/z$ [M+H]$^+$ calcd for $C_{20}H_{13}F_4N_4O_2$: 417.0975, found 417.0962, LC $t_R$ = 3.22 min, >98% Purity.

**(Z)-*N*-(3-((1H-imidazole-5-yl)methylene)-2-oxoindolin-5-yl)benzo[d][1,3]dioxole-4-carboxamide (124)**: Compound **124** was prepared by procedure A to afford a brown/red solid (47 mg, 0.126 mmol, 37%). MP 189–191 °C; $^1$H NMR (600 MHz, DMSO-$d_6$) δ 13.71 (s, 1H), 10.96 (s, 1H), 9.72 (s, 1H), 8.30 (s, 1H), 8.06–8.03 (m, 1H), 8.00 (d, $J$ = 4.2 Hz, 1H), 7.85–7.66 (m, 2H), 7.45 (dt, $J$ = 8.3, 3.1 Hz, 1H), 7.27 (dd, $J$ = 8.1, 1.1 Hz, 1H), 7.12 (dd, $J$ = 7.7, 1.1 Hz, 1H), 6.98 (t, $J$ = 7.9 Hz, 1H), 6.88 (d, $J$ = 8.3 Hz, 1H), 6.18 (s, 2H). $^{13}$C NMR (150 MHz, DMSO-$d_6$) δ 169.0, 161.9, 147.8, 145.3, 139.5, 136.3, 134.6, 132.9, 128.5, 124.6, 121.7, 121.1, 120.6, 120.3, 117.5, 112.0, 111.0, 109.7, 101.7, 43.8. HRMS $m/z$ [M+H]$^+$ calcd for $C_{20}H_{15}N_4O_4$: 375.1093, found 375.1081, LC $t_R$ = 2.85 min, >98% Purity.

***N*-[(3Z)-3-[(1H-imidazole-5-yl)methylidene]-2-oxo-2,3-dihydro-1H-indol-5-yl]-1,3-thiazole-2-carboxamide (125)**: Compound **125** was prepared by procedure A to afford a mustard green solid (60 mg, 0.178 mmol, 46%). MP 271–273 °C; $^1$H NMR (600 MHz, DMSO-$d_6$) δ 13.70 (s, 1H), 11.01 (s, 1H), 10.70 (s, 1H), 8.17 (s, 1H), 8.13–8.10 (m, 2H), 8.03 (s, 1H), 7.74 (d, $J$ = 24.9 Hz, 2H), 7.55 (d, $J$ = 8.0 Hz, 1H), 6.89 (d, $J$ = 8.3 Hz, 1H). $^{13}$C NMR (150 MHz, DMSO-$d_6$) δ 169.1, 164.1, 157.6, 157.6, 144.0, 139.7, 138.9, 136.6, 132.2, 126.4, 124.5, 123.0, 121.5, 120.1, 112.7, 109.8. HRMS $m/z$ [M+H]$^+$ calcd for $C_{16}H_{12}N_5O_2S$: 338.0712, found 338.0700, LC $t_R$ = 2.52 min, >98% Purity.

***N*-[(3Z)-3-[(1H-imidazole-5-yl)methylidene]-2-oxo-2,3-dihydro-1H-indol-5-yl]-1,3-oxazole-2-carboxamide (126)**: Compound **126** was prepared by procedure A to afford a dark orange solid (57 mg, 0.177 mmol, 43%). MP > 300 °C; $^1$H NMR (400 MHz, DMSO-$d_6$) δ 13.68 (s, 1H), 10.99 (s, 1H), 10.73 (s, 1H), 8.38 (dd, $J$ = 6.0, 0.8 Hz, 1H), 8.15–7.96 (m, 2H), 7.73 (d, $J$ = 14.6 Hz, 2H), 7.52 (dd, $J$ = 4.0, 0.8 Hz, 1H), 7.47 (d, $J$ = 7.7 Hz, 1H), 6.83 (dd, $J$ = 29.0, 8.3 Hz, 1H). $^{13}$C NMR (100 MHz, DMSO-$d_6$) δ 169.1, 155.1, 153.0, 142.6, 139.7, 138.9, 136.7, 132.0, 128.4, 128.0, 124.4, 123.1, 121.5, 119.9, 112.7, 109.8. HRMS $m/z$ [M+H]$^+$ calcd for $C_{16}H_{12}N_5O_3$: 322.0940, found 322.0930, LC $t_R$ = 2.21 min, >98% Purity.

***N*-[(3Z/E)-3-[(1H-imidazole-5-yl)methylidene]-2-oxo-2,3-dihydro-1H-indol-5-yl]-1,2-thiazole-5-carboxamide (127)**: Compound **127** was prepared by procedure A to afford an orange solid (48 mg, 0.142 mmol, 37%, *E*:Z ratio 30:70). MP > 300 °C; (*Z*)-*N*-(3-((1*H*-imidazole-5-yl)methylene)-2-oxoindolin-5-yl)isothiazole-5-carboxamide. $^1$H NMR (600 MHz, DMSO-$d_6$) δ 12.74 (s, 1H), 10.60 (s, 1H), 10.46 (s, 1H), 9.41 (d, $J$ = 2.1 Hz, 1H), 8.72 (dd, $J$ = 3.5, 1.7 Hz, 1H), 8.16 (d, $J$ = 1.8 Hz, 1H), 8.03 (s, 1H), 7.95 (s, 1H), 7.54 (s, 1H), 7.50–7.44 (m, 1H), 6.86 (d, $J$ = 8.2 Hz, 1H). (*E*)-*N*-(3-((1*H*-imidazole-5-yl)methylene)-2-oxoindolin-5-yl)isothiazole-5-carboxamide. $^1$H NMR (600 MHz, DMSO-$d_6$) δ 13.71 (s, 1H), 11.05 (s, 1H), 10.59 (s, 1H), 8.12 (s, 0H), 8.07 (s, 1H), 8.04 (s, 1H), 7.82 (s, 1H), 7.73 (s, 1H), 7.42 (d, $J$ = 7.5 Hz, 1H), 6.93 (d, $J$ = 8.3 Hz, 1H).HRMS $m/z$ [M+H]$^+$ calcd for $C_{16}H_{12}N_5O_2S$: 338.0712, found 338.0699, LC $t_R$ = 2.41 min, >98% Purity.

***N*-[(3Z)-3-[(4-methyl-1H-imidazole-5-yl)methylidene]-2-oxo-2,3-dihydro-1H-indol-5-yl]benzamide (128)**: Compound **128** was prepared by procedure A to afford a light orange solid (59 mg, 0.171 mmol, 43%). MP > 270 °C (decomp.); $^1$H NMR (400 MHz, DMSO-$d_6$) δ 13.91 (s, 1H), 11.02 (s, 1H), 10.23 (s, 1H), 8.15 (d, $J$ = 2.0 Hz, 1H), 8.07–8.02 (m, 2H), 7.99 (s, 1H), 7.71 (d, $J$ = 0.7 Hz, 1H), 7.67–7.62 (m, 1H), 7.62–7.56 (m, 2H), 7.51 (dd, $J$ = 8.4, 2.0 Hz, 1H), 6.94 (d, $J$ = 8.3 Hz, 1H), 2.50 (s, 3H). $^{13}$C NMR (100 MHz, DMSO-$d_6$) δ 169.5, 165.2, 147.6, 138.2, 135.9, 134.8, 133.1, 131.5, 128.4 (s, 2C), 127.5 (s, 2C), 124.8, 124.4, 122.3, 121.4, 118.1, 113.4, 109.5, 13.1. HRMS $m/z$ [M+H]$^+$ calcd for $C_{20}H_{17}N_4O_2$: 345.1352, found 345.1342, LC $t_R$ = 2.76 min, >98% Purity.

***N*-[(3Z)-2-oxo-3-(1H-pyrazol-5-ylmethylidene)-2,3-dihydro-1H-indol-5-yl]benzamide (129)**: Compound **129** was prepared by procedure A to afford a dark red/purple solid (87 mg, 0.263 mmol, 66%). MP 218–220 °C; $^1$H NMR (600 MHz, DMSO-$d_6$) δ 13.54 (s, 1H), 10.53 (s, 1H), 10.21 (s, 1H), 7.99–7.97 (m, 2H), 7.91 (d, $J$ = 2.2 Hz, 1H), 7.72–7.44 (m, 6H), 6.88 (s, 1H), 6.86 (d, $J$ = 8.3 Hz, 1H). $^{13}$C NMR (150 MHz, DMSO-$d_6$) δ 169.6, 165.3, 165.2, 139.2, 136.8, 135.0, 134.9, 132.5, 131.5, 131.4, 128.42, 128.36, 127.59, 127.55, 125.3, 123.9, 121.7, 109.8, 109.1. HRMS $m/z$ [M+H]$^+$ calcd for $C_{19}H_{15}N_4O_2$: 331.1195, found 331.1185, LC $t_R$ = 3.56 min, >98% Purity.

## Notes

The authors declare no competing financial interests.

## CRediT authorship contribution statement

**Christopher R.M. Asquith:** Writing – review & editing, Writing – original draft, Validation, Project administration, Methodology, Investigation, Formal analysis, Conceptualization. **Michael P. East:** Writing – review & editing, Validation, Methodology, Investigation, Formal analysis. **Tuomo Laitinen:** Writing – review & editing, Validation, Software, Methodology, Investigation, Formal analysis. **Carla Alamillo-Ferrer:** Writing – review & editing, Validation, Methodology, Investigation, Formal analysis. **Erkka Hartikainen:** Writing – review & editing, Investigation. **Carrow I. Wells:** Writing – review & editing, Investigation. **Alison D. Axtman:** Writing – review & editing, Investigation. **David H. Drewry:** Writing – review & editing, Investigation. **Graham J. Tizzard:** Writing – review & editing, Validation, Resources, Methodology, Investigation, Funding acquisition. **Antti Poso:** Writing – review & editing, Validation, Software, Methodology, Investigation, Funding acquisition. **Timothy M. Willson:** Writing – review & editing, Investigation, Formal analysis, Funding acquisition. **Gary L. Johnson:** Writing – review & editing, Validation, Resources, Methodology, Investigation, Formal analysis, Funding acquisition, Conceptualization.

## Declaration of competing interest

The authors declare that they have no known competing financial

interests or personal relationships that could have appeared to influence the work reported in this paper.

## Data availability

All data has been included in this submission.

## Acknowledgement

The SGC is a registered charity (number 1097737) that receives funds from AbbVie, Bayer Pharma AG, Boehringer Ingelheim, Canada Foundation for Innovation, Eshelman Institute for Innovation, Genome Canada, Innovative Medicines Initiative (EU/EFPIA) [ULTRA-DD grant no. 115766], Janssen, Merck KGaA Darmstadt Germany, MSD, Novartis Pharma AG, Ontario Ministry of Economic Development and Innovation, Pfizer, São Paulo Research Foundation-FAPESP, Takeda, and Wellcome [106169/ZZ14/Z]. The US National Institutes of Health (NIH) is acknowledged for support (U24DK11604). We thank Biocenter Finland/DDCB for financial support and the CSC-IT Center for Science Ltd. (Finland) for allocation of computational resources. We also thank Dr. Brandie Ehrmann and Ms. Diane E. Wallace for LC-MS/HRMS support provided by in the Mass Spectrometry Core Laboratory at the University of North Carolina at Chapel Hill. The core is supported by the National Science Foundation under Grant No. (CHE-1726291). We thank the EPSRC UK National Crystallography Service for funding and collection of the small molecule crystallographic data. In addition, we thank the University of North Carolina's Department of Chemistry NMR Core Laboratory for the use of their NMR spectrometers, along with Dr. Marc ter Horst and Dr. Andrew Camp for their assistance with NMR spectroscopy. The core is supported by the National Science Foundation under Grant No. (CHE-1828183).

## Appendix A. Supplementary data

Supplementary data to this article can be found online at https://doi.org/10.1016/j.ejmech.2024.116357.

## References

[1] I.M. Klimovskaia, C. Young, C.B. Strømme, P. Menard, Z. Jasencakova, J. Mejlvang, K. Ask, M. Ploug, M.L. Nielsen, O.L. Jensen, A. Groth, Tousled-like kinases phosphorylate Asf1 to promote histone supply during DNA replication, Nat. Commun. 5 (2014) 3394, https://doi.org/10.1038/ncomms4394.

[2] H.H. Silljé, K. Takahashi, K. Tanaka, G. Van Houwe, E.A. Nigg, Mammalian homologues of the plant Tousled gene code for cell-cycle-regulated kinases with maximal activities linked to ongoing DNA replication, EMBO J. 18 (1999) 5691–5702, https://doi.org/10.1093/emboj/18.20.5691.

[3] C.M. Hammond, C.B. Strømme, H. Huang, D.J. Patel, A. Groth, Histone chaperones as Cardinal Players in development, Nat. Rev. Mol. Cell Biol. 18 (2017) 141–158, https://doi.org/10.3389/fcell.2022.767773.

[4] M. Pilyugin, J. Demmers, C.P. Verrijzer, F. Karch, Y.M. Moshkin, Phosphorylation-mediated control of histone chaperone ASF1 levels by Tousled-like kinases, PLoS One 4 (2009) e8328, https://doi.org/10.1371/journal.pone.0008328.

[5] W. Bruinsma, J. van den Berg, M. Aprelia, R.H. Medema, Tousled-like kinase 2 regulates recovery from a DNA damage-induced G2 arrest, EMBO Rep. 17 (2016) 659–670, https://doi.org/10.15252/embr.201540767.

[6] S. Lee, S. Segura-Bayona, M. Villamor-Payà, G. Saredi, M.A.M. Todd, C.S. Attolini, T.Y. Chang, T.H. Stracker, A. Groth, Tousled-like kinases stabilize replication forks and show synthetic lethality with checkpoint and PARP inhibitors, Sci. Adv. 4 (2018) eaat4985, https://doi.org/10.1126/sciadv.aat4985.

[7] S. Segura-Bayona, M. Villamor-Payà, C.S. Attolini, L.M. Koenig, M. Sanchiz-Calvo, S.J. Boulton, T.H. Stracker, Tousled-like kinases Suppress innate immune signaling Triggered by alternative lengthening of telomeres, Cell Rep. 32 (2020) 107983, https://doi.org/10.1016/j.celrep.2020.107983.

[8] M. Wang, J. Li, X. Yang, Q. Yan, H. Wang, X. Xu, Y. Lu, D. Li, Y. Wang, R. Sun, S. Zhang, Y. Zhang, Z. Zhang, F. Meng, Y. Li, Targeting TLK2 inhibits the progression of gastric cancer by reprogramming amino acid metabolism through the mTOR/ASNS axis, Cancer Gene Ther. 30 (2023) 1485–1497, https://doi.org/10.1038/s41417-023-00653-8.

[9] S.H. Lelieveld, M.R. Reijnders, R. Pfundt, H.G. Yntema, E.J. Kamsteeg, P. de Vries, B.B. de Vries, M.H. Willemsen, T. Kleefstra, K. Löhner, M. Vreeburg, S.J. Stevens, I. van der Burgt, E.M. Bongers, A.P. Stegmann, P. Rump, T. Rinne, M.R. Nelen, J. A. Veltman, L.E. Vissers, H.G. Brunner, C. Gilissen, Meta-analysis of 2,104 trios provides support for 10 new genes for intellectual disability, Nat. Neurosci. 19 (2016) 1194–1196, https://doi.org/10.1038/nn.4352.

[10] A. Töpf, Y. Oktay, S. Balaraju, E. Yilmaz, E. Sonmezler, U. Yis, S. Laurie, R. Thompson, A. Roos, D.G. MacArthur, A. Yaramis, S. Güngör, H. Lochmüller, S. Hiz, R. Horvath, Severe neurodevelopmental disease caused by a homozygous TLK2 variant, Eur. J. Hum. Genet. 28 (2020) 383–387, https://doi.org/10.1038/s41431-019-0519-x.

[11] M.R.F. Reijnders, K.A. Miller, M. Alvi, J.A.C. Goos, M.M. Lees, A. de Burca, A. Henderson, A. Kraus, B. Mikat, B.B.A. de Vries, B. Isidor, B. Kerr, C. Marcelis, C. Schluth-Bolard, C. Deshpande, C.A.L. Ruivenkamp, D. Wieczorek, Developmental Disorders Study Deciphering, D. Baralle, E.M. Blair, H. Engels, H. J. Lüdecke, J. Eason, G.W.E. Santen, J. Clayton-Smith, K. Chandler, K. Tatton-Brown, K. Payne, K. Helbig, K. Radtke, K.M. Nugent, K. Cremer, T.M. Strom, L. M. Bird, M. Sinnema, M. Bitner-Glindzicz, M.F. van Dooren, M. Alders, M. Koopmans, L. Brick, M. Kozenko, M.L. Harline, M. Klaassens, M. Steinraths, N. S. Cooper, P. Edery, P. Yap, P.A. Terhal, P.J. van der Spek, P. Lakeman, R.L. Taylor, R.O. Littlejohn, R. Pfundt, S. Mercimek-Andrews, A.P.A. Stegmann, S.G. Kant, S. McLean, S. Joss, S.M.A. Swagemakers, S. Douzgou, S.A. Wall, S. Küry, E. Calpena, N. Koelling, S.J. McGowan, S.R.F. Twigg, I.M.J. Mathijssen, C. Nellaker, H.G. Brunner, A.O.M. Wilkie, De Novo and Inherited loss-of-function variants in TLK2: clinical and genotype-phenotype evaluation of a distinct neurodevelopmental disorder, Am. J. Hum. Genet. 102 (2018) 1195–1203, https://doi.org/10.1016/j.ajhg.2018.04.014.

[12] G.B. Mortuza, D. Hermida, A.K. Pedersen, S. Segura-Bayona, B. López-Méndez, P. Redondo, P. Rüther, I. Pozdnyakova, A.M. Garrote, I.G. Muñoz, M. Villamor-Payà, C. Jauset, J.V. Olsen, T.H. Stracker, G. Montoya, Molecular basis of tousled-like kinase 2 activation, Nat. Commun. 9 (2018) 2535, https://doi.org/10.1038/s41467-018-04941-y.

[13] P.J. Dillon, S.M. Gregory, K. Tamburro, M.K. Sanders, G.L. Johnson, N. Raab-Traub, D.P. Dittmer, B. Damania, Tousled-like kinases modulate reactivation of gammaherpesviruses from latency, Cell Host Microbe 13 (2013) 204–214, https://doi.org/10.1016/j.chom.2012.12.005.

[14] Y. Kim, J.L. Anderson, S.R. Lewin, Getting the "kill" into "shock and kill": strategies to eliminate latent HIV, Cell Host Microbe 23 (2018) 14–26, https://doi.org/10.1016/j.chom.2017.12.004.

[15] M. Lin, Z. Yao, N. Zhao, C. Zhang, TLK2 enhances aggressive phenotypes of glioblastoma cells through the activation of SRC signaling pathway, Cancer Biol. Ther. 20 (2019) 101–108, https://doi.org/10.1080/15384047.2018.1507257.

[16] J.A. Kim, M. Anurag, J. Veeraraghavan, R. Schiff, K. Li, X.S. Wang, Amplification of TLK2 induces genomic instability via impairing the G2-M checkpoint, Mol. Cancer Res. 14 (2016) 920–927, https://doi.org/10.1158/1541-7786.MCR-16-0161.

[17] J.A. Kim, Y. Tan, X. Wang, X. Cao, J. Veeraraghavan, Y. Liang, D.P. Edwards, S. Huang, X. Pan, K. Li, R. Schiff, X.S. Wang, Comprehensive functional analysis of the tousled-like kinase 2 frequently amplified in aggressive luminal breast cancers, Nat. Commun. 7 (2016) 12991, https://doi.org/10.1038/ncomms12991.

[18] S. Segura-Bayona, P.A. Knobel, H. González-Burón, S.A. Youssef, A. Peña-Blanco, É. Coyaud, T. López-Rovira, K. Rein, L. Palenzuela, J. Colombelli, S. Forrow, B. Raught, A. Groth, A. de Bruin, T.H. Stracker, Differential requirements for Tousled-like kinases 1 and 2 in mammalian development, Cell Death Differ. 24 (2017) 1872–1885, https://doi.org/10.1038/cdd.2017.108.

[19] S.B. Lee, T.Y. Chang, N.Z. Lee, Z.Y. Yu, C.Y. Liu, H.Y. Lee, Design, synthesis and biological evaluation of bisindole derivatives as anticancer agents against Tousled-like kinases, Eur. J. Med. Chem. 227 (2022) 113904, https://doi.org/10.1016/j.ejmech.2021.113904.

[20] C.H. Arrowsmith, J.E. Audia, C. Austin, J. Baell, J. Bennett, J. Blagg, C. Bountra, P. E. Brennan, P.J. Brown, M.E. Bunnage, C. Buser-Doepner, R.M. Campbell, A. J. Carter, P. Cohen, R.A. Copeland, B. Cravatt, J.L. Dahlin, D. Dhanak, A. M. Edwards, M. Frederiksen, S.V. Frye, N. Gray, C.E. Grimshaw, D. Hepworth, T. Howe, K.V. Huber, J. Jin, S. Knapp, J.D. Kotz, R.G. Kruger, D. Lowe, M. M. Mader, B. Marsden, A. Mueller-Fahrnow, S. Müller, R.C. O'Hagan, J. P. Overington, D.R. Owen, S.H. Rosenberg, B. Roth, R. Ross, M. Schapira, S. L. Schreiber, B. Shoichet, M. Sundström, G. Superti-Furga, J. Taunton, L. Toledo-Sherman, C. Walpole, M.A. Walters, T.M. Willson, P. Workman, R.N. Young, W. J. Zuercher, The promise and peril of chemical probes, Nat. Chem. Biol. 11 (2015) 536–541, https://doi.org/10.1038/nchembio.1867.

[21] M.A. Fabian, W.H. Biggs 3rd, D.K. Treiber, C.E. Atteridge, M.D. Azimioara, M. G. Benedetti, T.A. Carter, P. Ciceri, P.T. Edeen, M. Floyd, J.M. Ford, M. Galvin, J. L. Gerlach, R.M. Grotzfeld, S. Herrgard, D.E. Insko, M.A. Insko, A.G. Lai, J. M. Lelias, S.A. Mehta, Z.V. Milanov, A.M. Velasco, L.M. Wodicka, H.K. Patel, P. P. Zarrinkar, D.J. Lockhart, A small molecule-kinase interaction map for clinical kinase inhibitors, Nat. Biotechnol. 23 (2005) 329–336, https://doi.org/10.1038/nbt1068.

[22] M.W. Karaman, S. Herrgard, D.K. Treiber, P. Gallant, C.E. Atteridge, B.T. Campbell, K.W. Chan, P. Ciceri, M.I. Davis, P.T. Edeen, R. Faraoni, M. Floyd, J.P. Hunt, D. J. Lockhart, Z.V. Milanov, M.J. Morrison, G. Pallares, H.K. Patel, S. Pritchard, L. M. Wodicka, P.P. Zarrinkar, A quantitative analysis of kinase inhibitor selectivity, Nat. Biotechnol. 26 (2008) 127–132, https://doi.org/10.1038/nbt1358.

[23] M.I. Davis, J.P. Hunt, S. Herrgard, P. Ciceri, L.M. Wodicka, G. Pallares, M. Hocker, D.K. Treiber, P.P. Zarrinkar, Comprehensive analysis of kinase inhibitor selectivity, Nat. Biotechnol. 29 (2011) 1046–1051, https://doi.org/10.1038/nbt.1990.

[24] T. Anastassiadis, S.W. Deacon, K. Devarajan, H. Ma, J.R. Peterson, Comprehensive assay of kinase catalytic activity reveals features of kinase inhibitor selectivity, Nat. Biotechnol. 29 (2011) 1039–1045, https://doi.org/10.1038/nbt.2017.

[25] J.M. Elkins, V. Fedele, M. Szklarz, K.R. Abdul Azeez, E. Salah, J. Mikolajczyk, S. Romanov, N. Sepetov, X.P. Huang, B.L. Roth, A. Al Haj Zen, D. Fourches, E. Muratov, A. Tropsha, J. Morris, B.A. Teicher, M. Kunkel, E. Polley, K.E. Lackey,

F.L. Atkinson, J.P. Overington, P. Bamborough, S. Müller, D.J. Price, T.M. Willson, D.H. Drewry, S. Knapp, W.J. Zuercher, Comprehensive characterization of the published kinase inhibitor set, Nat. Biotechnol. 34 (2016) 95–103, https://doi.org/10.1038/nbt.3374.

[26] D.H. Drewry, C.I. Wells, D.M. Andrews, R. Angell, H. Al-Ali, A.D. Axtman, S. J. Capuzzi, J.M. Elkins, P. Ettmayer, M. Frederiksen, O. Gileadi, N. Gray, A. Hooper, S. Knapp, S. Laufer, U. Luecking, M. Michaelides, S. Müller, E. Muratov, R.A. Denny, K.S. Saikatendu, D.K. Treiber, W.J. Zuercher, T.M. Willson, Progress towards a public chemogenomic set for protein kinases and a call for contributions, PLoS One 12 (2017) e0181585, https://doi.org/10.1371/journal.pone.0181585.

[27] C.I. Wells, H. Al-Ali, D.M. Andrews, C.R.M. Asquith, A.D. Axtman, I. Dikic, D. Ebner, P. Ettmayer, C. Fischer, M. Frederiksen, R.E. Futrell, N.S. Gray, S. B. Hatch, S. Knapp, U. Lücking, M. Michaelides, C.E. Mills, S. Müller, D. Owen, A. Picado, K.S. Saikatendu, M. Schröder, A. Stolz, M. Tellechea, B.J. Turunen, S. Vilar, J. Wang, W.J. Zuercher, T.M. Willson, D.H. Drewry, The kinase chemogenomic set (KCGS): an open science resource for kinase vulnerability identification, Int. J. Mol. Sci. 22 (2021) 566, https://doi.org/10.3390/ijms22020566.

[28] S. Klaeger, S. Heinzlmeir, M. Wilhelm, H. Polzer, B. Vick, P.A. Koenig, M. Reinecke, B. Ruprecht, S. Petzoldt, C. Meng, J. Zecha, K. Reiter, H. Qiao, D. Helm, H. Koch, M. Schoof, G. Canevari, E. Casale, S.R. Depaolini, A. Feuchtinger, Z. Wu, T. Schmidt, L. Rueckert, W. Becker, J. Huenges, A.K. Garz, B.O. Gohlke, D.P. Zolg, G. Kayser, T. Vooder, R. Preissner, H. Hahne, N. Tonisson, K. Kramer, K. Gotze, F. Bassermann, J. Schlegl, H.C. Ehrlich, S. Aiche, A. Walch, P.A. Greif, S. Schneider, E.R. Felder, J. Ruland, G. Medard, I. Jeremias, K. Spiekermann, B. Kuster, The target landscape of clinical kinase drugs, Science 358 (2017) eaan4368, https://doi.org/10.1126/science.aan4368.

[29] S. Knapp, P. Arruda, J. Blagg, S. Burley, D.H. Drewry, A. Edwards, D. Fabbro, P. Gillespie, N.S. Gray, B. Kuster, K.E. Lackey, P. Mazzafera, N.C. Tomkinson, T. M. Willson, P. Workman, W.J. Zuercher, A public-private partnership to unlock the untargeted kinome, Nat. Chem. Biol. 9 (2013) 3–6, https://doi.org/10.1038/nchembio.1113.

[30] M. Reinecke, P. Brear, L. Vornholz, B.T. Berger, F. Seefried, S. Wilhelm, P. Samaras, L. Gyenis, D.W. Litchfield, G. Médard, S. Müller, J. Ruland, M. Hyvönen, M. Wilhelm, B. Kuster, Chemical proteomics reveals the target landscape of 1,000 kinase inhibitors, Nat. Chem. Biol. (2023), https://doi.org/10.1038/s41589-023-01459-3. Oct 30.

[31] L. Sun, C. Liang, S. Shirazian, Y. Zhou, T. Miller, J. Cui, J.Y. Fukuda, J.Y. Chu, A. Nematalla, X. Wang, H. Chen, A. Sistla, T.C. Luu, F. Tang, J. Wei, C. Tang, Discovery of 5-[5-fluoro-2-oxo-1,2- dihydroindol-(3Z)-ylidenemethyl]-2,4-dimethyl-1H-pyrrole-3-carboxylic acid (2-diethylaminoethyl)amide, a novel tyrosine kinase inhibitor targeting vascular endothelial and platelet-derived growth factor receptor tyrosine kinase, J. Med. Chem. 46 (2003) 1116–1119, https://doi.org/10.1021/jm0204183.

[32] N.K. Pryer, L.B. Lee, R. Zadovaskaya, X. Yu, J. Sukbuntherng, J.M. Cherrington, C. A. London, Proof of target for SU11654: inhibition of KIT phosphorylation in canine mast cell tumors, Clin. Cancer Res. 9 (2003) 5729–5734.

[33] S. Patyna, A.D. Laird, D.B. Mendel, A.M. O'farrell, C. Liang, H. Guan, T. Vojkovsky, S. Vasile, X. Wang, J. Chen, M. Grazzini, C.Y. Yang, J.O. Haznedar, J. Sukbuntherng, W.Z. Zhong, J.M. Cherrington, D. Hu-Lowe, SU14813: a novel multiple receptor tyrosine kinase inhibitor with potent antiangiogenic and antitumor activity, Mol. Cancer Therapeut. 5 (2006) 1774–1782, https://doi.org/10.1158/1535-7163.MCT-05-0333.

[34] R. Hoessel, S. Leclerc, J.A. Endicott, M.E. Nobel, A. Lawrie, P. Tunnah, M. Leost, E. Damiens, D. Marie, D. Marko, E. Niederberger, W. Tang, G. Eisenbrand, L. Indirubin Meijer, The active constituent of a Chinese antileukaemia medicine, inhibits cyclin-dependent kinases, Nat. Cell Biol. 1 (1999) 60–67, https://doi.org/10.1038/9035.

[35] S. Leclerc, M. Garnier, R. Hoessel, D. Marko, J.A. Bibb, G.L. Snyder, P. Greengard, J. Biernat, Y.Z. Wu, E.M. Mandelkow, G. Eisenbrand, L. Meijer, Indirubins inhibit glycogen synthase kinase-3 beta and CDK5/p25, two protein kinases involved in abnormal tau phosphorylation in Alzheimer's disease. A property common to most cyclin-dependent kinase inhibitors? J. Biol. Chem. 276 (2001) 251–260, https://doi.org/10.1074/jbc.M002466200.

[36] J.A. Bertrand, S. Thieffine, A. Vulpetti, C. Cristiani, B. Valsasina, S. Knapp, H. M. Kalisz, M. Flocco, Structural characterization of the GSK-3beta active site using selective and non-selective ATP-mimetic inhibitors, J. Mol. Biol. 333 (2003) 393–407, https://doi.org/10.1016/j.jmb.2003.08.031.

[37] M. Mapelli, L. Massimiliano, C. Crovace, M.A. Seeliger, L.H. Tsai, L. Meijer, A. Musacchio, Mechanism of CDK5/p25 binding by CDK inhibitors, J. Med. Chem. 48 (2005) 671–679, https://doi.org/10.1021/jm049323m.

[38] C.R.M. Asquith, D.K. Treiber, W.J. Zuercher, Utilizing comprehensive and mini-kinome panels to optimize the selectivity of quinoline inhibitors for cyclin G associated kinase (GAK), Bioorg. Med. Chem. Lett. 29 (2019) 1727–1731, https://doi.org/10.1016/j.bmcl.2019.05.025.

[39] S.D. Bembenek, G. Hirst, T. Mirzadegan, Determination of a focused mini kinase panel for early identification of selective kinase inhibitors, J. Chem. Inf. Model. 58 (2018) 1434–1440, https://doi.org/10.1021/acs.jcim.8b00222.

[40] P. Brandt, A.J. Jensen, J. Nilsson, Small kinase assay panels can provide a measure of selectivity, Bioorg. Med. Chem. Lett. 19 (2009) 5861–5863, https://doi.org/10.1016/j.bmcl.2009.08.083.

[41] L. Sun, N. Tran, F. Tang, H. App, P. Hirth, G. McMahon, C. Tang, Synthesis and biological evaluations of 3-substituted indolin-2-ones: a novel class of tyrosine kinase inhibitors that exhibit selectivity toward particular receptor tyrosine kinases, J. Med. Chem. 41 (1998) 2588–4603, https://doi.org/10.1021/jm980123i.

[42] G. Jones, The Knoevenagel condensation, Org. React. (2004) 204–273, https://doi.org/10.1002/0471264180.or015.02.

[43] E. Knoevenagel, Condensation von Malonsäure mit aromatischen Aldehyden durch Ammoniak und Amine [Condensation of malonic acid with aromatic aldehydes via ammonia and amines], Ber. Dtsch. Chem. Ges. 31 (1898) 2596–2619, https://doi.org/10.1002/cber.18980310308.

[44] R. Rueping, B.J. Nachtsheim, A review of new developments in the friedel-crafts alkylation - from green Chemistry to asymmetric catalysis, Beilstein J. Org. Chem. 6 (6) (2010), https://doi.org/10.3762/bjoc.6.6.

[45] C. Friedel, J.M. Crafts, Sur une Méthode Générale Nouvelle de Synthèse d'Hydrocarbures, d'Acétones, etc, Compt. Rend (84) (1877) 1392–1395.

[46] C. Friedel, J.M. Crafts, Sur une Méthode Générale Nouvelle de Synthèse d'Hydrocarbures, d'Acétones, etc, Compt. Rend (84) (1877) 1450–1454.

[47] J. Xiao, W. Westbroek, O. Motabar, W.A. Lea, X. Hu, A. Velayati, W. Zheng, N. Southall, A.M. Gustafson, E. Goldin, E. Sidransky, K. Liu, A. Simeonov, R. J. Tamargo, A. Ribes, L. Matalonga, M. Ferrer, J.J. Marugan, Discovery of a novel noniminosugar acid α glucosidase chaperone series, J. Med. Chem. 55 (2012) 7546–7559, https://doi.org/10.1021/jm3005543.

[48] O. Mitsunobu, Y. Yamada, Preparation of esters of carboxylic and phosphoric acid via quaternary phosphonium salts, Bull. Chem. Soc. Jpn. 40 (1967) 2380–2382, https://doi.org/10.1246/bcsj.40.2380.

[49] O. Mitsunobu, The use of diethyl azodicarboxylate and triphenylphosphine in synthesis and transformation of natural products, Synthesis (1) (1981) 1–28, https://doi.org/10.1055/s-1981-29317.

[50] S.D. Lepore, Y. He, Use of sonication for the coupling of sterically hindered substrates in the phenolic Mitsunobu reaction, J. Org. Chem. 68 (2003) 8261–8263, https://doi.org/10.1021/jo0345751.

[51] L.A. Carpino, H. Imazumi, A. El-Faham, F.J. Ferrer, C. Zhang, Y. Lee, B.M. Foxman, P. Henklein, C. Hanay, C. Mügge, H. Wenschuh, J. Klose, M. Beyermann, M. Bienert, The uronium/guanidinium peptide coupling reagents: finally the true uronium salts, Angew. Chem., Int. Ed. Engl. 41 (2002) 441–445, https://doi.org/10.1002/1521-3773(20020201)41:3<441::aid-anie441>3.0.

[52] G. Cavallo, P. Metrangolo, R. Milani, T. Pilati, A. Priimagi, G. Resnati, G. Terraneo, The halogen bond, Chem. Rev. 116 (2016) 2478–2601, https://doi.org/10.1021/acs.chemrev.5b00484.

[53] P. Auffinger, F.A. Hays, E. Westhof, P.S. Ho, Halogen bonds in biological molecules, Proc. Natl. Acad. Sci. U.S.A. 101 (2004) 16789–16794, https://doi.org/10.1073/pnas.0407607101.

[54] D. Stumpfe, J. Bajorath, Exploring activity cliffs in medicinal Chemistry, J. Med. Chem. 55 (2012) 2932–2942, https://doi.org/10.1021/jm201706b.

[55] A. Kohlmann, X. Zhu, D. Dalgarno, Application of MM-GB/SA and WaterMap to SRC kinase inhibitor potency prediction, ACS Med. Chem. Lett. 3 (2012) 94–99, https://doi.org/10.1021/ml200222u.

[56] C. Higgs, T. Beuming, W. Sherman, Hydration site thermodynamics explain SARs for triazolylpurines analogues binding to the A2A receptor, ACS Med. Chem. Lett. 1 (2010) 160–164, https://doi.org/10.1021/ml100008s.

[57] C.R.M. Asquith, T. Laitinen, J.M. Bennett, C.I. Wells, J.M. Elkins, W.J. Zuercher, G. J. Tizzard, A. Poso, Design and analysis of the 4-anilino-quin(az)oline kinase inhibition profiles of GAK/SLK/STK10 using quantitative structure activity relationships, ChemMedChem 15 (2020) 26–49, https://doi.org/10.1002/cmdc.201900521.

[58] C.R.M. Asquith, G.J. Tizzard, J.M. Bennett, C.I. Wells, J.M. Elkins, T.M. Willson, A. Poso, T. Laitinen, Targeting the water network in cyclin G-associated kinase (GAK) with 4-Anilino-quin(az)oline inhibitors, ChemMedChem 15 (2020) 1200–1215, https://doi.org/10.1002/cmdc.202000150.

[59] C.R.M. Asquith, K.A. Maffuid, T. Laitinen, C.D. Torrice, G.J. Tizzard, D.J. Crona, W. J. Zuercher, Targeting an EGFR water network with 4-Anilinoquin(az)oline inhibitors for chordoma, ChemMedChem 14 (2019) 1693–1700, https://doi.org/10.1002/cmdc.201900428.

[60] G.W. Bemis, M.A. Murcko, The properties of known drugs. 1. Molecular frameworks, J. Med. Chem. 39 (1996) 2887–2893, https://doi.org/10.1021/jm9602928.

[61] K.M. Kleman-Leyer, T.A. Klink, A.L. Kopp, T.A. Westermeyer, M.D. Koeff, B. R. Larson, T.J. Worzella, C.A. Pinchard, S.A. van de Kar, G.J. Zaman, J.J. Hornberg, R.G. Lowery, Characterization and optimization of a red-shifted fluorescence polarization ADP detection assay, Assay Drug Dev. Technol. 7 (2009) 56–67, https://doi.org/10.1089/adt.2008.175.

[62] H. Zegzouti, M. Zdanovskaia, K. Hsiao, S.A. Goueli, ADP-glo: a bioluminescent and homogeneous ADP monitoring assay for kinases, Assay Drug Dev. Technol. 7 (2009) 560–572, https://doi.org/10.1089/adt.2009.0222.

[63] H. Li, R.D. Totoritis, L.A. Lor, B. Schwartz, P. Caprioli, A.J. Jurewicz, G. Zhang, Evaluation of an antibody-free ADP detection assay: ADP-Glo, Assay Drug Dev. Technol. 7 (2009) 598–605, https://doi.org/10.1089/adt.2009.0221.

[64] D. Johnson, J. Hussain, S. Bhoir, V. Chandrasekaran, P. Sahrawat, T. Hans, M. I. Khalil, A. De Benedetti, V. Thiruvenkatam, S. Kirubakaran, Synthesis, kinetics and cellular studies of new phenothiazine analogs as potent human-TLK inhibitors, Org. Biomol. Chem. 21 (2023) 1980–1991, https://doi.org/10.1039/d2ob02191a.

[65] S. Ronald, S. Awate, A. Rath, J. Carroll, F. Galiano, D. Dwyer, H. Kleiner-Hancock, J.M. Mathis, S. Vigod, A. De Benedetti, Phenothiazine inhibitors of TLKs affect double-strand break repair and DNA damage response recovery and potentiate tumor killing with radiomimetic therapy, Genes Cancer 4 (2013) 39–53, https://doi.org/10.1177/1947601913479020.

[66] J.C. Uitdehaag, F. Verkaar, H. Alwan, J. de Man, R.C. Buijsman, G.J. Zaman, A guide to picking the most selective kinase inhibitor tool compounds for pharmacological validation of drug targets, Br. J. Pharmacol. 166 (3) (2012) 858–876, https://doi.org/10.1111/j.1476-5381.2012.01859.x.

[67] L.L. Rokosz, J.R. Beasley, C.D. Carroll, T. Lin, J. Zhao, K.C. Appell, M.L. Webb, Kinase inhibitors as drugs for chronic inflammatory and immunological diseases: progress and challenges, Expert Opin. Ther. Targets 12 (2008) 883–903, https://doi.org/10.1517/14728222.12.7.883.

[68] L. Sun, N. Tran, C. Liang, F. Tang, A. Rice, R. Schreck, K. Waltz, L.K. Shawver, G. McMahon, C. Tang, Design, synthesis, and evaluations of substituted 3-[(3- or 4-carboxyethylpyrrol-2-yl)methylidenyl]indolin-2-ones as inhibitors of VEGF, FGF, and PDGF receptor tyrosine kinases, J. Med. Chem. 42 (1999) 5120–5130, https://doi.org/10.1021/jm9904295.

[69] E.R. Wood, L. Kuyper, K.G. Petrov, R. N 3rd Hunter, P.A. Harris, K. Lackey, Discovery and in vitro evaluation of potent TrkA kinase inhibitors: oxindole and aza-oxindoles, Bioorg. Med. Chem. Lett 14 (2004) 953–957, https://doi.org/10.1016/j.bmcl.2003.12.002.

[70] H.N. Bramson, J. Corona, S.T. Davis, S.H. Dickerson, M. Edelstein, S.V. Frye, R.T. Jr. Gampe, P.A. Harris, A. Hassell, W.D. Holmes, R.N. Hunter, K.E. Lackey, B. Lovejoy, M.J. Luzzio, V. Montana, W.J. Rocque, D. Rusnak, L. Shewchuk, J. M. Veal, D.H. Walker, L.F. Kuyper, Oxindole-based inhibitors of cyclin-dependent kinase 2 (CDK2): design, synthesis, enzymatic activities, and X-ray crystallographic analysis, J. Med. Chem. 44 (2001) 4339–4358, https://doi.org/10.1021/jm010117d.

[71] K.C. Luk, M.E. Simcox, A. Schutt, K. Rowan, T. Thompson, Y. Chen, U. Kammlott, W. DePinto, P. Dunten, A. Dermatakis, A new series of potent oxindole inhibitors of CDK2, Bioorg. Med. Chem. Lett 14 (2004) 913–917, https://doi.org/10.1016/j.bmcl.2003.12.009.

[72] A. Dermatakis, K.C. Luk, W. DePinto, Synthesis of potent oxindole CDK2 inhibitors, Bioorg. Med. Chem. 11 (2003) 1873–1881, https://doi.org/10.1016/s0968-0896(03)00036-1.

[73] I. Islam, G. Brown, J. Bryant, P. Hrvatin, M.J. Kochanny, G.B. Phillips, S. Yuan, M. Adler, M. Whitlow, D. Lentz, M.A. Polokoff, J. Wu, J. Shen, J. Walters, E. Ho, B. Subramanyam, D. Zhu, R.I. Feldman, D.O. Arnaiz, Indolinone based phosphoinositide-dependent kinase-1 (PDK1) inhibitors. Part 2: optimization of BX-517, Bioorg. Med. Chem. Lett 17 (2007) 3819–3825, https://doi.org/10.1016/j.bmcl.2007.05.060.

[74] H. Guan, A.D. Laird, R.A. Blake, C. Tang, C. Liang, Design and synthesis of aminopropyl tetrahydroindole-based indolin-2-ones as selective and potent inhibitors of Src and Yes tyrosine kinase, Bioorg. Med. Chem. Lett 14 (2004) 187–190, https://doi.org/10.1016/j.bmcl.2003.09.069.

[75] M. Kaur, M. Singh, N. Chadha, O. Oxindole Silakari, A chemical prism carrying plethora of therapeutic benefits, Eur. J. Med. Chem. 123 (2016) 858–894, https://doi.org/10.1016/j.ejmech.2016.08.011.

[76] T. Troxler, P. Greenidge, K. Zimmermann, S. Desrayaud, P. Drückes, T. Schweizer, D. Stauffer, G. Rovelli, D.R. Shimshek, Discovery of novel indolinone-based, potent, selective and brain penetrant inhibitors of LRRK2, Bioorg. Med. Chem. Lett 23 (2013) 4085–4090, https://doi.org/10.1016/j.bmcl.2013.05.054.

[77] Z. Fang, Y. Song, P. Zhan, Q. Zhang, X. Liu, Conformational restriction: an effective tactic in 'follow-on'-based drug discovery, Future Med. Chem. 6 (2014) 885–901, https://doi.org/10.4155/fmc.14.50.

[78] C.R.M. Asquith, T. Laitinen, J.M. Bennett, P.H. Godoi, M.P. East, G.J. Tizzard, L. M. Graves, G.L. Johnson, R.E. Dornsife, C.I. Wells, J.M. Elkins, T.M. Willson, W. J. Zuercher, Identification and optimization of 4-anilinoquinolines as inhibitors of cyclin G associated kinase, ChemMedChem 13 (2018) 48–66, https://doi.org/10.1002/cmdc.201700663.

[79] J.M. Ellis, M.D. Altman, A. Bass, J.W. Butcher, A.J. Byford, A. Donofrio, S. Galloway, A.M. Haidle, J. Jewell, N. Kelly, E.K. Leccese, S. Lee, M. Maddess, J. R. Miller, L.Y. Moy, E. Osimboni, R.D. Otte, M.V. Reddy, K. Spencer, B. Sun, S. H. Vincent, G.J. Ward, G.H. Woo, C. Yang, H. Houshyar, A.B. Northrup, Overcoming mutagenicity and ion channel activity: optimization of selective spleen tyrosine kinase inhibitors, J. Med. Chem. 58 (2015) 1929–1939, https://doi.org/10.1021/jm5018169.

[80] B.G. Lawhorn, J. Philp, Y. Zhao, C. Louer, M. Hammond, M. Cheung, H. Fries, A. P. Graves, L. Shewchuk, L. Wang, J.E. Cottom, H. Qi, H. Zhao, R. Totoritis, G. Zhang, B. Schwartz, H. Li, S. Sweitzer, D.A. Holt, G.J. Gatto Jr., L.S. Kallander, Identification of purines and 7-deazapurines as potent and selective type I inhibitors of troponin I-interacting kinase (TNNI3K), J. Med. Chem. 58 (2015) 7431–7448, https://doi.org/10.1021/acs.jmedchem.5b00931.

[81] C.R.M. Asquith, T. Laitinen, C.I. Wells, G.J. Tizzard, W.J. Zuercher, New insights into 4-anilinoquinazolines as inhibitors of cardiac troponin I-interacting kinase (TNNi3K), Molecules 25 (2020) 1697, https://doi.org/10.3390/molecules25071697.

[82] J. Azuaje, W. Jespers, V. Yaziji, A. Mallo, M. Majellaro, O. Caamaño, M.I. Loza, M. I. Cadavid, J. Brea, J. Åqvist, E. Sotelo, H. Gutiérrez-de-Terán, Effect of nitrogen atom substitution in A3 adenosine receptor binding: *N*-(4,6-Diarylpyridin-2-yl) acetamides as potent and selective antagonists, J. Med. Chem. 60 (2017) 7502–7511, https://doi.org/10.1021/acs.jmedchem.7b00860.

[83] R. Geyer, U. Nordemann, A. Strasser, H.J. Wittmann, A. Buschauer, Conformational restriction and enantioseparation increase potency and selectivity of cyanoguanidine-type histamine H4 receptor agonists, J. Med. Chem. 59 (2016) 3452–3470, https://doi.org/10.1021/acs.jmedchem.6b00120.

[84] J. El Bakali, G.G. Muccioli, M. Body-Malapel, M. Djouina, F. Klupsch, A. Ghinet, A. Barczyk, N. Renault, P. Chavatte, P. Desreumaux, D.M. Lambert, R. Millet, Conformational restriction leading to a selective CB2 cannabinoid receptor agonist orally active against colitis, ACS Med. Chem. Lett. 6 (2014) 198–203, https://doi.org/10.1021/ml500439x.

[85] L.D. Pennington, D.T. Moustakas, The necessary nitrogen atom: a versatile high-impact design element for multiparameter optimization, J. Med. Chem. 60 (2017) 3552–3579, https://doi.org/10.1021/acs.jmedchem.6b01807.

[86] D.D. Robinson, W. Sherman, R. Farid, Understanding kinase selectivity through energetic analysis of binding site waters, ChemMedChem 5 (2010) 618–627, https://doi.org/10.1002/cmdc.200900501.

[87] D. Robinson, T. Bertrand, J.C. Carry, F. Halley, A. Karlsson, M. Mathieu, H. Minoux, M.A. Perrin, B. Robert, L. Schio, W. Sherman, Differential water thermodynamics determine PI3K-Beta/Delta selectivity for solvent-exposed ligand modifications, J. Chem. Inf. Model. 56 (2016) 886–894, https://doi.org/10.1021/acs.jcim.5b00641.

[88] Y. Hu, R. Kunimoto, J. Bajorath, Mapping of inhibitors and activity data to the human kinome and exploring promiscuity from a ligand and target perspective, Chem. Biol. Drug Des. 89 (2017) 834–845, https://doi.org/10.1111/cbdd.12919.

[89] E. Harder, W. Damm, J. Maple, C. Wu, M. Reboul, J.Y. Xiang, L. Wang, D. Lupyan, M.K. Dahlgren, J.L. Knight, J.W. Kaus, D.S. Cerutti, G. Krilov, W.L. Jorgensen, R. Abel, R.A. Friesner, OPLS3: a force field providing broad coverage of drug-like small molecules and proteins, J. Chem. Theor. Comput. 12 (2016) 281–296, https://doi.org/10.1021/acs.jctc.5b00864.

[90] CrysAlisPro Software System, Rigaku Oxford Diffraction, 2018.

[91] G.M. Sheldrick, Crystal structure refinement with SHELXL, Acta Crystallogr., Sect. A 71 (2015) 3–8, https://doi.org/10.1107/S2053229614024218.

[92] O.V. Dolomanov, L.J. Bourhis, R.J. Gildea, J.A.K. Howard, H. Puschmann, OLEX2: a complete structure solution, refinement and analysis program, J. Appl. Crystallogr. 42 (2009) 339–341, https://doi.org/10.1107/S0021889808042726.

[93] T.A. Fong, L.K. Shawver, L. Sun, C. Tang, H. App, T.J. Powell, Y.H. Kim, R. Schreck, X. Wang, W. Risau, A. Ullrich, K.P. Hirth, G. McMahon, SU5416 is a potent and selective inhibitor of the vascular endothelial growth factor receptor (Flk-1/KDR) that inhibits tyrosine kinase catalysis, tumor vascularization, and growth of multiple tumor types, Cancer Res. 59 (1999) 99–106.

[94] M.E. Lane, B. Yu, A. Rice, K.E. Lipson, C. Liang, L. Sun, C. Tang, G. McMahon, R. G. Pestell, S. Wadler, A novel cdk2-selective inhibitor, SU9516, induces apoptosis in colon carcinoma cells, Cancer Res. 61 (2001) 6170–6177.

[95] M.E. Dumas, G.Y. Chen, N.D. Kendrick, G. Xu, S.D. Larsen, S. Jana, A.G. Waterson, J.A. Bauer, W. Hancock, G.A. Sulikowski, R. Ohi, Dual inhibition of Kif15 by oxindole and quinazolinedione chemical probes, Bioorg. Med. Chem. Lett 29 (2019) 148–154, https://doi.org/10.1016/j.bmcl.2018.12.008.

[96] M.H. Kim, A.L. Tsuhako, E.W. Co, D.T. Aftab, F. Bentzien, J. Chen, W. Cheng, S. Engst, L. Goon, R.R. Klein, D.T. Le, M. Mac, J.J. Parks, F. Qian, M. Rodriquez, T. J. Stout, J.H. Till, K.A. Won, X. Wu, F.M. Yakes, P. Yu, W. Zhang, Y. Zhao, P. Lamb, J.M. Nuss, W. Xu, The design, synthesis, and biological evaluation of potent receptor tyrosine kinase inhibitors, Bioorg. Med. Chem. Lett 22 (2012) 4979–4985, https://doi.org/10.1016/j.bmcl.2012.06.029.